A Clean and Flexible Catalyst Synthesis Method

Metal nanoparticles on a fractal-like nanostructured metal oxide support

By

F.P. Braams

in partial fulfilment of the requirements for the degree of

Master of Science
in Chemical Engineering

at the Delft University of Technology,
to be defended publicly on Monday March 30, 2013 at 01:30 PM.

Student number:	1519093
Project Duration:	July 2014 – March, 2015
Faculty:	Applied Sciences
Department:	Chemical Engineering
Section:	Materials for Energy Conversion and Storage

Supervisor:	Prof. dr. A. Schmidt-Ott
Thesis committee:	Prof. dr. A. Schmidt-Ott,
	Dr. W. A. Smith,
	Dr. ir. J.R. van Ommen

TUDelft Delft University of Technology

Preface

At the start of each Master, every student knows that in the end a master thesis needs to be delivered. Without this final project no student can call him- or herself a Master of Science. But where to start or moreover, how to start? What I noticed when I started orienting on what I could do for my master thesis, was that there is so much yet to be discovered in the field of chemical engineering. Since my bachelor thesis I was interested in the world of nanoparticles, but that is still a very broad and vague term and so I was still a long way off from having a nicely demarcated research topic.

Luckily at that point in time I came into contact with Aaike van Vugt. He told me about his thesis research; how he was in the end phase of writing his report and that he was looking for someone who could continue on his work. One thing led to another and after an initial conversation with Andreas Schmidt-Ott, I started reading on the topic. A summer full of articles, papers and reports followed and in August last year I handed in my thesis proposal.

Then started months of brainstorms, experiments, bugging people for help, presentations and in the end of course writing this report. Some highlights in this journey:

- Creating my own set-up, it felt like playing with meccano again!

- Zooming in with an electron microscope and seeing with your own eyes the wonders of the nanoscale world.

- Performing Transmission Electron Microscopy (TEM) and getting the conformation that what you thought would happen actually is right.

- Sending in an abstract for a conference and being chosen to give a poster presentation.

These are just a handful of examples, but I could honestly say that (for the largest part) I had a great time doing my master thesis research. And of course I would like to thank a few people for their help during the course of this project. First of all Andreas Schmidt-Ott, Wilson Smith and Ruud van Ommen for doing me the honor of being part of my thesis committee. Aafke den Hollander for providing love and mental support during the whole project. Christien Braams for helping me in the lab, family and friends for listening to me talk about 'boring' science stuff and the girls in my office (Eva, Jessica and Eline) for welcome distractions in the everyday work life.

Abstract

A highly porous fractal-like nanostructured metal oxide catalyst support with characteristic dimensions of a few nanometers is formed by producing metal nanoparticles in the gas phase, oxidizing them and depositing/sintering them on a nanofiber network. By admixing nanoparticles in the aerosol phase, these can evenly be distributed in the fractal-like metal oxide structure. The nanofiber network is a polymer and is produced by electrospinning [77]. It serves as an initial support, while the structure supports itself after forming a certain thickness. Spark discharge is used to produce the active nanoparticles as well as the support [11]. Rapid diffusion limited aggregation governs the deposition process, guaranteeing formation of the fractal-like structure [38]. Due to the flexible nature of the spark discharge process, a virtually unlimited number of combinations of oxide supports, metals, alloys and bi-catalysts can be made. The method proved to work for titanium dioxide, aluminium oxide and magnesium oxide catalyst supports. Combinations of these metal oxides with gold and platinum proved the broad applicability of the method. The process can be called environmentally friendly, since it does not use any solvents or produce any hazardous waste.

Initial photocatalytic experiments on titanium dioxide nanostructures were carried out to test the catalytic activity of the material. It was observed that the titanium dioxide nanostructures were amorphous, but still exhibited catalytic properties. Adding gold nanoparticles to the nanostructures lowered the catalytic effect. In-situ annealing of amorphous titanium dioxide nanoparticles, before admixing gold nanoparticles, yielded highly porous fractal-like crystalline titanium dioxide nanostructures with gold nanoparticles on the surface.

Acknowledgements

Contents

List of Figures

List of Tables

Chapter 1

Introduction

Catalysis is everywhere; catalysts are present in chemical reactions on a scale that ranges from the largest chemical processes to the smallest organisms that can be found on this planet. Catalysis can be defined as: *"The increase in the rate of a chemical reaction due to the participation of an additional substance called a catalyst"* [4]. Catalysts are being used in various reactions and only looking at large scale industrial chemical processes, catalysts are being used in approximately 90% of all chemical reactions. It is stated that 80% of these catalysts are for heterogeneous catalysis, which is defined as *"Catalysis in which the phase of the reactants differs from the phase of the catalyst(s)"* [4]. Why is this relevant? The total market of catalysts is expected to grow to $ 27.59 billion by 2020; a huge market with lots of possibilities [5].

Van Vugt [2] developed a method to synthesize catalysts in a clean and efficient way. This method was based on combining the processes of polymer electrospinning and spark discharge nanoparticle generation. He showed that by combining these methods, highly fractal-like gold nanostructures (consisting of nanoparticles produced by spark discharge) could be made on top of a nanomaterial support (the electrospun polymer fibers). Both methods are explained in this thesis, in chapter 2. The method provided the possibility to create structures with high catalytic surface area and flexibility in catalyst material. Next to that (even more important) these promising structures were made without the downsides current (co)precipitation and impregnation/coating techniques production methods have: liquid waste streams and contaminated catalytic material. Below a summation of the main conclusions by van Vugt is given:

- The method yields highly fractal-like gold structures on polymer nanofibers.

- Combination of different metals is possible, providing a synthesis path for a metal oxide support for gold coatings.

- The synthesized microstructures seem to be stable up to 400 °C.

Of course every new invention has its downsides when first being discovered and this method was no exception. Although the overall conclusions were very promising, three main problems were identified. The main problems found by van Vugt were:

- Sintering of gold nanostructures, to improve the stability, induces loss of fractal-like nanostructure.

- Oxidation of a metal backbone to support the gold nanoparticles causes nanostructures to collapse.

- Gold nanoparticles become submerged in the metal oxide backbone upon oxidation.

These three observations gave enough ground to continue the research and encourage other scientists to come up with a solution to these problems. Therefore these three observations form the motivation of this master thesis research. The research objective of this master thesis can be described by the following sentence.

Design a general method to produce fractal-like metal oxide nanostructures with metal nanoparticles on the surface.

To achieve this goal, a dual spark chamber set-up with gas phase oxidation of the metal oxide support was proposed as the solution to the problems caused by the oxidation of the metal nanoparticles as observed in previous research [2].

To test whether this method proved to be the desired solution and at the same time make the next step towards applying the method in the field of catalysis, it was chosen to try and synthesize (in the first place) fractal-like titanium dioxide nanostructures on polymer fibers with gold nanoparticles on the surface of this titanium dioxide matrix. Nano-sized titanium dioxide exhibits interesting photocatalytic activity and was therefore chosen to be tested first.

Another part of the research objective is the desire to design a method for producing fractal-like metal oxide nanostructures that is applicable to all sorts of metal oxides, not only titanium dioxide. Therefore it was chosen to test the method also with other metals that tend to oxidize rapidly, for example aluminium and magnesium.

This thesis report consists of the following sections. First a literature overview is given that provides the theoretical framework of the thesis. In the second chapter, the experimental approach, results and discussion are being discussed. In chapter four, the conclusions of this thesis work are given and chapter five lists the recommendations for future research. Also added are various appendices that provide additional information.

Chapter 2

Literature Review

In this thesis various concepts, methods and phenomena are dealt with and used throughout the research. Many of these concepts are already thoroughly investigated by other researchers and many of these results are published. This chapter will give a short overview on these phenomena, concepts and methods that are already discussed in the literature. The outline is as follows:

- Spark discharge and electrospinning methods

- Aluminium and titanium nanoparticle oxidation

- Diffusion limited aggregation

- Fractal dimension

- Catalytic activity of gold nanoparticles on titania and alumina

- Applications of Au-TiO$_2$ and Au-Al$_2$O$_3$ catalysts

2.1   Spark discharge and Electrospinning method

2.1.1   Spark discharge

Two promising methods to efficiently produce nano size materials are spark discharge and electrospinning. Spark discharge is a method that has its roots already in the early 20th century [6], but was not used specifically for synthesis of nano-sized materials. It was not until the 1980's before the first publications on the use of spark discharge for the purpose of synthesising nanoparticles emerged [7, 8]. This early research showed that this method was able to produce nanoparticles as small as 1nm, from that point on other researchers set out to optimize the technique and extend the size range of produced particles [8, 9].

Spark discharge is a process where nanoparticles are generated with the use of spark generation between two electrodes. The process is based on the ablation of the electrodes upon the generation of a spark between them. When a spark is generated, it produces a plasma that will induce a sudden temperature increase up to approximately 20000K and even higher, for a duration of typically a few micro seconds [10]. This sudden increase causes ablation of

(a) Spark discharge mechanism

(b) Electrode configurations and nanoparticle mixing
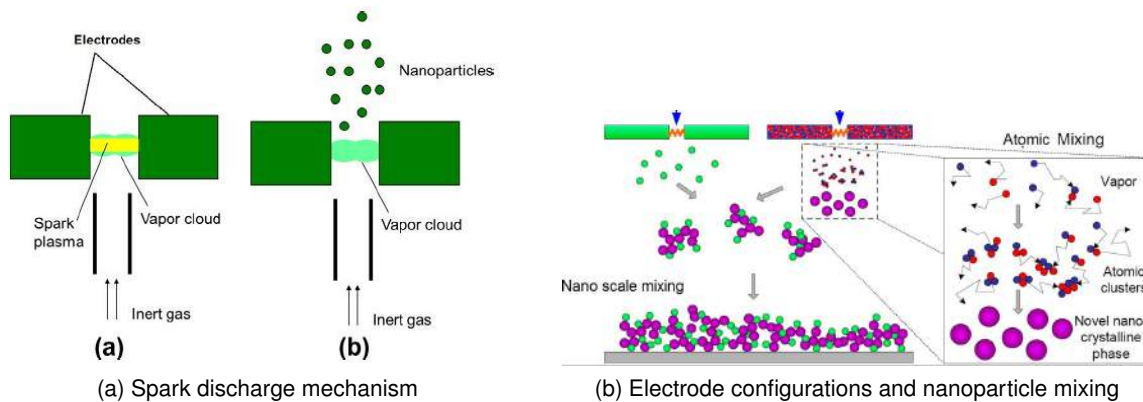
Figure 2.1: Spark discharge nanoparticle generation

the electrodes, generating nanoparticles in the size range of a single atom to 100 nm [9]. A schematic overview can be found in figure 2.1. The mechanism of spark discharge is relatively easy; a current source builds up a charge between the two electrodes to be ablated until the capacitance reaches a certain voltage. At this voltage, the so called gas breakdown voltage, a spark will transfer between the two electrodes discharging the capacitor and causing the ablation of the electrodes. A drawback in this design is that the breakdown voltage is not consistent and thus the energy per spark differs. Another drawback is that operation above a frequency of 500 Hz is not possible. A concept which better controls these drawbacks is available, however this is considered to be unnecessary for the small scale production in this thesis [1].

When looking more closely at the spark discharge mechanism, a few different parameters can be identified as being of influence on the particle size and composition. Research has shown that the primary size of the particles, just after the spark discharge, can effectively be controlled by the energy of the spark and the turbulent inert gas flow as shown in figure 2.2 [11]. The energy per spark determines the amount of ablated particles and the gas flow determines the size of the agglomerate. Particles that are ablated from the electrodes coagulate in the gas phase, so more particles in the gas phase would yield larger agglomerates. However, a larger flow causes more turbulence, reducing chances of particles coagulating [11, 12]. Although this is not done in this thesis research controlling the size of the particles can be done by mobility size classification in a Differential Mobility Analyser (DMA). Furthermore, changing the material of the electrodes will change the particle composition. Two alike electrodes will produce nanoparticles of the electrode material, but using two electrodes of different materials will create a variety in mixed nanoparticles; atomic mixed nanoparticles, nanoscale mixed nanoparticles, core-shell nanoparticles etc. as depicted in figure 2.1 [1, 13, 14].

2.1.2 Electrospinning

Electrospinning is a method that has been investigated for some time and is a process that is based on the uniaxial elongation of a jet from the surface of a polymer solution, due to the presence of an electric field between the polymer solution and a conductive collector [15, 16]. Elongation of a jet from the polymer surface happens when an electric field, that is applied between the polymer solution and the collector, is bigger than the surface tension of the specific polymer solution [17–19]. The Coulombic repulsion stretches the jets that elongate from
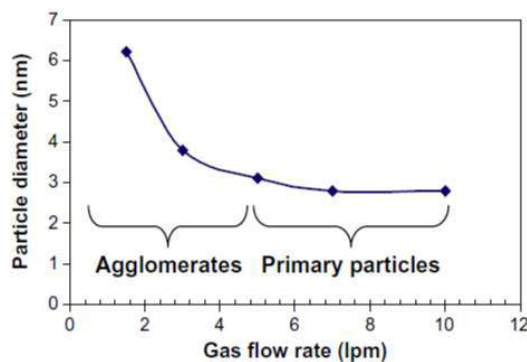
Figure 2.2: Particle mean diameter as function of Ar mass flow rate (C = 5 nF, d = 0.5 mm, f = 10 Hz). Taken from Pfeiffer *et al.* [1].

the polymer solution, creating nanometer scale polymer fibers. Due to the low order of magnitude (nanometer scale) of the jets the solvent of the solution evaporates, leaving practically dry polymer nanofibers [20]. A schematic representation of the electrospinning set up is given in figure 2.3. The figure shows a syringe with a metal needle attached, both are filled with the polymer solution and placed at a certain height above the collector. A syringe pump controls the flow rate of the polymer solution. The applications and industries in which nanofibers have been successfully used are nanocatalysis, tissue engineering scaffolds, protective clothing, filtration, biomedical, pharmaceutical, optical electronics, healthcare, biotechnology, defense and security, and environmental engineering [20].

Various kinds of polymers can be used for the electrospinning process. Previous research by van Vugt [2] used the polymer Poly Vinyl-Alcohol (PVA) as the backbone for deposition of the nanoparticles due to its low toxicity and solubility in water. These polymer nanofibers were however not stable at temperatures higher than 120 °C. A research by R. Saur [21] has shown that the polymers Poly Acrylo-Nitril (PAN) and a mixture of crosslinked PVA and Poly Acrylic-Acid (PAA) gave higher stability for the polymer nanofibers.

2.2 Aluminium and titanium nanoparticle oxidation

One of the limitations that occurred in previous research to produce fractal-like metal nanostructures on top of the polymer nanofibers is oxidation of aluminium nanoparticles once deposited on the polymer fibers [2]. Oxidation of the metal nanoparticles resulted in two things: 1. melting of the fractal-like nanostructures, causing them to collapse 2. submergence of gold nanoparticles placed on top of the structures into the aluminium oxide matrix. Therefore one of the main goals of this thesis was to overcome the problems the oxidation of the nanoparticles caused. Below a short overview of the literature of both aluminium and titanium nanoparticle oxidation is given.

2.2.1 Aluminium nanoparticle oxidation

Properties of particles drastically change once they enter the nanoparticle regime. Once in this size regime, most macroscopic properties and effects change and the normal way of treating these materials is not applicable anymore. Especially aluminium is a metal that has interesting
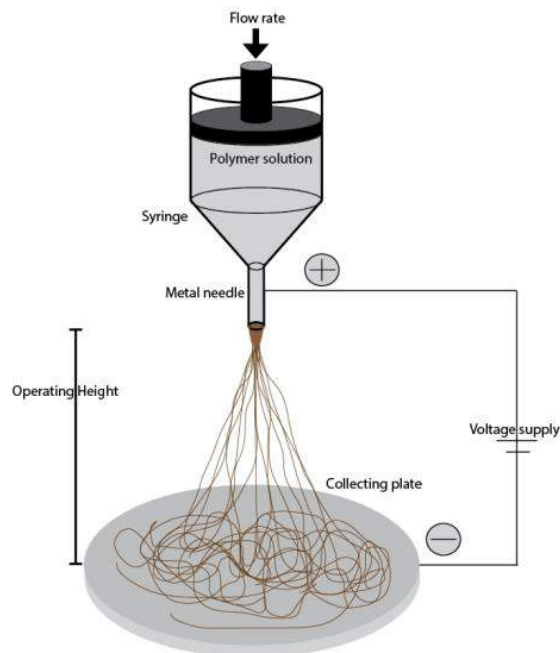
Figure 2.3: Electrospinning set-up, taken from van Vugt [2].

properties when the particles get in the nano-sized regime. Aluminium is nowadays used as an additive to propellants and explosives because of its high reaction enthalpy [22–25]. This made the material an interesting research topic and many research has been done on the reaction mechanism of aluminium. The mechanism on the combustion of aluminium was investigated by Yetter *et al.* [26, 27] in which they confirmed the gas phase combustion of micron size aluminium. Trunov *et al.* [3] studied the oxidation process with a core shell model, where the metal particle is surrounded by aluminium oxide shell. They stated that the oxidation process is based on the diffusion of oxygen and aluminium through this aluminium oxide shell, as is depicted in figure 2.4. This was opposed to the vapour phase phenomenon that was used by previous researchers.

All research up until this point focused on the oxidation process of micron sized aluminium, however as stated above, smaller particles means changing material properties. It has been reported that small sized metal particles (< 100 nm) are highly reactive and decreasing primary particle size increases reactivity [28]. Furthermore, making use of this high reactivity, it has been investigated that adding aluminium nanoparticles to propellants increases the propellant burning rate by a factor of 5-10 [22]. This has interested other researchers to investigate the oxidation of nanoparticle aluminium to better try to understand this process. Rai *et al.* [29, 30] wrote papers on understanding the process of aluminium nanoparticle oxidation, where they looked at the oxidation process from a mechanistic point of view. With previous data and new experiments they concluded that the oxidation proceeds in two regimes. They stated that at temperatures below the melting point of aluminium, the oxidation is limited by the diffusion of oxygen through the aluminium oxide shell. At higher temperatures this is described by the diffusion of both aluminium and oxygen, which may be enhanced by rupture and thinning of the oxide shell. The measurements and modelling of this process was for particles with a size bigger than 40nm. The research showed that temperatures of 400 °C were needed to fully oxidize the particles [30]. However, the particles used in this thesis are of the primary particle

6
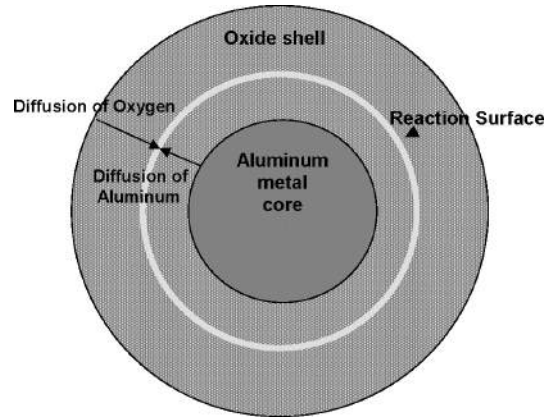
Figure 2.4: Core-shell model of aluminium nanoparticle oxidation, taken from Trunov *et al.* [3].

size of ±5nm and in this size regime no previous research has yet been done.

A.W. van Vugt [2] did not do significant research in the oxidation behaviour of aluminium nanoparticles, but reported that an interesting phenomenon was observed when aluminium was deposited on PVA nanofibers. It was observed that the aluminium nanoparticles oxidize rapidly and something much like a runaway reaction takes place on the fibers. During this process it looks like the aluminium nanoparticles react with the oxygen in air and sinter together to form a dense strucuture of aluminium oxide. When combining aluminium nanoparticles with gold nanoparticles it is hinted that the same phenomenon occurs and due to this sintering the gold nanoparticles submerge under a thin layer of aluminium oxide [2].

2.2.2 Titanium nanoparticle oxidation

As stated above, certain nanoparticles tend to react rather rapidly when exposed to oxygen and titanium is one of these materials. Titanium nanoparticle oxidation has not been researched often in the past and much is therefore unknown about the oxidation process on a nanoscale. Eventhough titanium nanoparticles have not (yet) been investigated in much detail, studies on the combustion and oxidation of microsize particles can be found [31, 32]. Some of this research focuses on the synthesis of titanium dioxide nanoparticles via combustion of microsize titanium, other research has focused on the addition of titanium to solid propellants (just like aluminium nanoparticle combustion research) [32]. The main goals of these studies were therefore not the oxidation mechanism of titanium particles, but using the oxidation process as a way of achieving other goals.

However an interesting phenomenon that was observed in several studies (and should be taken into account in this research) is the formation of titanium nitrogen bonds when a mixture of nitrogen and oxygen is used as the reactive gas [32]. As for the oxidation mechanism, one can state that the same "core-shell" model that is used for aluminium nanoparticles could possibly also be applicable for titanium nanoparticles. Thus when making smaller particles, further into the nanosize regime, rapid oxidation of these titanium nanoparticles is expected to occur.

2.3   Diffusion limited aggregation

The particles that are produced in the spark discharge process need to be deposited on the backbone of nanofibers that is produced by electrospinning. The nanoparticles are carried by the transporting gas flow to the fibers where they deposit on these fibers. This deposition process is thought to be influenced by four different mechanisms: Brownian motion, electrostatic forces, impaction and interception. In previous research it was investigated what the main force behind the deposition mechanism was and it was shown that deposition and aggregation of the particles was limited by Brownian motion only [2].

Diffusion limited aggregation (DLA) is a phenomenon that was first described in the early 1980's by Witten and Sander [33] and can be explained as a process where particles undergo a random walk due to Brownian motion and cluster together to form larger agglomerates. Brownian motion in this case refers to the random motion of a particle due to collisions with molecules in a liquid or a gas. Branch-like structures that are observed when simulating an aggregation process limited by diffusion, are often referred to as Brownian trees. Any system where diffusion is the primary means of particle transport can be described by DLA.

In the case of this research it is not only the clustering of the nanoparticles to one another that is important, but also the clustering and adhesion of the nanoparticles to the nanofiber backbone. One can assume that the deposition of the particles on the surface of the polymer is comparable to the deposition of particles on a flat surface, since the polymer diameter is a factor 40 larger than the mean primary particle size ($\pm$5nm). DLA computer simulation has made its entrance in the late 1980's, when (home) computers were able to quickly calculate the Brownian motion of particles in a fluid. The models that were developed over the years have been optimized and with the use of new numerical analysis software like MATLAB and Python, it has become increasingly easier to simulate three dimensional DLA systems that closely resemble real systems. In appendix H a MATLAB simulation of the nanoparticle deposition process and the structure growth on the polymer fiber is given.

2.4   Fractal dimension

A concept that is closely related to diffusion limited aggregation and more specifically brownian trees, is the concept of fractal dimensions. Fractal dimensions can be defined and used in various ways, but in the light of this research the most relevant manner of using fractal dimension is to use it as a measure of the space filling capacity of a (fractal) structure [34]. The fractal dimension tells in this case how a fractal structure scales differently from the space it is embedded in and thus tells us a lot about the porosity of a fractal structure [35]. The concept of porosity is especially interesting in this research, because a high porosity means high surface area with respect to the volume, e.g. a property of a good catalyst.

The concept of fractal dimensions has a lot to do with an atypical view on scaling and dimension. In traditional geometry a line has a dimension of 1, a square a dimension of 2 and a cube a dimension of 3. If one looks at scaling in a traditional way, measuring a line first with stick of length L and then with a smaller stick that is 1/2 L, will give for the smaller stick a total length of the line that is 2 times as many sticks long as with the first stick. This also holds for two and three dimensions as one can see in figure 2.5 (a).

The traditional view on scaling, as in the example above, can be mathematically explained by a general scaling rule given below in equation 2.1. In this equation, N stands for the number

(a) Example of the traditional view on fractal dimension

(b) First four iterations of a Koch snowflake
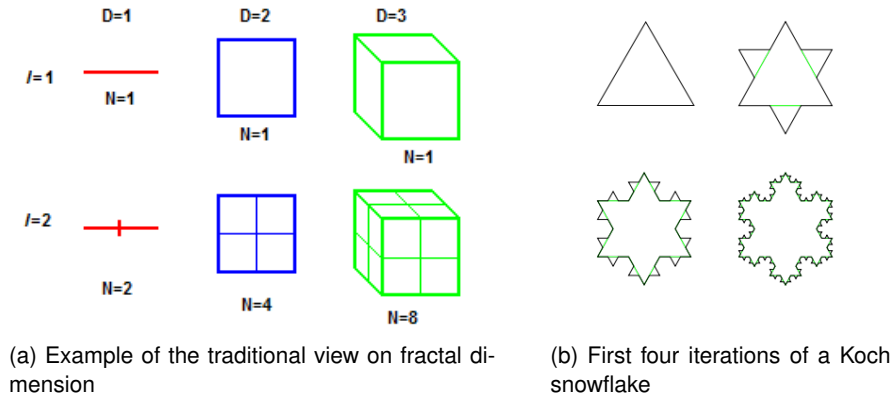
Figure 2.5: Examples of fractal dimensions

of new sticks (2 in the example), ε is the scaling factor (1/2 in the example; $1/I$ in figure 2.5 (a)) and D is the fractal dimension.

$$N \propto \varepsilon^{-D} \tag{2.1}$$

In the traditional view the concept of fractal dimensions comes rather intuitively and in the example above the fractal dimension of the line is 1; for a square $D = 2$ and for a cube $D = 3$. This same rule applies to fractal geometry, however this feels less intuitively; for example a line measured with one stick of lenght L measured in new sticks with length 1/3 L needs instead of three, four times as many scaled sticks. This can be visionilized by the Koch curve and snowflake, designed by the swedish mathematician Helge von Koch [36], as shown in figure 2.5 (b). In this case N will be 4, ε will be 1/3 and D can be found by substitution of N an ε in equation 2.1. This gives for D the value of 1.2619, wich is the approximate fractal dimension of the Koch Snowflake.

Intuitively, fractal dimensions are already hard to understand for ordered iterations like in the Koch snowflake. On top of that in real life systems these iterations are less ordered and even harder to understand, but to have an indication about the porosity of artificially synhesized structures an estimate needs to be made about the fractal dimension of these systems. One of these estimation models is the Minkowski-Bouligand dimension, also known as the box-counting dimension. To imagine this, one can have a look at figure 2.6. The box-counting dimension of a fractal, in this case the coast of Great Britain, can be calculated by counting the amount of boxes that are needed to cover the coast of Great Britain and see how this number changes as the grid (the size of the boxes) becomes smaller. This can be done by applying a box-counting algorithm to the fractal that needs investigation.

The example of the coast of Great Britain is an example of a fractal in a two-dimensional space, however the same method of box-counting holds for fractals in a three-dimensional space. Therfore this method of determining the fractal dimension can be used for fractals created by diffusion limited aggregation; the fractals created in this thesis research. Generally a fractal created in a diffusion limited aggregation system has a fractal dimension of 2.5 [37].

Interesting results have come from recent research on the fractal dimension of 3-dimensional DLA systems. It was observed in simulations of diffusion limited aggregation systems that the porosity (and with this the fractal dimension) varies within a fractal deposit [38]. The authors stated that the build-up of a fractal, characterized by plotting the packaging fraction as a func-
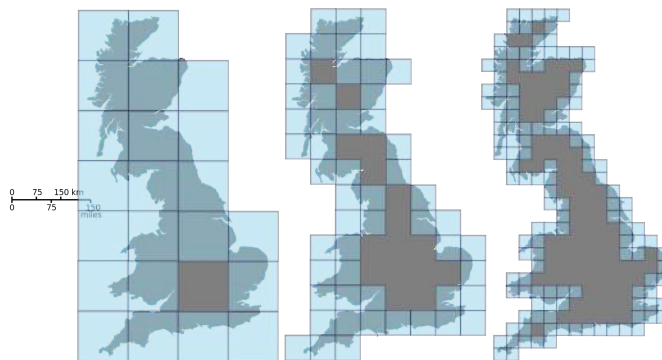
Figure 2.6: Box-counting of the coast of Great Britain

tion of the film thickness, could be described in three regimes. The first region, typically for low amounts of particle deposition, is a region where the packing fraction begins at its maximum value (relatively low porosity) and quickly decays to a constant value. In the second region, the packing fraction stays at a relative constant value and is unaltered after more particle deposition. Finally in the third region, with a subsequent deposition of new particles the film is still growing and this results in a decay of packaging fraction to zero.

Previous research [39–41] above reported that the scaling relation holds valid along the porous film's thickness. The recent research however suggests otherwise, stating that the scaling only applies to the first and third region [38]. After a sufficient number of deposits, the porosity becomes constant with the film thickness and in this second region (which occupies the majority of thicker films) it was found that the porosity of the fractal was solely dependent on the variables particle inertia, advection, and thermal motion. These variables were expressed in two dimensionless parameters; the diffusive Knudsen number Kn_D and χ_F; the ratio of translational kinetic energy to the thermal energy. By changing these two parameters various porosities can be made, independent of the roughness of the substrate the fractal is build upon. This indicates that in situ changing of these parameters could yield various different fractals with different porosities and therefore different properties.

The above findings are of particular interest in the current research since a combination of change in porosity (by varying the above parameters) and a change in deposited nanoparticles (by varying spark electrodes) could yield an endless amount of new catalytic materials, where not only changes in catalytic material within one film can be made but also changes in physical properties within the same film is a possibility.

2.5 Catalytic activity of gold nanoparticles on TiO$_2$ and Al$_2$O$_3$

Various research has been done on the catalytic effect of both aluminia and titania and the effect that gold nanoparticles on top of these structures have on the catalytical properties. This section will therefore describe in more detail the interesting catalytical properties of both aluminia and titania nanostructures with gold nanoparticles.

10

2.5.1 Catalytic activity of TiO$_2$ with gold nanoparticles

As will be discussed in section 2.7, the main use of TiO$_2$ is in the field of photocatalysis. Most research of the last decades on the material TiO$_2$ has thus been on (improving) the photocatalytic effect and many review articles have been written [42–45]. When looking at the interesting properties of the proposed electrospinning and spark discharge combination to synthesize the catalysts, one of the obvious advantages is the production of nanostructures. Various research has shown that the use of nanomaterials (nanotubes, nanorods, spherical nanoparticles etc.) as a photocatalyst is much more effective than using bulk TiO$_2$ [46]. It is proposed that when the particle diameter falls below 10 nm, the particles behave quantummechanically as a particle in a box [47] and it increases the bandgap of the material and shift the band edges to yield a higher redox potential [48].

Other interesting findings are the reported improvements in the photocatalytic effect when noble metals are added to the TiO$_2$ photocatalyst [43, 49–55]. Because the fermi levels of noble metals are generally lower than that of TiO$_2$, the excited electrons can be transferred to these quantumdots while the holes in the valance band stay in the TiO$_2$. Hereby the fast recombination of electrons and holes in the TiO$_2$ matrix is prohibited resulting in more efficient seperation of holes and electrons and thus increasing efficiency [42]. Combining this with the fact that nanomaterials show exceptional catalytic properties, research has shown that noble metal particles with a diameter of <20nm form composites that show exceptional catalytic behaviour [56]. Increases in efficiency of up to 30% are reported when adding gold, with respect to plain TiO$_2$ photocatalysts [57, 58]. Other research shows that only a few Au particles (0.5 wt% Au-TiO$_2$, with small Au particles) in electronic contact with the titania structure are enough to enable the charge transfer to the solute, thus acting as an efficient electron relay [59, 60].

2.5.2 Catalytic activity of Al$_2$O$_3$ with gold nanoparticles

When looking at the catalytic activity of Al$_2$O$_3$, it is clear that there are much less applications known for Al$_2$O$_3$ as a catalyst [61]. However, the importance of alumina as a catalyst support is still widely recognized, especially since it is used as a support in the Claus process of hydrodesulfurization, hydrodenitrogenation and hydrocracking reactions [62, 63]. With Al$_2$O$_3$ as a support it is of great relevance that the pore size of the alumina can be controlled, since optimal pore size varies with the desired reaction [64, 65]. Various kinds of metals can be used in different kinds of catalysts with an alumina (nano)structure as its backbone and especially gold turns out to be an interesting material to use as a catalyst in the nanosize regime of <10nm for various reactions [66–68]. However these structures were often made in a multi-step production process in contrast to the possibilities that this research provides.

By using a combination of electrospinning and spark discharge to synthesize the catalyst or catalyst supports, it is possible to generate alumina structures with controlled pore sizes. Next to that the spark discharge process provides the opportunity to make alumina supports for virtually any kind of metal. Therefore this research can provide a clean and flexible way to synthesize gold catalysts with an alumina catalyst support.

2.6 Annealing of TiO$_2$

As is discussed in the previous section, the photocatalytic activity of titanium dioxide is of great importance. Research has shown that the crystalline phase of the titanium dioxide has a big

impact on the photocatalytic activity of the material [69].

Titanium dioxide is the only naturally occurring oxide of titanium and exists in three polymorphs; anatase, rutile and brookite, of which rutile is the stable phase. However, anatase and brookite are both metastable and can easily be created by a process that is called annealing. Annealing is a heat treatment procedure that alters the physical properties of the material. Heating the material to above its glass transition temperature, so it is possible for the atoms to rearrange their structures, and subsequently cool the material to "freeze" the atoms in their new state induces the changes in physical properties.

In the case of titanium dioxide, the three different crystalline phases can be generated by heating the material at different temperatures. When increasing the temperature at which the material is being annealed, anatase is the first crystalline structure to be formed. Transformation from amorphous titanium dioxide to anatase is reported to occur at temperatures as low as 250 °C [70]. The transformation from anatase to rutile has also been widely studied. Reported transition temperatures vary in range between 400 °C and 1200 °C, because of the use of different methods of determining the transition temperatures, processing methods and raw materials [71–73]. Brookite is harder to synthesize and so is seldom studied.

The different phases can be distinguished from each other by performing X-ray diffraction (XRD) measurements. An explanation of the technique behind XRD is given in appendix B. When analyzing the anatase to rutile transition, the difference in peak intensity of the most prominent signal of both materials is used to determine the weight fractions of anatase and rutile.

Annealing of titanium dioxide is an essential part of creating highly active titanium dioxide photocatalysts, since amorphous material exhibits little to no photocatalytic activity [69]. When it comes to crystalline titanium dioxide, the anatase phase is considered superior to rutile when it comes to photocatalytic performance. Having said this, some papers have shown that a mixed-phase photocatalyst consisting of anatase and rutile have enhanced photoactivity relative to single-phase titania [70].

2.7 Applications of Au-TiO$_2$ catalysts and Au-Al$_2$O$_3$

Apart from the improvements in the field of science, research (preferably) also needs to have a direct link to modern day applications. This section is on the promising applications of the synthesized Au-TiO$_2$ catalysts, when produced correctly.

Titanium is the ninth-most abundant material on earth, making up for approximately 0.6 mass% of the earth its crust [74], which makes the material relatively cheap. Next to that the oxidized form of titanium, titanium dioxide, is a popular photocatalyst and has been investigated thoroughly over the past decades since these properties were first observed by Akira Fujishima in 1972 [75]. This gives also to the most obvious and promising application of this thesis research, the use of titanium dioxide nanoparticles on PVA nanofibers to produce photocatalysts with enhanced photochemical properties. As discussed in section 2.5, the photocatalytic activity of titanium nanoparticles rises when small amounts of gold nanodots are placed on top of the surface of the titanium dioxide. The combination of nanofibers and deposition of primary nanoparticles on top of these fibers creates a rather favourable surface to volume ratio. Electrospun polymer fibers and nanoparticle deposition via the spark discharge mechanism could therefore be a promising method to create these kind of photocatalysts.

As discussed in section 2.5.2, aluminium oxide in itself has no catalytic properties, but it is used in various reactions as a catalyst support. The biggest and most known process where

aluminium oxide is used as a catalyst support is the Claus process of hydrodesulfurization, hydrodenitrogenation and hydrocracking reactions [62, 63]. This alone makes it worthwile investigating the possibilities of synthesizing a fractal-like aluminium oxide nanostructure that in the future could serve as a support in this process.

Chapter 3

Experimental, Results and Discussion

This chapter will discuss the experimental part of this thesis research. First in section 3.1 the formation of a fractal-like metal oxide nanostructure by the proposed method of gas phase oxidation is investigated. In section 3.2 the method is tested on its applicability to synthesize fractal-like metal oxide nanostructures with metal nanoparticles on the surface. In these experiments polymer fibers act as the backbone for these structures. Section 3.3 discusses the photocatalytic activity of the, by the proposed method, produced titanium dioxide and mixed titanium dioxide-gold samples. In the last section, section 3.4 an analysis was done on the annealing of the titanium dioxide structures.

3.1 Metal-oxide nanoparticle structures on PVA fibers

The research of this report has had its focus on the synthesis of a TiO_2 fractal-like nanostructure on top of PVA nanofibers. To prepare these samples a one spark chamber set-up was used, a detailed overview of the set-up is given in appendix A.2. To determine if the hypothesis of a runaway reaction occurring when the nanoparticles are oxidized in air while on the fibers is true, this process was investigated.

3.1.1 Titanium nanoparticle oxidation after deposition

To investigate the deposition of titanium nanoparticles on polymer nanofibers and their oxidative behaviour, solid titanium electrodes were used in the spark discharge process and oxidized after deposition on the polymer nanofibers.

Sample preparation

These samples were prepared with the settings that are described in appendix A.1 and appendix A.2. The schematic overview of the process is given in appendix A, where in this case two titanium electrodes were used to produce the desired titanium dioxide nanostructures. The optimal spark settings were calibrated on 7 mA, 1.0 kV (corresponding to a breakdown voltage of approximately 1 kV), 6 nF and a deposition time of 25 minutes to ensure enough material was deposited on the fibers. After deposition of the titanium nanoparticles, the metal mashes
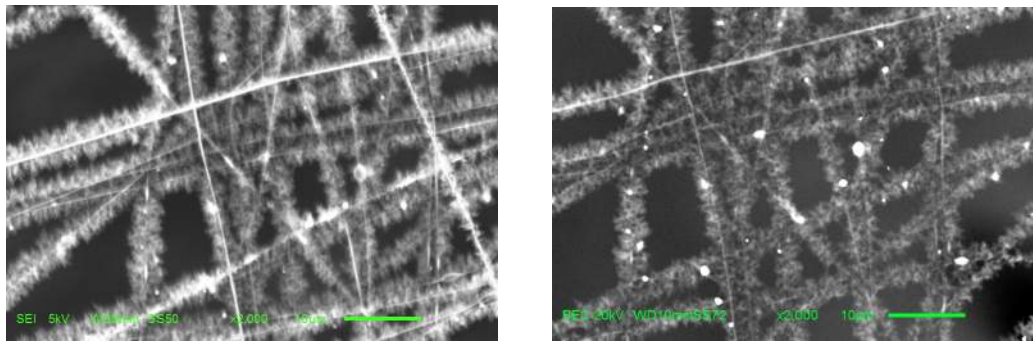
(a) SEM analysis with secondary electrons of ti-
tanium dioxide microstructures

(b) SEM analysis with backscattered electrons of
titanium dioxide microstructures

Figure 3.1: SEM images of fractal-like titanium dioxide nanostructures

were then taken out of the sample holder and instantaneously exposed to air. More details on
the gas flows and set-up can be found in appendix A.2.

Results

Scanning electron microscopy (SEM) was used to analyze the titanium dioxide microstructures.
Figure 3.1 shows the SEM pictures that provide a global overview of the structures on a mi-
croscopic scale. From these pictures it can be seen that fractal-like microscopic structures are
formed. To examine the fractal-like structures on a nanoscale, transmission electron microscopy
(TEM) can be used. An overview of these analysis techniques is given in appendix B. TEM was
not performed on these samples, since it will not add much value in achieving the main goal of
this thesis research. As SEM was easily accessible it was chosen to use SEM to get a quanti-
tative insight in the amount of material that is being deposited with the used settings, as basis
for the spark settings that could be used in subsequent experiments. TEM was not used for this
specific sample as it was less easily accessible and analogies can be made between this sam-
ple and the sample described in section 3.2.1. It was therefore chosen only to test the sample
produced in section 3.2.1 with TEM. These images show that no fractal-like *nano*structures are
formed with this synthesis method; oxidation of the nanoparticles after deposition. The images
show a dense, melted structure. No change in color from the initial state was observed when
taking the sample out of the sample holder. Exposing the sample to the outside air also did not
induce a color change of the sample.

Discussion

Looking at the images in figure 3.1, one can see that there are fractal-like *micro*structures
formed on a the polymer nanofibers. The images shown are of the same area of the sample,
one with secondary electron analysis and one with backscattered electrons. The observation
of fractal-like micromaterial is in line with the findings of both van Vugt [2] and Saur [21] who,
on a microscale, observed branch-like structures when depositing aluminium nanoparticles on
nanofibers. One can see on the SEM images in figure 3.1 that on a microscale the titanium is
evenly distributed on the polymer fibers, forming a branch like structure with the polymer fiber
as a base.

15

As mentioned before, analogies can be made between this experiment and the experiment discussed in section 3.2.1 when it comes to the oxidizing behaviour of the titanium nanoparticles. In this picture, figure 3.5, it can be seen that the titanium nanostructures clearly show a melting-like behaviour when the particles are oxidized, with a high oxygen concentration (20% of oxygen), after they are deposited on the polymer nanofibers. In line with these findings it can be argued that the structures in this section are indeed oxidized after they were exposed to air and due to the rapid oxidation they are not fractal-like at a nanoscale.

Conclusion

To conclude on this section, it can be argued that oxidizing titanium nanoparticles, after they are deposited on the nanofibers, is not desirable to achieve the main research objective. In line with the literature [31, 32], titanium nanoparticles tend to oxidize quite rapidly and the same oxidizing phenomenon observed for aluminium can be observed for the titanium nanoparticles [2]. Fractal-like structures on a microscale are observed, but in light of this research these structures are undesirable. Eventhough these *micro*structures can be of use for other applications, in this research the goal is to produce fractal-like structures on a *nano*scale.

3.1.2 Titanium nanoparticle oxidation before deposition

Since oxidation of the nanoparticles after deposition proved to be unsuitable to produce fractal-like nanostructures on the polymer fibers, oxidation of the metal needs to occur in the gas phase before deposition. This section will focus on synthesizing fractal-like nanostructures of pure titanium dioxide, oxidized in the gas phase before deposition. These samples needed to be synthesized under the same conditions as for the mixed nanoparticle structures on polymer fibers to be able to compare photocatalytic effect and other properties of the different samples.

Sample preparation

The preparation of this sample is a little different from the previous section. In the preparation of these samples two variations occur with respect to the oxidation of the titanium nanoparticles after deposition. First this sample is made as if it were a two spark chamber set-up as described in appendix A.3; maintaining the flows described in this appendix, but only running one spark with the settings of 7 mA, 1 kV (breakdown voltage of approximately 1 kV) and 6 nF. The second change with respect to the previous section, which is also explained in appendix A.3, is the addition of a second gas stream consisting of an argon/oxygen mixture to oxidize the titanium nanoparticles in the gas phase before deposition. The gas flows of the various streams are mentioned in this appendix and the nanoparticle production time is 30 minutes (the variation of production time with the previous discussed samples is due to the needed similarity with the experiment discussed in section 3.2.3).

Results

To examine these samples, various kinds of analysis techniques were used. First, a light gray color was observed when taking the sample out of the sample holder. To examine the microscopic and nanoscale structures, electron microscopy was used on the samples. Both TEM and SEM measurements have been performed, these images are shown in figure 3.2. One

(a) TEM image of titanium dioxide nanostructures

(b) TEM image of titanium dioxide nanostructures

(c) SEM image of titanium dioxide microstructures
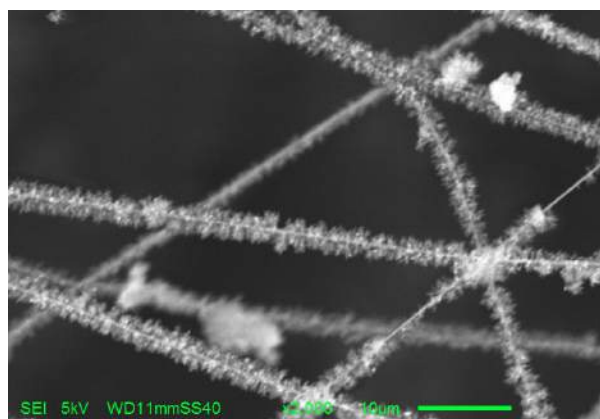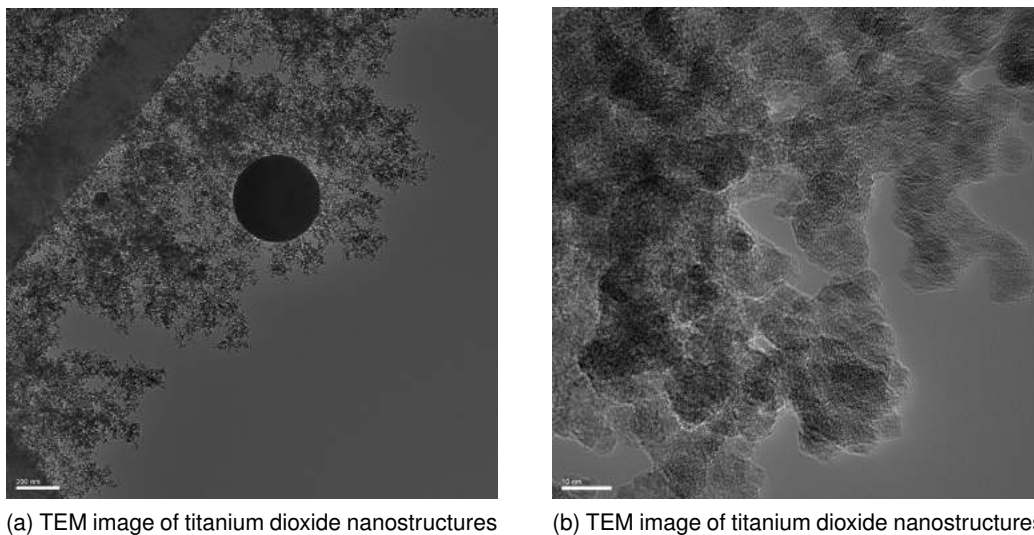
Figure 3.2: Micrograph images of titanium dioxide nanostructures, oxidized after deposition

can see in these figures that fractal-like structures are formed both on a microscopic and on a nanoscale.

To examine the extent of oxidation, energy dispersive x-ray diffraction (EDX) was performed on the sample. EDX was performed to check whether the particles had fully oxidized and not core-shell particle had formed. This was done on both the large sphere shown in figure 3.2 (b) and another on the separate nanostructures build up of smaller particles shown in the figure (a). The figure shows that the smaller particles are completely oxidized and the larger particle oxidizes partly. This can be concluded from the respective counts of oxygen and titanium. For the small particle EDX these are relatively equal, while for the large particle a high titanium count with respect to oxygen can be observed.

To examine the catalytic effect of the sample, a propane oxidation reaction was performed on the sample, these tests show that a conversion of 154 ppm of CO_2 is formed in 30 minutes. Because these results are quite interesting they will be discussed in more detail in a separate section; section 3.3. More elaboration on the propane oxidation reaction can be found in appendix B.3.

(a) EDX measurement on titanium dioxide nanostructure

(b) EDX measurement on large titanium dioxide sphere
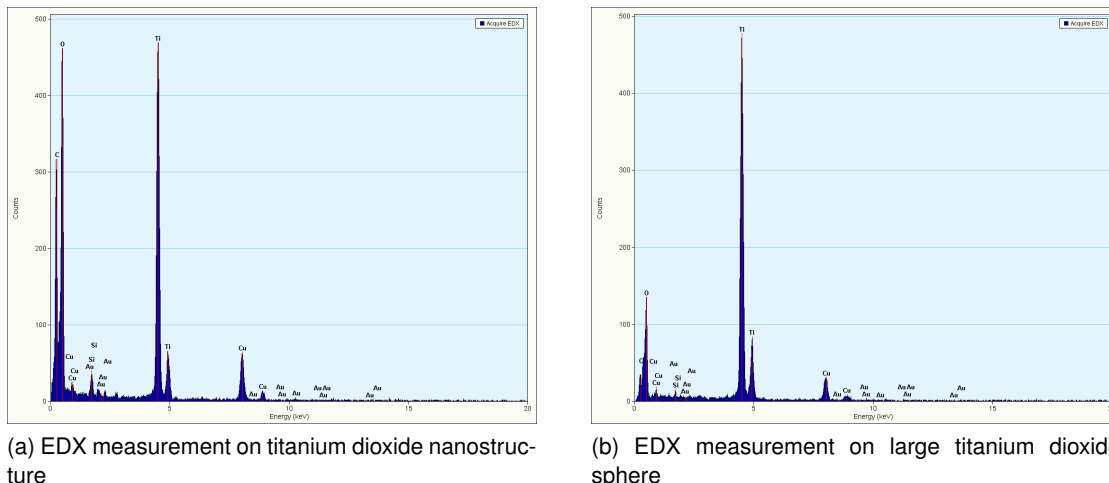
Figure 3.3: Energy dispersive x-ray diffraction (EDX) graphs of the titanium dioxide fractal-like nanostructure and large titanium sphere

Discussion

The images shown in figure 3.2 give a promising result when it comes to the creation of fractal-like nanostructures. Small primary particles of approximately 5-10 nm are produced in the spark discharge process and an average fiber diameter of 200-400 nm can be observed. As expected the small nanoparticles form fractal-like structures on a micro- and nanoscale on top of the polymer fibers, as shown in the figure 3.2. It can be stated that the structures are fractal-like, as the deposition process in these experiments is similar to the deposition process that was used in the simulations by Hogan *et. al.* [38]. From the TEM images it looks as if the structures consist of primary particles sticking together, not forming sintered necks between the particles, indicating that the particles are oxidized before forming larger agglomerates. Arguably, these same TEM images show that the titanium dioxide nanoparticles produced are amorphous, something that is line with the findings of the photocatalytic experiments done on the titanium dioxide samples, described in section 3.3. However, previous research has shown that nanoparticles produced by spark discharge is usually in a crystalline phase [1].

Next to these results it can be concluded from the EDX measurements that the small particles have been oxidized due to the high oxygen count in the EDX measurements, shown in figure 3.3 (a). Figure 3.3 (b) shows the EDX measurements of the larger titanium dioxide sphere. It can be observed that the oxygen particle count is a lot lower with respect to the titanium particle count for the large titanium dioxide sphere than for the EDX measurements on the small particle nanostructures in figure 3.3 (a). It can thus be concluded that the larger particles only partly oxidize and form a protective titanium dioxide shell that is less penetrable for both oxygen and titanium atoms [3]. Nice to notice here is thus that, in line with the literature, the assumption of a core-shell model for the oxidation of titanium particles is correct [3].

The larger titanium sphere most likely originates from the fact that during the spark discharge process some of the produced particles recirculate in the spark chamber and therefore grow to larger sizes than the particles that exit the spark chamber almost immediately after being generated by the spark. The EDX results also show some peaks that indicate the presence of gold and copper. The presence of gold can be explained by the fact that the set-up was not entirely clean and some gold nanoparticles were still in the set-up after previous use. The

signal for copper can be explained by the fact that the TEM-grids are made of copper.

Conclusion

It can be concluded from this section that with the designed spark method, of in the gas phase oxidation of the metal nanoparticle before deposition, fractal-like titanium dioxide nano- and microstructures can be produced, arguably consisting of amorphous material. The primary particles of approximately 5-10 nm are oxidized in the gas phase and form a fractal-like nanostructure on top of the produced polymer fibers of approximately 200-400 nm in diameter. In the oxidation of titanium nanoparticles, it can be assumed that a core-shell model is a suitable way of depicting the oxidation process of the nanoparticles. Both the SEM- and TEM images and the EDX graphs support these conclusions.

3.1.3 Aluminium nanoparticle oxidation before deposition

Van Vugt [2] observed an interesting phenomenon when trying to produce fractal-like nanostructures with aluminium and gold. It was observed that when the aluminium nanoparticles are exposed to the oxygen in air, the particles oxidize rapidly, creating 'melted' structures. This reduces not only the total surface area of the structures, but it was observed that the created alumina encapsulates the gold nanoparticles. To determine if one can control this oxidation process, the experiment discussed in this was done. Apart from this it also provided an insight in the applicability of the proposed method of in the gas phase oxidation of nanoparticles. The experiment in this chapter resembles the experiment discussed in section 3.1.2, however in this case not titanium, but aluminium electrodes were used.

Sample preparation

These samples were prepared in the same manner as the samples in section 3.1.2, but with different electrodes. In this case solid aluminium electrodes were used to generate aluminium nanoparticles. The aluminium nanoparticle sample was made as if it were a two spark chamber set-up as described in appendix A.3; maintaining the flows described in this appendix, but only running one spark with the settings of 7 mA, 1 kV (breakdown voltage of approximately 1 kV) and 6nF. After the spark chamber, a second gas stream is added, consisting of an argon/oxygen mixture to oxidize the aluminium nanoparticles before deposition. The gas flows of the various streams are mentioned in this appendix and the nanoparticle production time is 30 minutes. The choice for this spark time is based on earlier findings by van Vugt [2].

Results

Taking the samples out of the sample holder did not induce a color change on the sample; the sample could be indicated as light gray. The micro and nanostructures of the sample were analyzed by SEM and TEM; these images are shown in 3.4. The images show highly fractal-like structures on both a microscopic level and a nanoscale. No further analysis was done to characterize these samples, as the main objective of these experiments can be extracted from these figures.
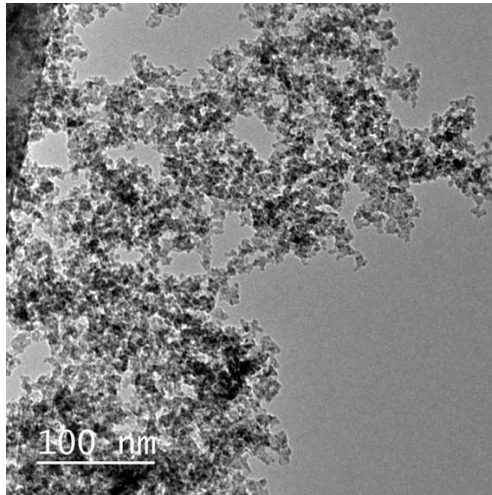
(a) TEM image of aluminium oxide nanostructures
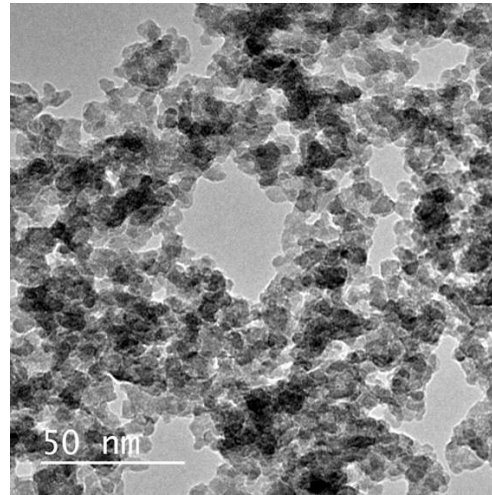
(b) TEM image of aluminium oxide nanostructures
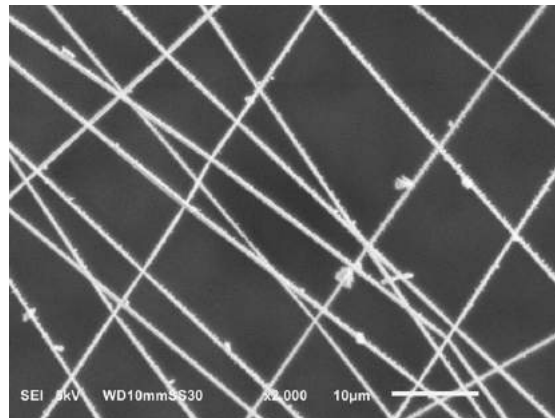
(c) SEM image of aluminium oxide microstructures

Figure 3.4: Micrograph images of aluminium oxide nanostructures, oxidized after deposition

Discussion

The images shown in figure 3.4 show fractal-like aluminium oxide micro- and nanostructures, in contrast to the findings of van Vugt [2]. The difference with the production method of van Vugt was the point of oxidation of the aluminium nanoparticles, which in the case of this research was before deposition on the polymer nanofibers. The images (a) and (b) clearly show, just as for the titanium dioxide nanostructures in section 3.1.2, fractal-like nanostructures consisting of primary particles of approximately 5-10 nm. Just as observed in section 3.1.2, no necks are formed between the primary particles.

Although no EDX was performed on these samples, it can be argued from previous research that the aluminium nanoparticles oxidize in the same way as the titanium nanoparticles; according to a core-shell oxidation mechanism [3]. In previous research it was observed that the aluminium nanoparticles sinter together when they are oxidized, which makes the fractal-like nanostructures collaps [2]. Since figure 3.4 shows fractal-like structures on a nanoscale, and the only change in production method is the place of oxidation, the oxidation of the nanoparti-

cles must have occured before deposition.

Conclusion

From the images shown above, it can be concluded that fractal-like aluminium oxide micro- and nanostructures can be made with the proposed method of the gas phase oxidation of the, by spark discharge produced, aluminium nanoparticles. Fractal-like nanostructures of aluminium oxide consisting of primary particles of 5-10 nm in diameter on top of polymer fibers of 200-400 nm in diameter are produced. Oxidation of the primary particles has occured in the gas phase before deposition on the polymer fibers.

3.1.4   Conclusion section 3.1

To conclude this section, a fair assumption can be made that the proposed experimental design is suitable for producing the desired metal oxide nanostructures on top of polymer nanofibers. Metal nanoparticles are produced by spark discharge with a size of 5-10 nm. Polymer nanofibers, functioning as supports for deposition of the metal nanoparticles, are produced by electrospinning and have a diameter ranging from 200 to 500 nm. Oxidation of the metal nanoparticles occurs in the gas phase when a second stream, consisting of an argon/oxygen mixture, is introduced. This method ensures the formation of fractal-like structures on a micro- and nanoscale, where the formation of the fractal-like structures is in line with the literature on diffusion limited aggregation [33]. In line with previous research, the same fractal-like nanostructures cannot be made when the metal particles are oxidized after deposition on the, by electrospinning produced, polymer nanofibers [2].

The produced titanium dioxide nanoparticles seem to be amorphous, which is in contrast to previous works in the field of spark discharge generation of nanoparticles [1]. This result would indicate that the oxidation of the crystalline metal nanoparticles causes a change in crystallinity to the amorphous phase.

Strong evidence is found to assume that a core-shell oxidation model is a feasible way of depicting the oxidation mechanism of the metal nanoparticles. According to the literature, rapid oxidation occurs when the nanoparticles come in contact with oxygen [3]. From EDX measurements it can be assumed that the produced small metal nanoparticles are fully oxidized before deposition. Larger metal particles only oxidize partly due to the formation of a, for metal and oxygen atoms, difficult to penetrate metal oxide layer.

The proposed method has shown to yield good results for a few different metal oxides, indicating the possibility of the method to be applicable for other metal oxides.

3.2   Mixed nanoparticle structures on PVA fibers

This section will focus on the synthesis of mixed fractal-like metal oxide nanostructures with gold nanoparticles on top of electrospun PVA fibers. As explained in section 2.5, mixtures of metal nanoparticles or metal nanoparticles on metal oxides could be favourable structures in catalyst production. The electrodes used in this process are made of gold and titanium and various mass ratios are investigated. Two different set-ups were used in these measurements, which can be found in appendix A. As is explained in chapter 2, various metal nanoparticles tend to oxidize rapidly when exposed to air. One of the hypotheses of van Vugt was that the rapid oxidation causes gold nanoparticles to submerge in the formed metal oxide support. To examine this,

various configurations of electrodes and spark chambers are used and the following set ups will be discussed in more detail:

- Gold and titanium electrodes in one spark chamber

- Gold and titanium electrodes in separate spark chambers

- Gold and aluminium electrodes in separate spark chambers

As for the first experiment (gold and titanium electrodes in one spark chamber), two variations have been investigated: 1. oxidation of the titanium nanoparticles *after* deposition on the fibers and 2. oxidation of the titanium nanoparticles *before* deposition on the fibers.

3.2.1 Gold and titanium electrodes in one spark chamber (1)

As a first explorative experiment, based on the research of van Vugt [2], the spark discharge process was done with two different electrodes. As is explained in the literature study of this thesis it is expected that by ablating two different electrodes, a gaseous mixture of the two separate materials is formed. This experiment explores the fractal-like nanostructures of gold and titanium dioxide made on the fibers with oxidation of the titanium nanoparticles *after* deposition on the fibers.

Sample preparation

The samples were made in the same way as described in section 3.1 and explained in appendix A.1 and appendix A.2. The electrodes used were a titanium electrode and gold electrode. The optimal spark settings used in this experiment were a voltage of 0.75 kV (corresponding to a breakdown voltage of 1.5 kV), a current of 5 mA, a capacitance of 4 nF and a production time of 25 minutes. The particles were then deposited on the nanofibers and oxidized in air after they were taken out of the sample holder.

Results

When the samples were taken out of the sample holder a dark gray colour was observed; no colour change was observed by the eye after exposion to air. The analysis of these samples was done in various ways. First a SEM image was made to analyze the microstructure of the deposited particles, depicted in 3.5 (a) and (b). From these pictures a relatively open microstructure can be observed. The EDX function of the scanning electron microscope was used to determine the relative atom percentages in the observed sample, which is depicted in table 3.1. An atomic ratio of approximately 1:10 for Ti:Au can be observed. The SEM does not give an insight in the nanoscale morphology of the synthesized sample, therefore TEM was used to examine the nanostructure of the sample. TEM images of the sample are shown in figure 3.5 (c) and (d). The TEM image shows that there is no fractal-like nanostructure formed.

Discussion

Looking at the images in figure 3.5, a few things catch the eye. First of all, figures 3.5 (a) and (b) show that on a microscale, metal oxide structures have formed on the polymer nanofibers. One could indicate these structures as flocks or clouds of metal oxide nanoparticle clusters.
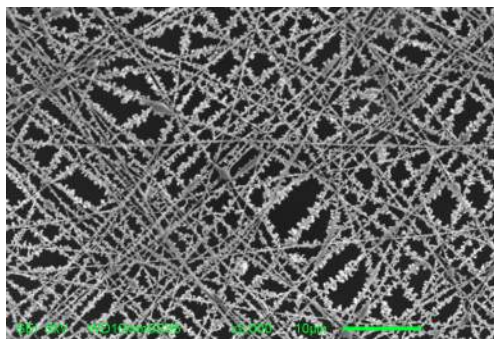
(a) SEM image of mixed titanium dioxide-gold microstructures
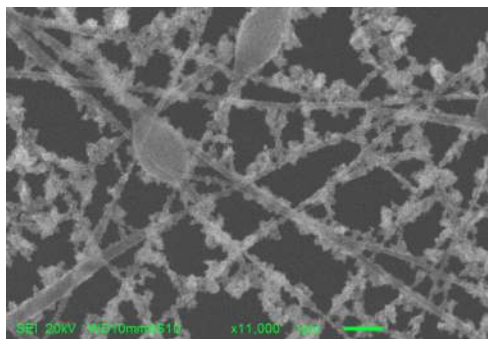
(b) SEM image of mixed titanium dioxide-gold microstructures
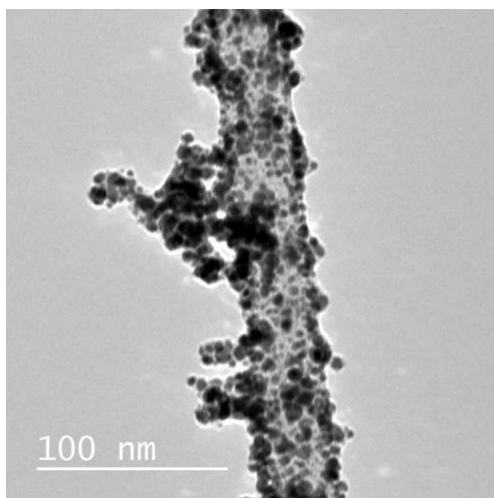
(c) TEM image of mixed titanium dioxide-gold nanostructures
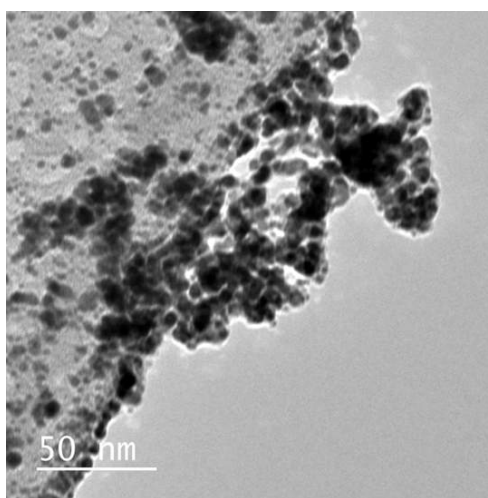
(d) TEM image of mixed titanium dioxide-gold nanostructures

Figure 3.5: Micrograph images of mixed titanium dioxide-gold nanostructures, single spark set-up, oxidized after deposition

However the figures 3.5 (c) and (d) show that on a nanoscale the structures are not fractal-like. Using the findings of section 3.1.2, it can be assumed that the produced titanium dioxide is in an amorphous phase. It seems as thought the structures, build up of titanium dioxide particles ranging in diamter of 5 to 10 nm and gold nanoparticles of 2 to 5 nm, have melted and collapsed.

This is in line with the previously found results by van Vugt, who showed that when a mixture of aluminium and gold nanoparticles is deposited on polymer nanofibers and these structures were oxidized after deposition, the structures collapsed and the produced gold nanoparticles were embedded in the aluminium oxide [2]. This might be explained by the fact that the oxidation process is an exothermic process and because of the rapid oxidation the sample might heat-up locally, causing the structures to melt and collapse. Combining these results with (and projecting them on) the results from the experiment in section 3.1.1, it can be stated that the oxidation of titanium occurs rapidly when exposed to a high oxygen concentration. This is in line with previous research on the oxidation of titanium nanoparticles [31, 32].

As figures 3.5 (c) and (d) show, dark gray and light gray particles can be distinguished. It is assumed that the darker particles are gold nanoparticles and the light gray particles are

titanium dioxide nanoparticles. The difference in colour between the two is related to the extent that a particle blocks the electron beam of the TEM. Gold is a relatively large atom (especially in comparison to titanium) and will therefore block the electron beam more than the titanium particles [76].

The images shown in this report do not conclusively yield the same results as van Vugt; it looks as if there are also gold particles on the surface of the material. This might be explained by the fact that the atom ratio for the two experiments was different [2]. In the case of this experiment, more gold was deposited than aluminium. One could argue that if enough gold is added, some of the gold nanoparticles are bound to end up on the surface of the aluminium oxide structures. No further investigation into this phenomenon is done however, since the mixture does in any case not yield the desired fractal-like structures on a nanoscale.

The atom ratio between gold and titanium also needs some discussion. A single spark set-up, with one gold and one titanium electrode, was used. Previous research showed that, when using a pair of different electrodes, the cathode is always ablated more strongly [1]. In this set-up the gold electrode was the cathode, explaining the higher concentration of gold in the sample.

Figure 3.5 (b) also shows some 'beads' in the microstructures. These beads occur during the electrospinning process and are related to the viscosity of the polymer solution. A too low viscosity results in the formation of these beads [77]. Even though not many of these beads can be observed, it might indicate that the polymer solution needs further optimisation. However this was outside of the scope of this thesis project.

Conclusion

A few conclusions can be drawn on the basis of the previous results and discussion. First of all, SEM and TEM images show that on a microscale flock like structures are formed on the polymer nanofibers, however on a nanoscale the samples do not appear to be fractal-like. In line with previous research it is expected that the oxidation of the titanium nanoparticles causes the fractal-like structures to collapse [2]. The formed structures consist of primary particles roughly ranging in diameter between 5 to 10 nm (for the titanium dioxide nanoparticles) and 2 to 5 nm (for the gold nanoparticles) and can be assumed to be amorphous. The particles can be distinguished from each other by their contrast in the TEM figures. The dark gray parts resemble gold nanoparticles and the lighter gray areas resemble the titanium dioxide nanoparticles.

Table 3.1: Atomic percentage of mixed titanium dioxide-gold nanostructures, single spark set-up, oxidized after deposition (EDX). * Background signal of the metal mash support

Chemical formula	Atom%
C	83.41
O	12.82
Ti	0.13
Cr	0.63
Fe	1.92
Au	1.09
Total	100.00

It is observed from EDX measurements, that the atomic ratio between titanium and gold is 1:10 respectively. It therefore can be concluded that a mixture of titanium dioxide and gold structures can be made on top of polymer nanofibers by combining spark discharge and electrospinning. The found atomic ratio results in a high loading of gold. The high gold loading can be explained by the fact that the gold electrode was the cathode in the experiment, which ablates the most in each spark system [1]. In contrast to previous research it cannot conclusively be said that all the gold is embedded in a titanium dioxide matrix, completely covering the gold nanoparticles [2]. This is most probably due to the high gold loading.

Formation of beads in the electrospinning of polymer fibers is observed, concluding that the parameters in the electrospinning process need more optimisation with respect to (especially, but not only) the viscosity of the polymer solution [77].

3.2.2 Gold and titanium electrodes in one spark chamber (2)

This section also describes experiments done with gold and titanium electrodes in one spark chamber, however the difference with the previous section is the place of oxidation of the titanium nanoparticles in the synthesis process. This section describes the experiment which explored the synthesized fractal-like nanostructures when titanium nanoparticles are oxidized *before* deposition on the fibers.

Sample preparation

The samples were made in the same way as described in section 3.1 and explained in appendix A.1 and appendix A.2. The electrodes used were a titanium electrode and gold electrode. The optimal spark settings used in this experiment were a voltage of 0.75 kV (breakdown voltage of approximately 1.5 kV), a current of 5 mA and capacitance of 4 nF and a production time of 25 minutes was used. The particles were then oxidized in the gas phase before deposition on the nanofibers. The samples were then taken out of the sample holder.

Results

When the sample was taken out of the sample holder a dark gray colour could be observed. No change in colour was observed after being exposed to air. This would indicate that the titanium nanoparticles had oxidized before exposition to air. For this experiment SEM was performed on the sample to investigate the fractal-like structure on a microscale, as shown in figures 3.6 (a) and (b). A relatively open and spiky structure can be observed in these images. The sample was prepared in the same way as in section 3.2.1, the titanium to gold atomic ratio therefore was approximately 1:10 respectively, as depicted in table 3.1. Images taken with the transmission electron microscope are given in figures 3.6 (c) and (d). The TEM image shows a fractal-like structure on a nanoscale.

Discussion

Just like the previous experiments, SEM analysis shows fractal-like structures on a microscale. However if one compares the result of figure 3.6 (a) and (b) to the results from section 3.2.1, oxidation after deposition, more spiky structures are formed, instead of the flocky structures found in figure 3.5. This indicates that already on microscale there is an influence of the moment of oxidation in the process on the fractal-like structures that are formed. Zooming in on the structures
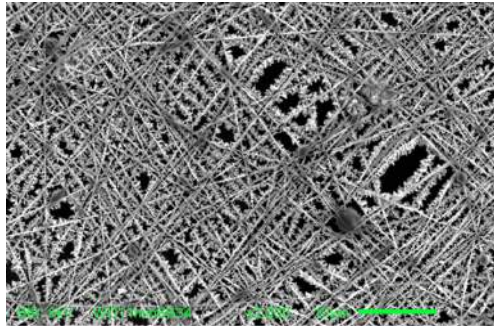
(a) SEM image of mixed titanium dioxide-gold microstructure
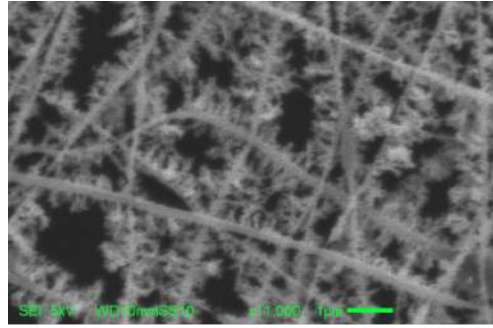
(b) SEM image of mixed titanium dioxide-gold microstructure
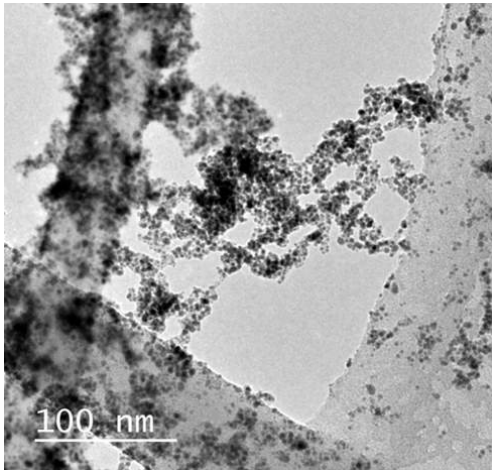
(c) TEM image of mixed titanium dioxide-gold nanostructure
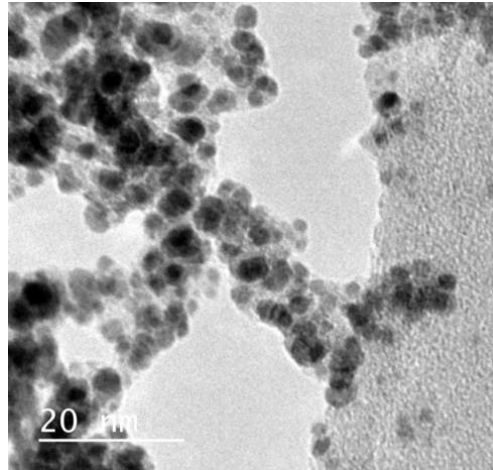
(d) TEM image of mixed titanium dioxide-gold nanostructure

Figure 3.6: Micrograph images of mixed titanium dioxide-gold nanostructures, single spark set-up, oxidized before deposition

confirms this assumption, yielding a fractal-like structure on a nanoscale, as depicted in figures 3.5 (c) and (d). Structures formed of titanium dioxide nanoparticles (approximately 5-10 nm in diameter) and gold nanoparticles (approximately 2-5 nm in diameter) can be observed. The structures clearly consist of primary particles agglomerated together, but not forming sintered necks between them.

Comparing these results to the results in section 3.2.1, fractal-like structures are formed also on a nanoscale, consisting of a mixture of titanium dioxide and gold nanoparticles. Therefore the oxidation of titanium nanoparticles occurs most likely in the gas phase, before deposition on the polymer nanofibers. This is also in line with the results found in sections 3.1.2 and 3.1.3, where fractal-like nanostructures of titanium dioxide and aluminium oxide were formed by oxidation of the respective metal nanoparticles in the gas phase before deposition on polymer nanofibers. From these same experiments it can be assumed that the formed titanium dioxide matrix consists of an amorphous phase.

It can be seen that gold nanoparticles appear on the surface of the fractal-like nanostructures, this could be due to two reasons. The first would be that fractal-like structures of titanium dioxide are formed and gold particles are deposited on these structures. However since the

26

titanium nanoparticles are mixed with the gold nanoparticles in the gas phase *before* oxidation, a case can be made that most of the gold is still embedded in a titanium dioxide matrix. Only due to the large gold loading some gold particles are placed on the surface of the titanium dioxide matrix. In general embedded particles could of course have an application, but gold is an expensive material and as the embedded particles do not have any catalytic effect it is in light of this research undesirable the have embedded particles. The high gold loading can be explained by the fact that the cathode was again the gold electrode and the anode was made of titanium.

Conclusion

To sum up, the following conclusions can be drawn. The method of in the gas phase oxidation of metal nanoparticles is also applicable to a system with one spark with two different electrodes. A single spark system with a gold and a titanium electrode, where oxidation of the titanium nanoparticles occurs before deposition, yields fractal-like nanostructures of a mixture of titanium dioxide and gold (particles of 5-10 nm and 2-5 nm in diameter respectively). With respect to the experiment in section 3.2.2 a change in material, induced by the place of oxidation, can even be seen in the difference in structure on a microscale (more spiky structures).

It looks as if there are gold nanoparticles on the surface of the produced fractal-like nanostructures. For this observation two explanations can be given. The first explanation is the fact that the titanium oxidizes and gold nanoparticles are placed on these structures. However, the gold nanoparticles are mixed with the titanium nanoparticles even *before* oxidation of these nanoparticles occurs, so another explanation seems more likely. Since the atomic ratio between the two materials is approximately 1:10 (titanium to gold) some gold particles are bound to end up on the surface of the material. Changing the atomic ratio between the two materials could give a definitive answer on this question.

3.2.3 Gold and titanium electrodes in separate spark chambers

To overcome the problem of an unfavourable titanium to gold ratio when producing the mixed nanoparticles on PVA nanofibers in one spark chamber, a dual spark system was proposed. In this section the experiments will be discussed where gold and titanium are produced in separate spark chambers. The previous experiments have shown that oxidation *after* deposition does not provide the desired results, therefore it was chosen only to experiment with titanium nanoparticle oxidation in the gas phase *before* deposition on the fibers. On top of that it is suggested that mixing of the gold and titanium nanoparticles before oxidation might be unfavourable in the process, thus mixing occurs after oxidation of the titanium nanoparticles.

Sample preparation

The experimental approach is similar to the various experiments described in the previous sections. However in this case two separate spark chambers, placed in parallel, are used to produce the nanoparticles. The process used in this experiment, a set-up with two parallel spark chambers, is described in Appendix A.3.

The electrodes used were two solid titanium electrodes in one spark chamber and two hollow gold electrodes in the other spark chamber. Various experiments have been done to determine the influence of different spark settings on the ratio of titanium to gold, as is described in Appendix A.4. The spark settings that were ultimately used were a current of 7 mA, voltage
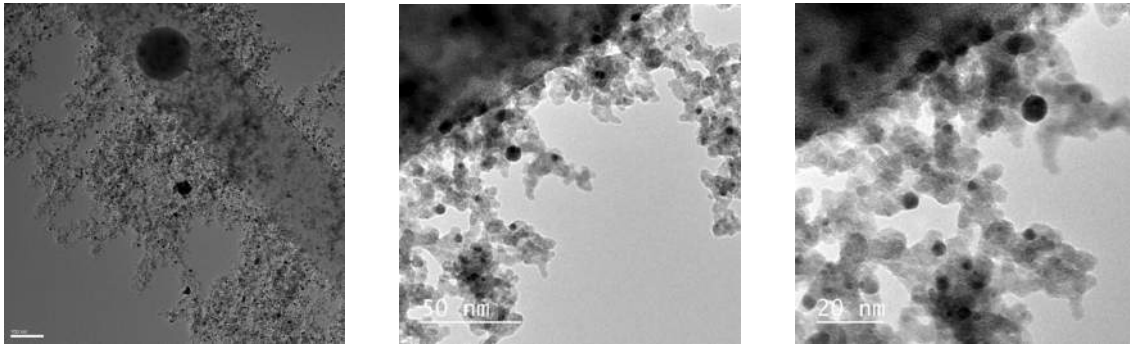
Figure 3.7: TEM images of mixed titanium dioxide-gold nanostructures, dual spark set-up, oxidized before deposition

of 1 kV (breakdown voltage of 1 kV) and a capacitance of 6 nF for the spark chamber for production of titanium nanoparticles and 1 mA and 0.35 kV (breakdown voltage of 0.7 kV) in the chamber where gold nanoparticles were produced. Experiments where the time was varied determined that a deposition time of 30 minutes was optimal with respect to amount of deposited material. Titanium nanoparticles were oxidized before being mixed with the gold nanoparticles, after which the mixture was deposited on PVA nanofibers. After the above mentioned run time of deposition, the samples were taken out of the sample holder.

Results

When the samples were taken out of the sample holder, a light gray colour could be observed. Indicating the presence of gold nanoparticles on the titanium dioxide. To analyze these samples, various tools have been used. Both SEM and (high resolution) TEM is used to visualize the nanoscopic structures. HR-TEM was used to get an even better insight into the nanoscale structures that are formed. The images produced by these analysis techniques are shown in figures 3.7 and 3.10. The figures show that highly porous titanium dioxide nanostructures are formed, with gold particles on the surface. The EDX function on the SEM was used to determine the titanium to gold ratio, a detailed overview of the various ratios that can be achieved by varying the spark settings can be found in Appendix A.4. The samples tested here had an approximate titanium to gold ratio of 13:1.

To analyze the catalytic properties of the samples propane oxidation under the influence of light was done. As these structures should have an increased performance, due to the fractal-like structure on a nanoscale and the addition of gold nanoparticles, this sample was examined on its catalytic properties. It was found that for a sample made under the above described conditions, the oxidation of propane to CO_2 was 80 ppm in 30 minutes of reaction time. The settings of the oxidation reactor and a broader overview of these measurements are described in appendix B.3. To examine the extent of oxidation of the titanium nanoparticles, EDX measurements were also performed by the TEM. These results are shown in figure 3.8. Full oxidation of the titanium nanoparticles can be assumed according to this graph.

Elemental mapping was done to determine the dispersity of the gold nanoparticles, figure 3.9 shows that the gold nanoparticles are well dispersed in the titanium dioxide matrix on a nanoscale.

Discussion

If one takes a look at the images produced by TEM, figure 3.7, one can see that highly porous structures on a nanoscale are produced; consisting of a mixture of titanium dioxide nanoparticles (5-10 nm in diameter) and gold nanoparticles (2-5 nm in diameter). The titanium to gold ratio was 13:1, yielding highly dispersed gold particles that are, according to figure 3.7, on the surface of the titanium dioxide matrix. As discussed in section 3.2.1, the gold nanoparticles can be distinguished from the matrix by the colour in the TEM images. Dark gray particles are gold, light gray particles can be indicated as titanium dioxide nanoparticles. The SEM images in figure 3.10 also show a more porous and fractal-like structure on a microscale than the images in section 3.2.2.

A fair assumption can be made that this matrix indeed consists of (arguably amorphous) titanium dioxide, as the production method was the same as in section 3.1.2. The titanium nanoparticles are oxidized in the gas phase before they are mixed with gold nanoparticles and subsequently deposited on the polymer nanofibers. This also points out one of the differences between this experiment and the experiment done in section 3.2.2, where oxidation of the titanium nanoparticles occured *after* mixing with gold nanoparticles (which happens right after the spark). In comparison to the fractal-like nanostructures created in section 3.2.2, the structures produced by the dual spark method in this experiment are even more porous.

This result could be explained in two ways. One explanation is the difference in atomic ratio between the two experiments. In the first experiment, in section 3.2.2, the structures consisted of more gold atoms than titanium atoms. Since gold nanoparticles behave almost liquid like, the high gold loading could have had an effect on the overall porosity of the structures. In the second experiment, this was changed and a real fractal-like titanium nanostructure was created with only a few gold particles placed throughout the material. If one compares the results of this experiment with the structures produced in section 3.1.2, it can be seen that (except for the addition of gold nanoparticles) the fractals are similar; indicating that this might be the correct explanation.

Another explanation could be that, because the gold and titanium nanoparticles are mixed before oxidation of the titanium particles, the gold is still incorporated in a titanium dioxide matrix which would change the morphology of the created fractal-like nanostructures. This could be investigated in more detail by changing the electrode configuration (anode and cathode switch) to change the atomic ratio between the gold and titanium, as is already discussed in section 3.2.2.
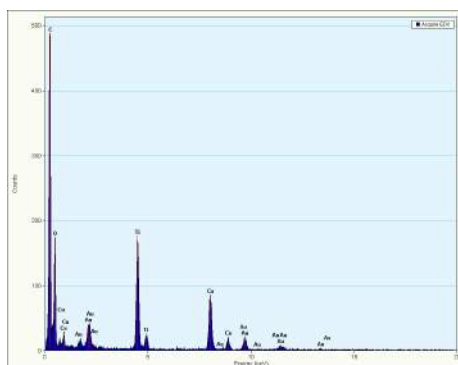
Figure 3.8: Energy dispersive x-ray diffraction (EDX) graphs of the mixed titanium dioxide - gold fractal-like nanostructure
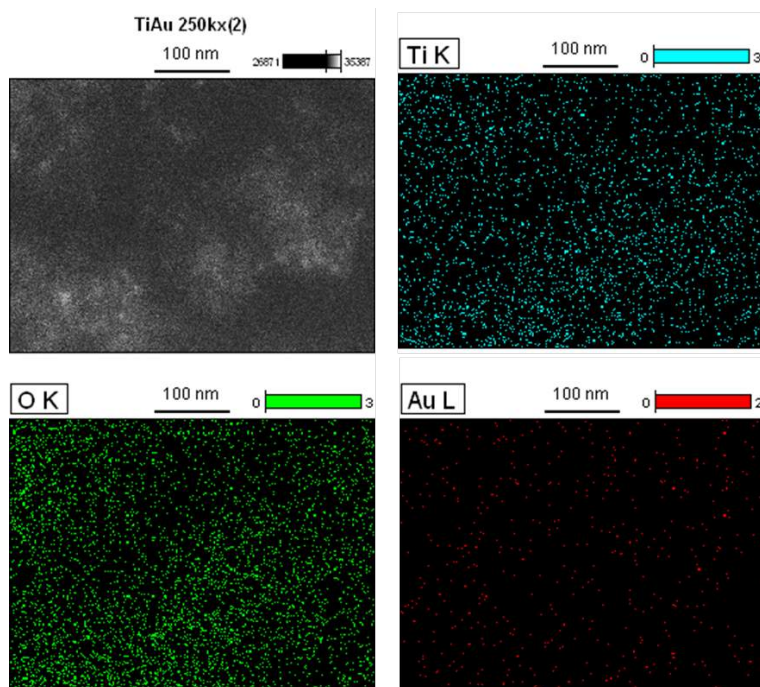
Figure 3.9: Elemental map of the mixed titanium dioxide-gold nanostructures

Elemental mapping was done to determine the dispersity of the gold particles throughout the titanium dioxide matrix. It can be seen from figure 3.9 that the gold nanoparticles are well distributed throughout the matrix on a nanoscale, indicating that the gold does not form larger agglomerates and are more or less immobilized on the surface of the titanium dioxide.

A discussion on the lower catalytic effect of these samples in comparison to the samples produced in section 3.1.2 can be found in section 3.3, where the photocatalytic measurements on the different samples is discussed in more detail.

Conclusion

To conclude this section, it can be stated that a dual spark set-up with gas phase oxidation of titanium nanoparticles is suitable to produce highly porous titanium dioxide nanostructures with gold nanoparticles on the surface of the titanium dioxide nanostructure. It can be stated that the formed titanium dioxide nanoparticles have an amorphous crystalline structure. The titanium dioxide primary particles have a diameter in the range of approximately 5 to 10 nm, the produced gold nanoparticles are in the range of approximately 2 to 5 nm.

In comparison to earlier experiments, the fractals produced were more porous than the sample produced in section 3.2.2 and exhibited the same fractal-like structure as the structures produced by the experiment in section 3.1.2. These two observations combined would suggest that a high gold loading, in combination with the moment of oxidation of the titanium nanoparticles (before or after mixing with gold) induces the differences with section 3.2.2.

The elemental mapping of the fractal-like mixed titanium dioxide-gold nanostructures suggest that the gold nanoparticles are well distributed throughout the whole structure on a nanoscale.
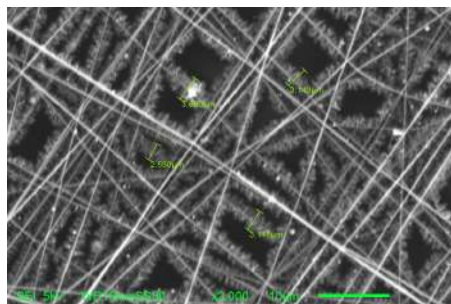
(a) SEM overview image of the fractal-like mixed titanium dioxide-gold nanostructures
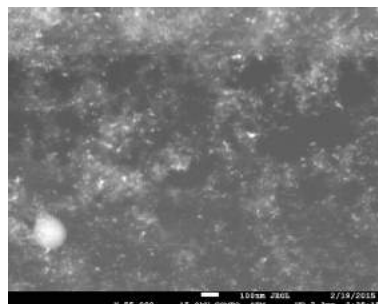
(b) High Resolution SEM image of the fractal-like mixed titanium dioxide-gold nanostructures

Figure 3.10: (High Resolution) SEM images of mixed titanium dioxide-gold nanostructures, dual spark set-up, oxidized before deposition

3.2.4 Gold and aluminium electrodes in separate spark chambers

The previous section (section 3.2.3) showed that a dual spark system is suitable for producing a titanium dioxide nanoparticle matrix with gold nanoparticles on the surface. As this report aims on providing a general method to produce fractal-like supports of metal oxides, more experiments were done on the applicability of this method to other metals. In the light of previous research by van Vugt it was chosen to test the method with aluminium oxide and gold nanoparticles.

Sample preparation

The samples prepared for these experiment were prepared in exactly the same way as the samples prepared in section 3.2.3, but the titanium electrodes were switched to aluminium electrodes. The process used in this experiment, a set-up with two parallel spark chambers, is described in Appendix A.3.

The main objective of these experiments was not to produce a sample consisting of fractal-like aluminium oxide nanostructures with gold nanoparticles on the surface. It is therefore that not an exact aluminium to gold atomic ratio is needed; the most prominent requirement is a high aluminium to gold atomic ratio. This way one could get around the same problem that occured in section 3.2.2, where a too high gold loading might have lead to gold particles on the surface by accident. Since the spark settings in section 3.2.3 provided a high atom ratio between titanium and gold it was chosen to hold onto the spark settings used in section 3.2.3. The spark settings used were a current of 7 mA and voltage of 1 kV for the spark chamber for production of aluminium nanoparticles and 1 mA and 0.35 kV in the chamber where gold nanoparticles were produced. The optimal run time of the process turned out to be 30 minutes [2]. Aluminium nanoparticles were oxidized before being mixed with the gold nanoparticles, after which the mixture was deposited on PVA nanofibers. After the above mentioned run time of deposition, the samples were taken out of the sample holder.
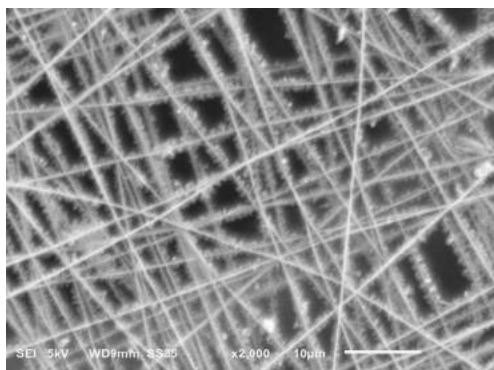
(a) SEM image of mixed aluminium oxide-gold microstructure
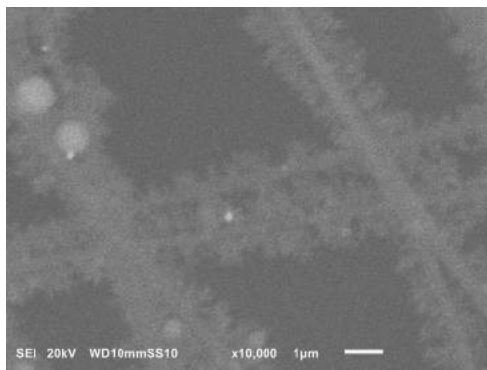
(b) SEM image of mixed aluminium oxide-gold microstructure
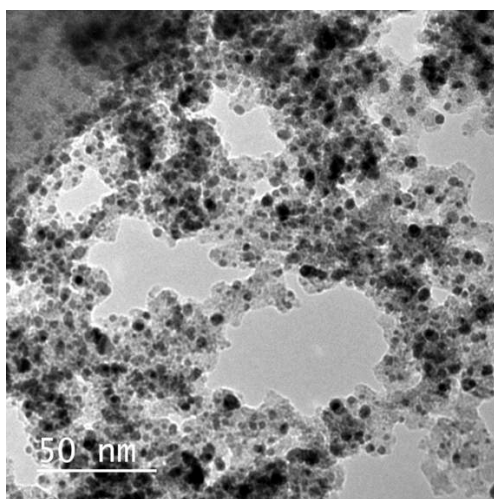
(c) TEM image of mixed aluminium oxide-gold nanostructure
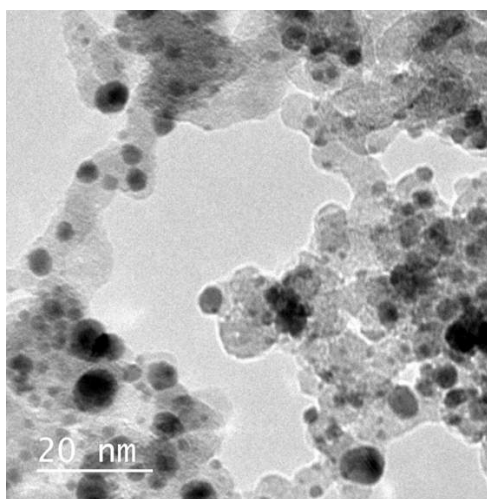
(d) TEM image of mixed aluminium oxide-gold nanostructure

Figure 3.11: Micrograph images of mixed aluminium oxide-gold nanostructures, dual spark set-up, oxidized before deposition

Results

When the samples were taken out of the sample holder a light gray colour could be observed. The samples were analyzed by both TEM and SEM, these micrographs are given in figure 3.11. The figures show that the particles are well distributed along the polymer fiber, generating fractal-like nanostructures of aluminium oxide. The images also show that gold nanoparticles are on the surface of the aluminium oxide.

Discussion

It can be seen from the images in figure 3.11 that fractal-like structures of aluminium oxide and gold is formed. These structures consist of a fractal-like base structure of aluminium oxide particles (approximately between 5 and 10 nm) and gold nanoparticles on top of the surface (approximately 2 to 5 nm). We assume here that aluminium oxide is formed, since previous research had shown that if the particles are exposed to oxygen they tend to oxidize rapidly

[2, 3, 29, 30]. Next to that, the experiments done in the previous sections show that oxidation of titanium nanoparticles fully oxidize in the gas phase, providing a basis to assume the same happens to aluminium nanoparticles.

In line with the previous experiments from section 3.1.3 fractal-like structures are formed on a nanoscale. Next to that, the structures look like the fractals made in section 3.2.3, indicating that the method of a dual spark set-up, with oxidation of the (in this case aluminium) nanoparticles before mixing and deposition on polymer nanofibers, is applicable to a wider range of metals.

No measurements on the crystallinity of the material are done, since the experiment was mainly done to prove the wide applicability of the system and not to synthesize a specific material. However one can argue that due to the oxidation of the aluminium nanoparticles, the crystalline state is amorphous. This phenomenon was observed for titanium nanoparticles in section 3.1.2 and because of the similarity in structure and the oxidative behaviour of the different nanoparticles a case can be made to assume that the aluminium oxide matrix is amorphous. To make sure that this is indeed the case, measurements should be done on the crystallinity of the material.

Conclusion

It can be concluded that fractal-like aluminium oxide nanostructures can be made with gold nanoparticles on its surface. Aluminium oxide nanoparticles of approximately 5-10 nm in diamater agglomerate together on polymer nanofibers to form a fractal-like nanostructure on which gold nanoparticles of approximately 2-5 nm are placed. The same sort of fractal-like structures are formed for this experiment as for the experiments in sections 3.2.3 and 3.1.3, in which the differences were the fractal-like base material (titanium in section 3.2.3) and the addition of gold (with respect to pure aluminium oxide in section 3.1.3).

The method of a dual spark system with oxidation of aluminium nanoparticles before mixing with gold nanoparticles and deposition on polymer nanofibers seems to work very well to produce the desired fractal-like structures. In combination with the findings in 3.2.3 it can be stated that the method is applicable to a wider range of metals, to yield the same kind of fractal-like metal oxide nanostructures with gold nanoparticles on the surface.

3.2.5 Gold and magnesium electrodes in separate spark chambers

The method of in the gas phase oxidation of metal nanoparticles has proven to work for both titanium and aluminium nanoparticles. To test the method validity for other nanoparticles, magnesium (whose nanoparticles readily oxidize when exposed to oxygen) was used as electrode material.

Sample preparation

The samples prepared for these experiment were prepared in exactly the same way as the samples prepared in section 3.2.3, but the titanium electrodes were switched to magnesium electrodes. The process used in this experiment, a set-up with two parallel spark chambers, is described in Appendix A.3.

Just as explained in section 3.2.4 the main objective of these experiments was to check whether fractal-like nanostructures are formed by the magnesium oxide and if the produced gold particles are on top of these nanostructures. Therefore the same spark settings were used
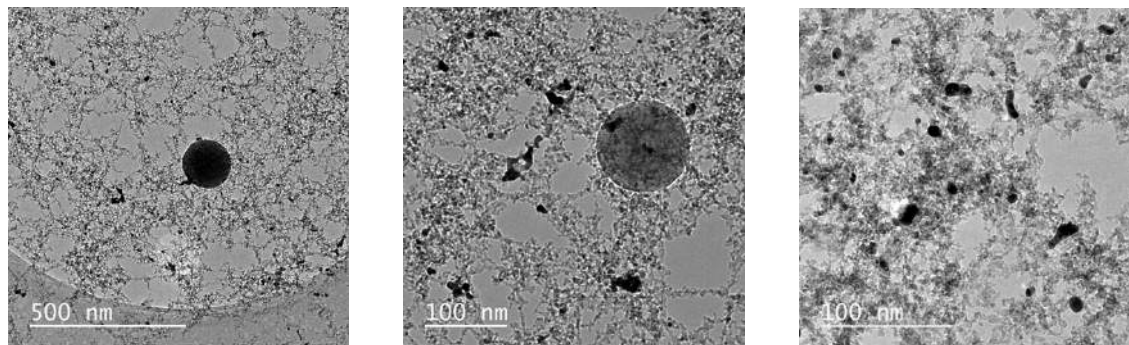
Figure 3.12: TEM images of mixed magnesium oxide-gold nanostructures, dual spark set-up, oxidized before deposition

as in sections 3.2.4 and 3.2.3, to ensure more magnesium nanoparticles were produced than gold nanoparticles.

Results

With TEM the nanostructures were analysed. The best images were taken from fractal-like structures deposited on the TEM-grid, figure 3.12 shows these micrographs. It can be seen that very open and fractal-like structures of, arguably, magnesium oxide are produced. The same micrograph shows that the gold nanoparticles are on the surface of the magnesium oxide matrix.

Discussion

Looking at the micrographs generated by transmission electron microscopy, it can be stated that with the proposed method of in the gas phase oxidation of the produced magnesium nanoparticles a fractal-like magnesium oxide nanostructure can be formed. Adding a second stream of gold nanoparticles, after the oxidation of magnesium, yields highly porous magnesium nanostructures with gold nanoparticles on the surface. This is in line with what is observed in the previous sections 3.2.3 and 3.2.4. This once again provides a basis to assume that the method is applicable to many other metals.

Conclusion

To conclude this section it can be stated that the proposed method is a useful tool to produce magnesium oxide nanostructures with gold nanoparticles on the surface. The section once again points out the possibilities that lie in the proposed method.

3.2.6 Platinum and magnesium electrodes in separate spark chambers

The previous sections proved that with the proposed method a fractal-like metal oxide matrix can be made with gold nanoparticles on the surface. To show the applicability to other metals, platinum electrodes were used instead of gold. The goal of this experiment was therefore to produce a magnesium oxide matrix with platinum nanoparticles on the surface.
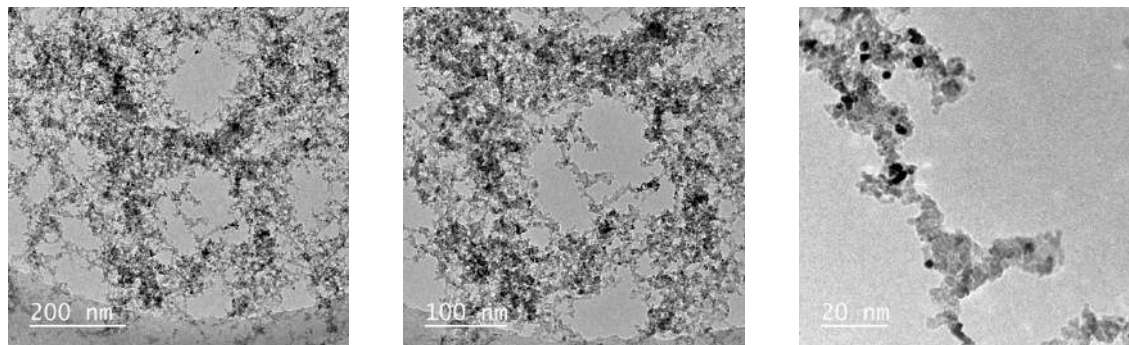
Figure 3.13: TEM images of mixed magnesium oxide-platinum nanostructures, dual spark set-up, oxidized before deposition

Sample preparation

The sample is prepared in the same manner as discussed in section 3.2.5, however the gold electrodes are replaced by electrodes made of platinum. The process used in this experiment, a set-up with two parallel spark chambers, is described in Appendix A.3.

The same spark settings were used as in section 3.2.5 to ensure the ratio of magnesium to platinum is sufficiently high. Creating a magnesium oxide framework for platinum nanoparticles and not the other way around.

Results

No observable colour change on the sample was noticed when the sample was taken out of the sample holder and exposed to air, indicating the magnesium was already oxidized. TEM was used to examine the nanostructure of the samples. Figure 3.13 shows the TEM images and it can be noticed that the structures are very porous and look fractal-like. Selected area diffraction SAD was performed on the sample to examine whether the samples were crystalline, these images are shown in figure 3.14. Information on SAD can be found in appendix B. It can be seen that a crystalline mixture is formed of both crystalline magnesium oxide and platinum.

Discussion

The images made by TEM show that the proposed method is also applicable for producing fractal metal oxides with nanoparticles on the surface other than gold. In this case platinum was used and it can be seen from figure 3.13 that the platinum nanoparticles are on top of the metal oxide matrix.

Table 3.2: XRD data of crystalline magnesium oxide, platinum and the mixed titanium dioxide-gold sample, annealed in-situ at 500 °C. Data from webmineral.com

D_1 (Å)	I_1 (%)	D_2 (Å)	I_2 (%)	D_3 (Å)	I_3 (%)	Mineral
2.106	100	1.489	52	1.216	12	Periclase (MgO)
2.265	100	1.962	53	1.183	33	Platinum
1.921	100	1.415	unknown	1.153	unknown	MgO-Pt sample
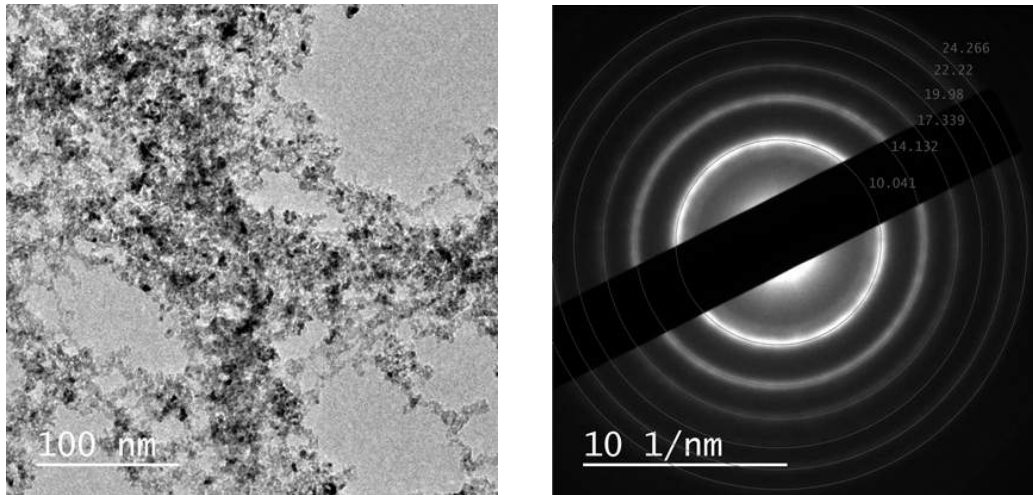
Figure 3.14: TEM image and corresponding SAD pattern of mixed magnesium oxide-platinum nanostructures

An interesting observation can be obtained from the SAD pattern, depicted in figure 3.14. It can be noticed that a clear crystalline material was made, which is in contrast to earlier findings in sections 3.1.2 and 3.2.3. Table 3.2 shows the specific d-spacing values for magnesium oxide, platinum (taken from literature) and those of the produced sample consisting of a mixture of platinum and magnesium oxide. If one should assign the peaks in the SAD pattern, one could argue that both crystalline platinum (in line with literature [1]) and crystalline magnesium oxide are formed. Especially the second observation, crystalline magnesium oxide, raises eyebrows. One should expect from the earlier observations in sections 3.1.2 and 3.2.3 that amorphous magnesium oxide is formed. This is however not the case and indicates that more research needs to be done on the oxidation of various nanoparticles. Magnesium is known to burn rather well and it might be that high local temperatures cause the particles to anneal due to the oxidation. That this is not observed for titanium nanoparticles might be because titanium oxidizes less easily.

Conclusion

This section once again underlines the flexibility of the proposed method. Fractal-like magnesium oxide nanostructures with platinum particles on the surface are produced. In contrast to earlier results these structures were highly crystalline, indicating that understanding the oxidation process might be of use when producing crystalline nanomaterials.

3.2.7 Conclusion section 3.2

From this section it can be concluded that a fractal-like nanostructure of a mixture of different metal nanoparticles can be made on top of polymer nanofibers. The results show that this can be done in either a one spark set-up with oxidation of the (to be oxidized) metal before deposition on polymer nanofibers or in a dual spark set-up where oxidation also occurs before deposition. This is a prerequisite of the set-up, since oxidation after deposition did not yield the fractal-like structures on a nanoscale.

Both set-ups show promising results when it comes down to the porosity of the structure on a nanoscale. However with respect to the mixing of the nanoparticles, the results show that the dual spark set-up is favourable over a single spark set-up. For one, the dual spark set-up makes it easier to control the amount of produced nanoparticles, making it easy to change the atomic ratio between the elements of the nanoparticles that are produced in the separate spark chambers. Next to that, the dual spark set-up gives conclusive evidence of gold nanoparticles on the surface of the metal oxide support, where oxidation of the metal (titanium or aluminium) takes place before mixing with the other metal nanoparticles (in this case gold). This is not conclusively shown by the single spark set-up, where mixing occurs before oxidation.

The fractal-like nanostructures in these experiments consisted of metal oxides (titanium and aluminium) with gold nanoparticles on the surface of the fractal. The diameter of the metal oxide nanoparticles ranged from 5 to 10 nm and the gold nanoparticles where in the range of 2 to 5 nm. The fractals exhibit the same structure as the fractals described in literature for a diffusion limited aggregation system [33]. Next to that, when produced in a dual spark set-up, with a low gold atomic percentage and oxidation before mixing and deposition, the fractals have the same structures as can be found in sections 3.1.2 and 3.1.3.

The last two sections focused on demonstrating the wide applicability of the method. It was shown that the method also produces fractal-like magnesium oxide nanostructures with gold nanoparticles on the surface. Next to that it was proven that other metal nanoparticles can be placed on the surface throughout the structure by switching gold with platinum; still obtaining the same results.

3.3 Photocatalytic measurements on TiO_2 and Au-TiO_2 samples

To measure the photocatalytic effect of the produced titanium dioxide and the mixed titanium dioxide-gold samples, some propane oxidation experiments were done with the help of Bindikt Fraters from the University of Twente. In these measurements, the formation of CO_2 was investigated when a gas with a small percentage of propane was transferred over the samples under irradiation of light. A comparison was made between the titanium dioxide, the mixed titanium dioxide-gold samples and a good performing reference sample yielding high conversions. The main idea of these measurements was to get a first estimate of the photocatalytic effect of the samples and if addition of gold nanoparticles would have an effect on the photocatalytic activity.

Sample preparation

Two samples were tested in the photocatalytic measurements; one with fractal-like titanium dioxide nanostructures and one sample with mixed titanium dioxide-gold nanostructures. These samples were prepared in the same was as discussed in sections 3.1.2 and 3.2.3 for the titanium dioxide and mixed nanostructures respectively. Making use of these preparation methods it can be assumed that the only difference between the samples is the addition of gold; the titanium dioxide amount on both samples was the same.

A reference sample was prepared by Bindikt Fraters; this sample consisted of a 2 micrometer thick coating with approximately 1 mg of titanium dioxide. The titanium dioxide had a crystalline structure that was 100% anatase. Samples produced with these properties had relative conversions between 1300-1400 ppm.

Results

Table 3.3 shows the different CO_2 conversions for the different samples. It can be seen that both the prepared samples by the proposed method perform less than the best performing reference sample of titanium dioxide. The fractal-like nanostructures with solely titanium dioxide had a relative conversion of 172.2 ppm. Next to that the measurements show that the samples prepared *with* gold perform less than the samples with only titanium dioxide. These mixed nanostructures had a relative conversion of 93.6 ppm.

Discussion

The most interesting result is that the nanostructures produced by the dual spark method with gas phase oxidation exhibit significantly lower photocatalytic activity than the best performing reference sample. A hypothesis to explain this phenomenon could be the fact that the titanium dioxide of the samples is not crystalline. The anatase phase is preferred over amorphous phase in the propane oxidation reaction, which would explain the lower catalytic effect. However there is still some catalytic activity in the samples which is quite interesting. One could argue that the fractal-like nanostructures are suitable as photocatalytic material and might even have higher conversions when the material was not amorphous but anatase. To test this, crystalline titanium dioxide fractal-like nanostructures need to be synthesized.

Another interesting result is the lowest catalytic effect for the mixed titanium dioxide-gold nanostructures. Indicating that addition of gold nanoparticles lowers the catalytic effect of the samples, which is contradictionary to the findings in previous research [43, 49–55]. However a yet to be published PhD thesis by Bindikt Fraters, from the University of Twente, observed the same lower catalytic effect. One could try to explain this lower catalytic effect in two ways; the first would be the size of the gold nanoparticles. It could be the case that the majority of the gold nanoparticles is of a too large size. If this is the case, the addition of the gold particles would only do more bad than good by covering part of the titanium dioxide nanostructure and do not exhibit the quantummechanical properties of the smaller particles.

The second explanation is linked to this, which is a too high loading of gold. The mixed fractal-like nanostructures were produced to prove that placing gold nanoparticles on the surface of a metal oxide matrix was possible. If one looks at the literature, weight percentages of around 0.5 % gold nanoparticles is the optimal loading. If one looks at the samples produced for this experiment, the weight percentage of gold is approximately more than 15 % (calculated from an atomic ratio of 13:1 for Ti:Au). Again the gold would take up too much of the surface area of the titanium dioxide matrix, lowering its photocatalytic properties.

An upside from these experiments is the fact that, if the hyphtesis is true, it would indicate that the gold is indeed on the surface of the titanium dioxide nanostructures, instead of being

Table 3.3: Photocatalytic measurements on titanium dioxide and mixed titanium dioxide-gold nanostructures

Sample	Amount of TiO_2 (mg)	Amount of gold (mg)	Total sample conversion to CO_2 (ppm)	Conversion time (min)	Relative Conversion (ppm/(mg · min))
Titania (1)	0.024 mg	0 mg	124 (ppm)	30 min	172.2
Titania-gold (2)	0.024 mg	0.0045 mg	80 (ppm)	30 min	93.6
Reference of titania	1 mg	0 mg	6500-7000 (ppm)	5 min	1300-1400

burried under a layer of titanium dioxide (forming the core-shell structures found by van Vugt [2]).

Conclusion

To conclude on the photocatalytic measurements, it can be stated that the fractal-like nanostructures produced in a dual spark method with oxidation before deposition do not exhibit extraordinary photocatalytic activity. The produced samples have a photocatalytic activity of roughly 10 times lower than the best performing reference sample provided by Bindikt Fraters.

The low catalytic activity can be due to the structure of the material. In the case of the produced samples it was most likely amorphous, while the reference was of a 100 % anatase crystalline phase. Knowing that the titanium dioxide particles in the sample are amorphous, the relatively high conversion is surprising and would be very promising if the material can be made anatase.

Next to this, it can be concluded that the addition of gold in the samples only lowered the catalytic effect. This could be due to two reasons, the size of the nanoparticles (too large; too small) and the high loading of gold. However both would indicate that the gold would be on the surface of the material, lowering the catalytically active area of the titanium dioxide nanostructures and thereby lowering the total photocatalytic effect.

3.4 Annealing

One of the conclusions from the previous sections was that there is strong evidence to believe that the produced titanium dioxide nanoparticles are amorphous. Especially in photocatalytic catalysis the anatase phase of titanium dioxide is desirable. Therefore two experiments were carried out to anneal the titanium dioxide nanoparticles to get fractal-like structures with a crystalline phase. The two experiments that were carried out are:

- Annealing of TiO_2 and Au-TiO_2 fractal-like nanostructures

- In-situ annealing of TiO_2 nanoparticles

The first experiment focuses on first building the fractal-like nanostructures and then proceeds to annealing them in an tube oven. The second experiment investigates the annealing behaviour of the primary titanium dioxide nanoparticles by annealing them before deposition on the polymer fibers.

3.4.1 Annealing of TiO_2

To investigate the possibility of producing crystalline titanium dioxide fractal-like nanostructures, an experiment was carried out to anneal the fractal-like nanostructures that are formed when carrying out the experiment discussed in section 3.1.2. This experiment mainly focused on producing a crystalline material and determining the temperature at which the fractal-like structures would anneal. To investigate the degree of crystallinity, selected area diffraction was performed on the sample with a transmission electron microscope.

(a) Titanium dioxide annealed at 200 °C

(b) Titanium dioxide annealed at 300 °C

(c) Titanium dioxide annealed at 400 °C
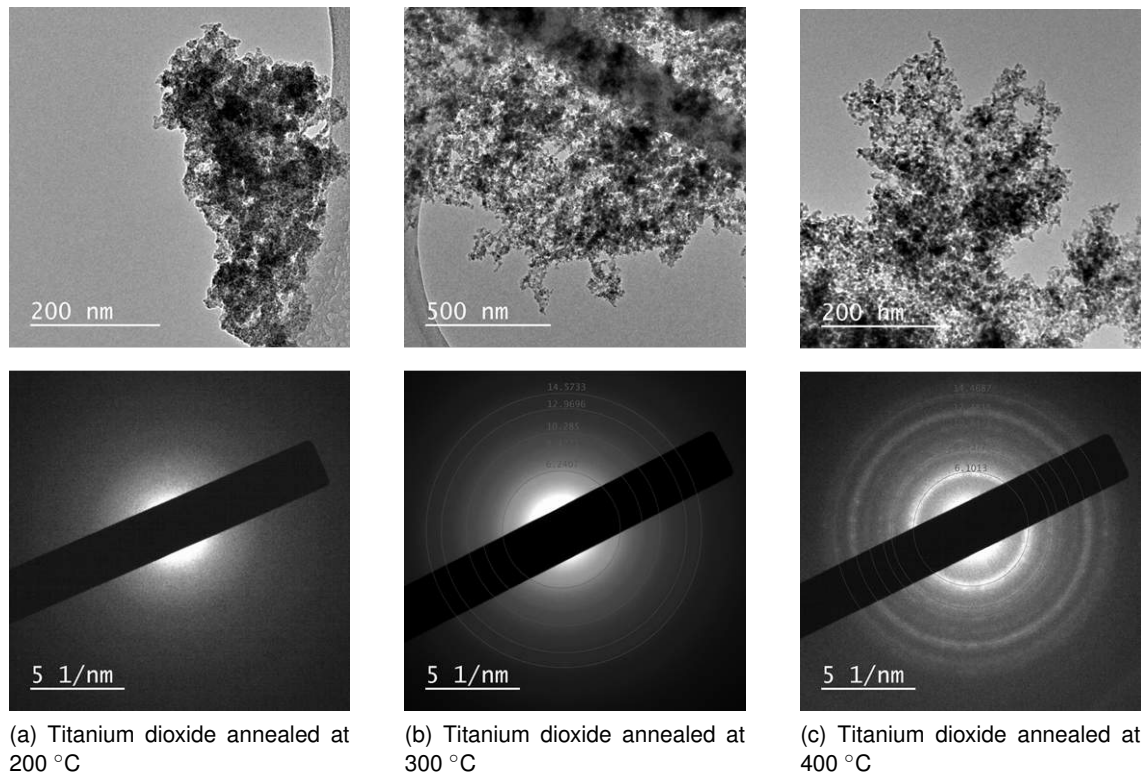
Figure 3.15: TEM images and associated SAD pattern of titanium dioxide annealed at different temperatures

Sample preparation

Samples were made in the same way as discussed in sections 3.1.2 and 3.2.3, for TiO_2 and Au-TiO_2 fractal-like nanostructures respectively. After the deposition process, the metal meshes were placed in a tube oven for 30 minutes at various temperatures. The heat-up rate of the oven was set at 5 °C per minute. The annealing of the samples was done under an argon atmosphere. The various temperatures that were investigated were 200, 300 and 400 °C, all with the same temperature settings. After annealing, material was scratched off the metal support and put onto a TEM grid for further investigation.

Results

When the samples were taken out of the oven, a colour change of the metal grids could be observed. Furthermore it could be seen by the bare eye that for the largest part the polymer fibers had disappeared, indicating that the PVA fibers cannot withstand the heat of the oven. This occured for oven temperatures of 300 and 400 °C, but not for 200 °C, which is in line with previous research [2, 21]. TEM was used to analyze both the structures on a nanoscale and to determine the crystallinity of the material (by SAD). It can be seen from figure 3.15 that fractal-like structures remain intact to a certain extent. From the same figure it can be concluded that a temperature increase induces the crystallinity of the material.

Table 3.4: XRD data of different crystalline phases of titanium dioxide and the titanium dioxide samples annealed at different temperatures. Data from webmineral.com

D_1 (Å)	I_1 (%)	D_2 (Å)	I_2 (%)	D_3 (Å)	I_3 (%)	Mineral
3.510	100	1.891	33	2.379	22	Anatase
3.245	100	1.687	50	2.489	41	Rutile
3.510	100	2.900	90	2.379	80	Brookite
3.278	100	1.602	unknown	2.370	unknown	Sample at 400 °C
3.204	100	1.944	unknown	2.361	unknown	Sample at 300 °C

Discussion

The most interesting result from this experiment is the formation of crystalline material. Even though this is in line with previous research, the dimensions of the titanium dioxide nanoparticles would suggest that crystalline material would form at even lower temperatures. No crystalline material was found when the sample was annealed at 200 °C. However it can be clearly seen from the images in figure 3.15 that at 300 and 400 °C a crystalline phase was formed. The circles that can be seen in figure 3.15 (b) and (c) represent the corresponding d-spacing of the crystalline lattice of the tested material (supposedly titanium dioxide). Looking at the different values in the figure and the intensities of the circles, one cannot conclusively point out the corresponding crystalline phase of the titanium dioxide.

Table 3.4 shows the different d-spacing values of the three possible crystalline phases of titanium dioxide (anatase, rutile and brookite) and the d-spacing values found for the tested samples. The table shows that the most prominent signal in the SAD patterns, of both annealing at 300 and 400 °C, corresponds to a rutile phase. This is not in line with the literature, since it can be found that the rutile phase regularly does not form until the sample is heated up above 550 °C. This might indicate that indeed the nanoparticles exhibit different annealing properties.

From the other signals of the SAD pattern, two interesting observations can be made. The first observation is that there is a shift in the second d-spacing value between the sample annealed at 300 °C and 400 °C. Annealing at 300 °C would suggest that the signal comes from an anatase material, while annealing at 400 °C suggests an rutile phase. The second observation is that the third strongest d-spacing signal for both annealing temperatures suggest an anatase phase.

Combining all of these observations, no conclusive answer can be given on which crystalline phase the samples are made of. The most obvious explanation would be a combination of both phases, where increasing the temperature from 300 to 400 °C changes the ratio of occurrence between the phases in the sample. This would also suggest that annealing the material at higher temperatures than 400 °C would yield a high percentage of rutile material and annealing at lower temperatures, between 200 and 300 °C, yields a higher percentage of anatase, both not in line with what is found in literature [71–73].

Nice to mention is also the fact that it is definitely not the heating up of the structures by the electron beam that induces the formation of crystalline material. Three different SAD patterns are observed for samples, pre-treated in different ways, indicating it is not the electron beam that causes a change in structure.

The TEM images in figure 3.15 (b) and (c) show that the nanostructures are still relatively

fractal-like. It can even be seen in figure (b) that the polymer fiber is still intact after being annealed at 300 °C. However, when comparing these results with the not annealed material in section 3.1.2, the structures look more dense (especially figure (c)).

Conclusion

Some interesting conclusions can be drawn from this section. The SAD patterns show that annealing at different temperatures can induce the crystallinity of the material. No crystalline material was observed when annealing was done at 200 °C, whilst different crystalline phases were observed for annealing at 300 °C and annealing at 400 °C.

No conclusive answer can be given on the crystalline phase of the material, however most likely a combination of anatase and rutile is formed when annealing the fractal-like titanium dioxide nanostructures at 300 °C and above. The d-spacing values for the samples show a shift when annealed at different temperatures, indicating a change in crystalline structure. According to what can be found in literature, the shift in peaks can be credited to the various d-spacing values of anatase and rutile. When looking at previous research, the results presented here are consistent with previous research [78]. The appearance of circles in the SAD pattern for rutile and de gradual decrease in intensity of anatase material is frequently found in literature [70]. Arguably a transition from anatase to rutile is occuring between 300 to 400 °C and maybe even beyond. In combination with the information from the sample annealed at 200 °C, a solely anatase phase should be formed when annealing the sample somewhere between 200 and 300 °C.

Fractal-like structures remain relatively intact when annealing at 300 and 400 °C, indicating that the material is quite stable. The structures on the TEM images in figure 3.15 look denser than what is observed for the structures in section 3.1.2, indicating that some sintering occurs.

Nice to mention in this section is that literature has shown that a combination of both rutile and anatase phase could actually be favourable for the photocatalytic properties of the material.

3.4.2 Annealing of Au-TiO$_2$ fractal-like nanostructures

As the previous section shows, it is possible to make a crystalline material by annealing after deposition of the nanoparticles on the polymer fibers. However the next step would be to determine if the gold nanoparticles stay on the surface of the titanium dioxide matrix when the annealing process takes place. Previous research showed that upon oxidation gold nanoparticles become submerged in the formed aluminium oxide matrix. This could be due to the oxidation process itself, but might also be caused by the fact that upon oxidation the temperatures locally rises to above the glass transition temperature of the aluminium oxide causing the gold particles to "sink" in the matrix. This experiment will also provide an insight in this phenomenon.

Sample preparation

The samples are prepared as described in section 3.2.3; a titanium dioxide fractal-like nanostructure with gold nanoparticles on the surface. After which these samples were transferred to a tube oven to be annealed for 30 minutes at 300 °C. The heat-up rate of the oven was set at 5 °C per minute. The annealing of the samples was done under an argon atmosphere. After annealing, material was scratched off the metal support and put onto a TEM grid for further investigation with a TEM.
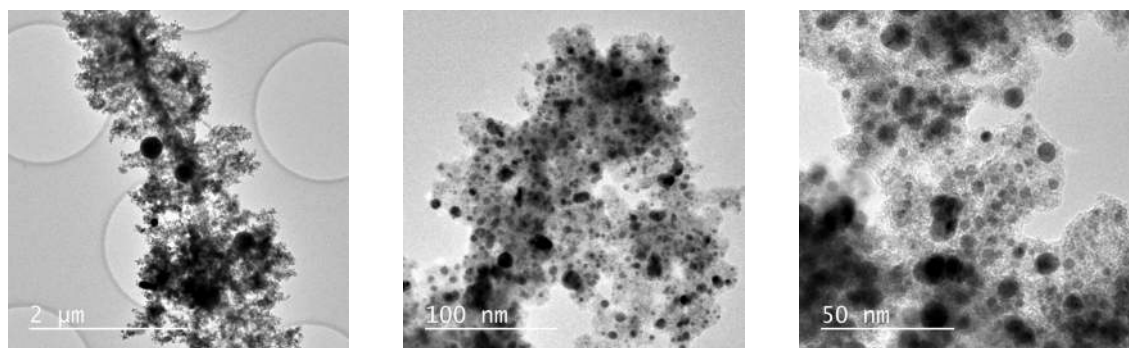
Figure 3.16: TEM images of mixed titanium dioxide-gold nanostructures, annealed at 300 °C

Results

A colour change could be observed when taking the sample out of the oven. The colour had changed from light gray to reddish in colour. This might indicate that the gold nanoparticles are distributed *inside* the titanium dioxide matrix as was also observed by van Vugt for gold nanoparticles in aluminium oxide [2]. The sample was further analyzed by performing TEM. As figure 3.16 shows, the nanostructures have remained relatively intact, however the gold nanoparticles have submerged in the titanium dioxide matrix. Figure 3.17 shows the SAD pattern of the fractal-like nanostructure and the corresponding TEM image, indicating that the sample has increased in crystallinity.

Discussion

The most prominent change of this sample upon annealing is the fact that the gold nanoparticles submerge into the titanium dioxide matrix. This would indicate that the elevation in temperature causes the gold nanoparticles to "sink" into the titanium dioxide matrix. With respect to the earlier research by van Vugt this results would conclude that it is not the oxidation of the aluminium matrix itself that is the cause of an aluminium oxide layer on the gold nanoparticles. It is the secondary effect of a locally elevated temperature, due to the oxidation, that causes this phenomenon.

   Furthermore it can be observed that the fractal-like nanostructures are more or less intact after the annealing process. However, looking more closely it can be seen that the particles sinter together to form denser structures than before they were annealed (as shown in the

Table 3.5: XRD data of different crystalline phases of titanium dioxide, gold and the mixed titanium dioxide-gold sample, annealed after deposition at 300 °T. Data from webmineral.com

D_1 (Å)	I_1 (%)	D_2 (Å)	I_2 (%)	D_3 (Å)	I_3 (%)	Mineral
3.510	100	1.891	33	2.379	22	Anatase
3.245	100	1.687	50	2.489	41	Rutile
2.355	100	2.039	52	1.230	36	Gold
2.195	100	1.894	unknown	1.361	unknown	Au – TiO$_2$ at 300 °C

(a) SAD pattern of mixed TiO$_2$-Au nanostructures

(b) Corresponding TEM image of mixed TiO$_2$-Au nanostructures
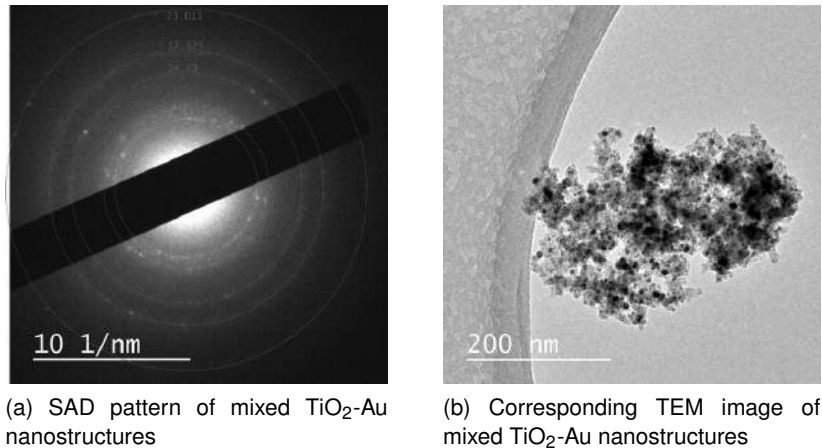
Figure 3.17: TEM image and corresponding SAD pattern of mixed titanium dioxide-gold nanostructures, annealed at 300 °C

figures of section 3.2.3). It can be stated that the process of annealing does have an influence on the structure, but at the tested temperature(s) it does not completely destroy the fractal-like nanostructures. This would also indicate that annealing at different temperatures can be used to influence the degree of sintering and can thus be used to increase the stability of the material.

Looking at the SAD pattern in figure 3.17, it can be seen that the material has increased in crystallinity. Apart from the circles, that can also be observed in figure 3.15 in section 3.4.1, small dots are present in the SAD pattern. This indicates an even higher degree of crystalline material in the sample. As the only difference between the sample from figure 3.17 and the sample discussed in figure 3.15 (b) is the addition of gold nanoparticles, the dots in the SAD pattern must (for the larger part) be due to the signal coming from the gold nanoparticles.

In table 3.5 the three main signals of the sample and the reference x-ray signals from literature are given. Comparing the main signals from the sample to the values found in literature, one can argue that the first signal is most probably caused by the gold nanoparticles. The signal could also be attributed to the third strongest signal of anatase titanium dioxide (assuming a little error in the measurement), however looking at table 3.4 this seems less likely. In this table the third strongest signal of anatase titanium dioxide was measured at a higher d-spacing value (2.361) and on top of that no specific dots (indicating specific particles) were identified. The second signal would clearly indicate the presence of anatase titanium dioxide in the sample and the same peak was also observed in the sample annealed without gold nanoparticles. The third signal has a low intensity, but could be best attributed to the gold nanoparticles present in the sample.

Conclusion

Three main conclusions can be drawn from these annealing experiments. First, it can be stated that the gold nanoparticles submerge in the titanium dioxide during the annealing process at 300 °C. This indicates that in previous research it was the oxidation that only indirectly caused the submergence of the gold nanoparticles; it was mainly caused by the locally increase in temperature due to the oxidation [2]. The fractal-like structures seem to stay intact at the annealing temperature (as was also observed in section 3.4.1). However it is safe to say that this path of

synthesizing a crystalline fractal-like titanium dioxide nanostructure with gold nanoparticles *on* the surface is not possible.

Secondly, as expected, clear signals from the gold nanoparticles can be seen in the SAD pattern of the sample. Less clear but in line with what was found in section 3.4.1, there is evidence to assume that the titanium dioxide matrix has become (to a certain extent) crystalline.

3.4.3 In-situ annealing of TiO$_2$ nanoparticles

The previous section has shown that annealing of the large fractal-like structures is a possibility to get a crystalline material. However there were some downsides to the proposed method. Upon annealing the structures become more dense, resulting in higher stability, but lower porosity. Next to that it was not possible to synthesize a crystalline material with gold nanoparticles on the surface of the matrix; the gold nanoparticles became submurged upon annealing. To overcome these problems it was proposed to anneal the titanium dioxide nanoparticles before mixing with gold nanoparticles and subsequent deposition on the polymer nanofiber support. This section discusses the in-situ annealing of only titanium dioxide nanoparticles.

Sample preparation

These samples were prepared in the same manner as discussed in section 3.1.2. The difference with the synthesis of the samples discussed in this section was the in-situ annealing of the titanium dioxide nanoparticles with the aid of a tube oven (Vecstar furnaces), that was placed in synthesis process before deposition of the particles. The oven was 35cm in length and the oven diameter was 1.2 cm. With the flowrates used in the experiment this resulted in an average annealing time of approximately 0.6 s. Annealing was tested at a temperature of 300 °C, this temperature was chosen because literature and previous results show that at higher temperatures the preferred anatase phase would probably not form.

Results

No obvious change in colour of the sample could be observed when taking the sample out of the sample holder. Transmission electron microscopy was performed to get an insight in the fractal-like nanostructures of the titanium dioxide matrix. As shown in figure 3.19, it can be seen that highly porous structures are formed with the method of in-situ annealing. Selected area diffraction was used to determine the crystallinity of the structures. Figure 3.18 shows the SAD patterns and it can be observed that crystalline material is formed at the investigated temperature.

Discussion

From figure 3.19 it can be concluded that highly porous structures are formed when the particles are annealed in flight before deposition. At 300 °C the structures are fractal-like on a nanoscale, consisting of titanium dioxide nanoparticles. When comparing these structures with the structures found in section 3.1.2, the structures made in this section look even more porous. This could be explained by the fact that during the annealing process the nanoparticles coalesce and form large agglomerates. These agglomerates are more porous than when the individual particles are deposited on the fiber support (the reasoning behind this is further explained in appendix H). Fractal-like nanostructures made of these larger agglomerates could therefore

45
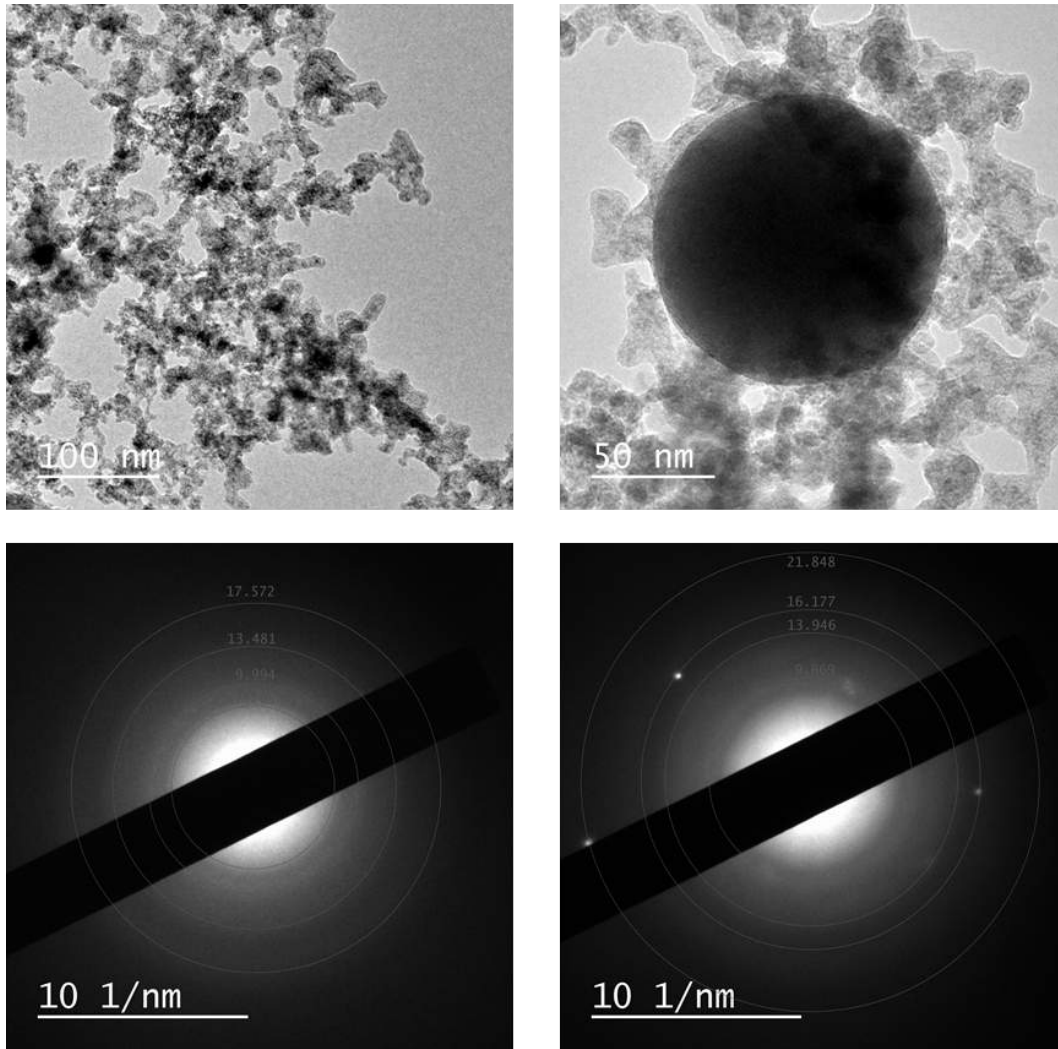
Figure 3.18: TEM images and associated SAD pattern of titanium dioxide nanostructures and splash particle, annealed in-situ at 300 /degree C

be more porous than the structures build up of individual primary particles. No conclusive answer can be given on this matter for now, because that would require an in-situ analysis of the agglomeration process of the particles or a quantitative measurement of the porosity of the different samples.

The second major result from this section is the production of crystalline material. Figure 3.18 shows the SAD patterns of the fractal-like nanostructures and splash particles in these structures for an annealing temperature of 300 °C. Table 3.6 shows the observed d-spacing values of the different samples. Striking is the mismatch between the diffraction peaks of titanium dioxide (anatase and rutile) found in literature and the values observed in the SAD patterns. As the only difference between this sample and the sample in section 3.1.2 is the annealing process; previous experiments show that the material must be titanium dioxide. One could argue that the oven could cause impurities in the sample, however that would not mean that one part of sample would consist of only impure material. Looking at the d-spacing values of the titanium dioxide nanostructures annealed at 300 °C, with a little imagination one could assign

(a) Titanium dioxide annealed at 300 °C   (b) Titanium dioxide annealed at 300 °C
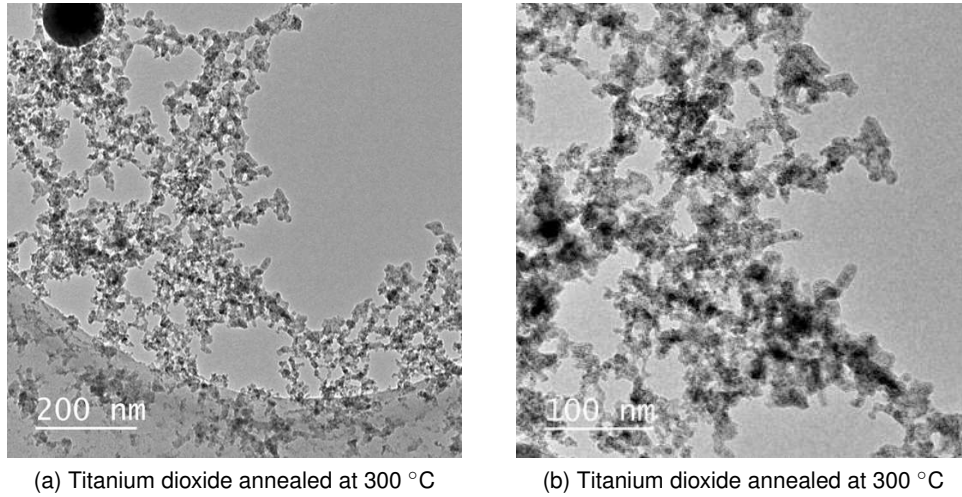
Figure 3.19: TEM images of produced fractal-like structures of titanium dioxide, annealed in-situ at 300 °C

the first and second peak to the second and third values of crystalline titanium dioxide found in literature. By eye one cannot state that the intesities of the observed values can be assigned to either anatase or rutile. Literature would suggest that the formed phase is anatase, but no conclusive answer can be given based on the findings in this section.

Comparing the observed d-spacings of the splash particle to values found in literature, it would suggest that it is an impurity in the material. Running the observed values in a search query on webmineral.com gives an almost 100 % match with chromium, giving a base to assume that the observed splash particle is an impurity consisting of (crystalline) chromium.

Conclusion

Three conclusions can be drawn from the results in this section. In-situ annealing of titanium dioxide nanoparticles, produced by spark discharge, is a method suitable for creating fractal-like nanostructures of crystalline material. Annealing at different temperatures has an effect on the crystallinity of the material; it is observed that a higher annealing temperature increases the crystallinity in the end product. Literature would suggest that the formed crystalline phase

Table 3.6: XRD data of different crystalline phases of titanium dioxide and the samples of titanium dioxide, annealed in-situ at different temperatures. Data from webmineral.com

D_1 (Å)	I_1 (%)	D_2 (Å)	I_2 (%)	D_3 (Å)	I_3 (%)	Mineral
3.510	100	1.891	33	2.379	22	Anatase
3.245	100	1.687	50	2.489	41	Rutile
2.596	100	2.001	unknown	1.483	unknown	Sample at 300 °C (nanostructures)
2.068	100	1.236	unknown	0.915	unknown	Sample at 300 °C (splash particle)

47

of titanium dioxide, annealed at 300 °C, is anatase. The SAD patterns do however not yield a conclusive answer on this hypothesis.

3.4.4   In-situ annealing of Au-TiO$_2$ fractal-like nanostructures

The previous section showed that in-situ annealing of titanium dioxide nanoparticles produces (semi-) crystalline material. Combining this with the problem that arose in section 3.4.2 (the submerging of gold nanoparticles in the titanium dioxide matrix upon annealing), it should be possible to synthesize a fractal-like titanium dioxide with gold nanoparticles on the surface with this method of in-situ annealing.

Sample preparation

This sample was prepared in practically the same way as the samples in section 3.2.3. The difference was the addition of a tube oven, just as discussed in section 3.4.3. This tube oven was placed after the place of oxidation of the titanium nanoparticles, but before the stream of gold nanoparticles is mixed in. The stepwise process would thus look like:

Titanium nanoparticle production → oxidation → annealing → mixing with gold nanoparticles → deposition

The oven was 35cm in length and the oven diameter was 1.2 cm. With the flowrates used in the experiment this resulted in an average annealing time of approximately 0.6 s. Annealing was tested at 500 °C, this temperature was chosen to rule out the possibility that a too low annealing temperature could be the cause of the gold nanoparticles not submerging in the titanium dioxide matrix.

Results

The samples were analyzed by transmission electron microscopy on their crystallinity and nanostructure. The TEM images given in figure 3.22 show the fractal-like structures made by the proposed method. It can be seen that highly porous structures are made with gold nanoparticles on top of the titanium dioxide matrix. Selected area diffraction was used to determine the crystallinity of the material. The SAD pattern and associated TEM image is shown in figure 3.23. The figure shows that both the investigated nanostructures and splash particle consist of crystalline material.

Discussion

It can be observed from the TEM images that the proposed method of in-situ annealing of titanium dioxide before mixing with gold nanoparticles yields the desired fractal-like nanostructures with gold nanoparticles on the crystalline titanium dioxide matrix. That the particles are indeed on top of the titanium dioxide matrix and not, as described in section 3.4.2, embeded in the titanium dioxide matrix can be concluded from the TEM images in figure 3.22.

The fractal-like structures observed in this figure are quite similar to what is observed in section 3.4.3, only the addition of extra gold nanoparticles can be observed. An interesting phenomenon can be seen in figure 3.22 (a), where various larger splash particles can be observed. Although in the previous section a SAD measurement stated that such a particle was

an impurity of chromium, it is expected that most of these larger splash particles are due to the in-situ annealing of the titanium dioxide. Due to the induced heat the particles coalesce in flight. When two same size particles meet, the particles will coalesce with the intermediate step as depicted in figure 3.20 below.

Figure 3.20: Schematic process of coalescence of same size particles

This intermediate is energetically favourable than proceeding immediately to the large sphere. Putting in more energy (in this case heat) will cause the complete process to irreverisbly move to the right. However when a larger particle meets a much smaller particle, this intermediate step does not exist (or better: can be neglected) and the smaller particle will be gobbled by the larger particle, as described in figure 3.21.
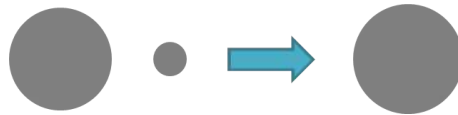
Figure 3.21: Schematic process of coalescence of large and small particle

From these assumptions it can be assumed that the presence of these larger spherical splash particles in the sample are due to the recirculation of titanium dioxide particles in the oven, causing them to grow. Removing the oven from the process would, according to this reasoning, yield structures with less to no splash particles at all, which is exactly the case for the experiment from section 3.2.3.

When looking at the fractal-like nanostructures themselves, it is hard to say wheter the particles are partly sintered together (the intermediate step in figure 3.20). Partial sintering of the sample would enhance the stability of the nanostructures. The structures are highly porous and arguably more porous than what was observed in section 3.2.3. These titanium dioxide nanostructures are in line with what was observed in section 3.4.3, where a case is made that the fractal-like structures are build up of agglomerates instead of primary titanium dioxide nanoparticles. In any case, the structures produced by this method are more porous than the
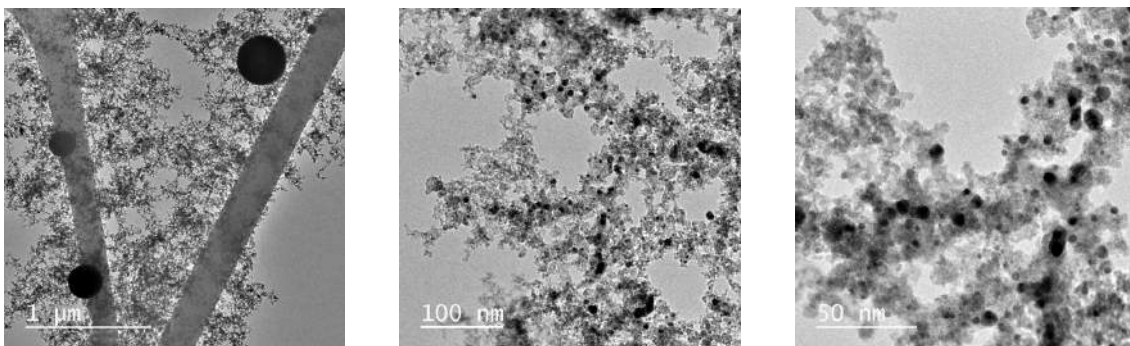
Figure 3.22: TEM images of mixed titanium dioxide-gold nanostructures, annealed in-situ at 500 °C

(a) TEM and SAD pattern of fractal-like mixed titanium dioxide-gold nanostructure

(b) TEM and SAD pattern of splash particle
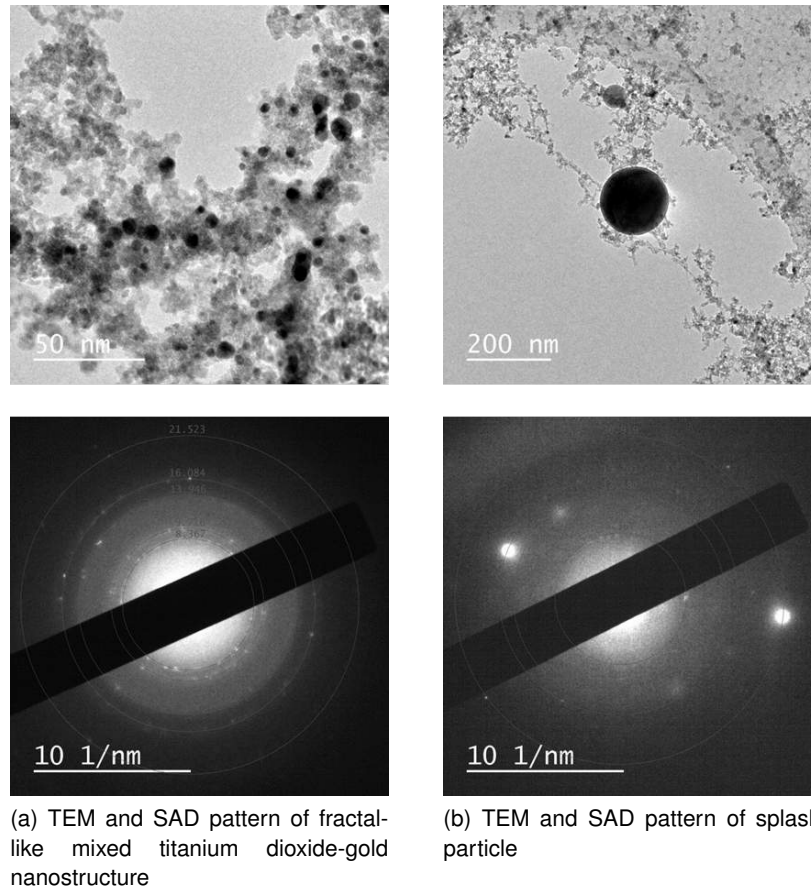
Figure 3.23: TEM images and associated SAD pattern of mixed titanium dioxide-gold nanostructures, annealed in-situ at 500 °C

structures produced by annealing after deposition, as described in section 3.4.2, making this a more suitable method to produce the desired end product.

The SAD pattern shows a relatively high degree of crystallization, especially when compared to the in-situ annealing at 300 and 400 °C in section 3.4.3. Table 3.7 shows the observed d-spacing values of the sample and the expected d-spacings taken from literature. The results only show an increase in crystalline material due to the annealing. Assigning the various peaks to a certain material would be speculating without a real basis. One could argue that most of the bright dots in the SAD pattern are due to the presence of gold. In line with this one could state that the first and second signal can be assigned to gold. Next to that there should be a signal for crystalline titanium dioxide as crystalline material was observed with in-situ annealing for the synthesis of only titanium dioxide nanostructures, as discussed in section 3.4.3. Knowing this, one could argue that the first peak should be assigned to the titanium dioxide.

Comparing the SAD pattern of the splash particle and the SAD pattern of the nanostructures it can be observed that one two peaks coincide. This would indicate that these peaks should be assigned to crystalline titanium dioxide, as the larger splash particles are most likely formed in the oven during the annealing process. It should be noted that this splash particle could also be an impurity, just as discussed in section 3.4.3. This seems unlikely as for these assigned peaks no clear match can be found for any material on webmineral.com.

However all these assumptions and discussion would make any statement about the findings presented here very weak. Literature has little to no information on the annealing of very small nanoparticles (<10nm) and it is therfore suggested to do more research on the annealing process to get a better insight.

Conclusion

To conclude, it is possible to synthesize a fractal-like crystalline titanium dioxide matrix with gold nanoparticles on the surface. This can be done by annealing titanium dioxide nanoparticles in-situ before mixing with gold nanoparticles and subsequent deposition on the polymer fiber support. The structures have a, to the eye, very high porosity, arguably more porous than the structures made when the particles are not annealed before deposition. Selected area diffraction suggest that crystalline material is present in the sample. With the obtained data it is however not possible to give a conclusive answer on the crystalline form of the material.

3.4.5   Conclusion section 3.4

This section examined the possibilities of annealing the amorphous titanium dioxide nanostructures and design a method that would make it possible to synthesize fractal-like crystalline titanium dioxide nanostructures with gold nanoparticles on the surface. To achieve this goal, two different approaches were tried. One was annealing after deposition of the particles and one was annealing in-situ before deposition.

Annealing after deposition yielded relatively porous titanium dioxide nanostructures that increased in crystallinity when annealing occurred at higher temperatures. A temperature higher than 200 °C was needed to anneal the material. A shift in crystalline phase (anatase to rutile) was observed when the annealing temperature was increased from 300 to 400 °C. A difference in porosity could be observed when annealing occurred at different temperatures; usually the higher the temperature, the denser the material.

It was not possible to synthesize crystalline titanium dioxide nanostructures with gold nanoparticles on the surface with this method. Upon annealing of the material at 300 °C, the gold nanoparticles submerge in the titanium dioxide matrix. The fractal-like nanostructures stay intact and the material shows some crystallinity, but in light of this research the submergence of gold nanoparticles is undesirable.

Annealing in-situ, e.g. before deposition, yields highly porous crystalline titanium dioxide nanostructures. The material became more crystalline after annealing at a higher temperature,

Table 3.7: XRD data of different crystalline phases of titanium dioxide, gold and the mixed titanium dioxide-gold sample, annealed in-situ at 500 °C. Data from webmineral.com

D_1 (Å)	I_1 (%)	D_2 (Å)	I_2 (%)	D_3 (Å)	I_3 (%)	Mineral
3.510	100	1.891	33	2.379	22	Anatase
3.245	100	1.687	50	2.489	41	Rutile
2.355	100	2.039	52	1.230	36	Gold
2.390	100	2.058	unknown	1.434	unknown	Mixed sample at 500 °C (nanostructures)
1.316	100	2.390	unknown	1.481	unknown	Mixed sample at 500 °C (splash particle)

51

just as was observed when annealing after deposition. The main difference between annealing in-situ and after deposition, is that the annealing temperature does (for the tested temperatures) not influence the porosity of the nanostructures when annealing is done in-situ.

This method proved to be suitable for synthesizing fractal-like crystalline titanium dioxide nanostructures with gold nanoparticles on the surface. When annealing of titanium dioxide is done before mixing with gold nanoparticles (and subsequent deposition on the polymer fiber support), the desired material was synthesized. A concluding answer on the crystalline phase of the titanium dioxide could not be given, but the point here is that a crystalline material was observed. This result alone points out the possibilities of the method and the annealing process needs further optimization.

Chapter 4

Conclusions Summary

This chapter gives an overview of the conclusions that can be drawn from the experimental results of the previous sections. The experimental section of this research was divided into four parts: metal-oxide nanoparticle structures on PVA fibers, mixed nanoparticle structures on PVA fibers, photocatalytic measurements on TiO_2 and Au-TiO_2 samples and annealing of TiO_2 and Au-TiO_2 nanostructures.

The main conclusion from the first section is the fact that the proposed method of in the gas phase oxidation of, by spark discharge produced, metal nanoparticles before deposition on the PVA fiber support yields fractal-like metal oxide nanostructures. The method proved to yield fractal-like structures for both titanium and aluminium nanoparticles, suggesting a wide range of metal oxide nanostructures might be possible. Synthesized titanium dioxide nanostructures had an amorphous crystalline phase.

Section two discussed mixed nanoparticle structures on PVA nanofibers. It could be concluded from this section that the proposed catalyst production method, with a dual spark chamber set-up, can be applied to synthesize highly porous metal oxide nanostructures with metal nanoparticles on the surface. The method is applicable to a wide range of metal oxides (titanium, aluminium and magnesium) and it was possible to put both gold and platinum nanoparticles on the surface of these metal oxide nanostructures throughout the whole structure. In contrast to amorphous titanium dioxide, crystalline magnesium oxide was formed. Indicating that the oxidation process is of influence on the crystalline structure of the metal oxide.

Photocatalytic experiments were done on the synthesized titanium dioxide and mixed titanium dioxide-gold nanostructures. It turned out that the material did not exhibit much catalytic activity. This was probably due to the fact that the synthesized titanium dioxide was amorphous. Next to that, the mixed titanium dioxide-gold sample performed less than a sample of only titanium dioxide.

The last section focused on the annealing of titanium dioxide. The proposed catalyst synthesis method, extended with in-situ annealing of titanium dioxide nanoparticles (before admixing gold nanoparticles and subsequent deposition on PVA nanofibers) proved to be suitable for synthesizing fractal-like crystalline titanium dioxide nanostructures with gold nanoparticles on the surface.

Chapter 5

Recommendations

As for almost every research, each result and subsequent new knowledge raises even more questions and provides new possibilities in various fields of research. As for this research, it is no different. The main result of this thesis research is the design of a method with which fractal-like metal oxide nanostructures can be synthesized with metal nanoparticles on the surface. This result opens up a whole new range of possible research topics, of which a few are listed below:

- Although in this research PVA nanofibers were used as a backbone for the metal-oxide nanostructures, research can be done on the applicability of the method on other backbone materials. One can for example think of synthesizing metal oxide nanostructures on carbon nanofibers, textiles and other materials than can be suitable as a catalyst support.

- The samples prepared in this research are classified as "fractal-like", because of the similarity in the synthesis process with previous research [38]. More research should be done on the actual fractal properties of the material.

- In this research the rate of production was too low to be able to for example conduct a BET analysis. A possibility for future research could therefore be scaling up of the process and get a better insight in the characteristic properties of new catalytic materials.

- As the method is designed for the production of various catalysts, more research should be done in synthesizing catalysts that are being used in the everyday life. Optimizing and synthesizing a catalyst with extraordinary catalytic properties should be the goal of such a research.

- In line with the previous point, synthesis of an excellent performing titanium dioxide photocatalysts with the proposed method could be the basis for further research. One could investigate doping of the titanium oxide with for example nitrogen [49].

- Oxidation of (small) nanoparticles is still a topic that has not been researched very often. Interesting results in this research show that the oxidation process can influence the crystalline phase of the material. A thorough research should be done on the oxidation behaviour of different metals.

- Crystalline phase transitions. due to annealing, of titanium dioxide nanoparticles seems to occur at different temperature ranges than what can be found in literature for larger particles. To optimize the catalyst synthesis process, this phenomenon needs further investigation.

- As catalysts are often subject to extreme conditions (high temperatures, high pressures), more research should be done in the stability of the produced nanostructures. Can these materials withstand such extreme conditions, or are the catalysts produced by the proposed method only suitable for chemical reactions under mild conditions?

These are just a handful of examples of new research topics for future scientists. It is still a long way to industrial catalysts production with the proposed method, but the possibilities are virtually endless and are worthwile investigating.

Appendix A

Experimental Set-up

During this research various experimental methods were used in series. First there is the electrospinning process to produce the supporting polymer nanofibers, then the spark discharge mechanism was used to produce the desired nanoparticles and these two combined formed the production process of the mixed gold-metal oxide nanostructures. The nanoparticles produced during the spark discharge process are transferred via a transporting gas to a metal mash on which the nanofibers are spun. A schematic overview of this process is given below in figure A.1. Next to that, both the electrospinning set-up and the spark discharge set-up are depicted in the figures below. The various parts of- and alterations to this process that were performed during the time span of the project are discussed in this appendix.
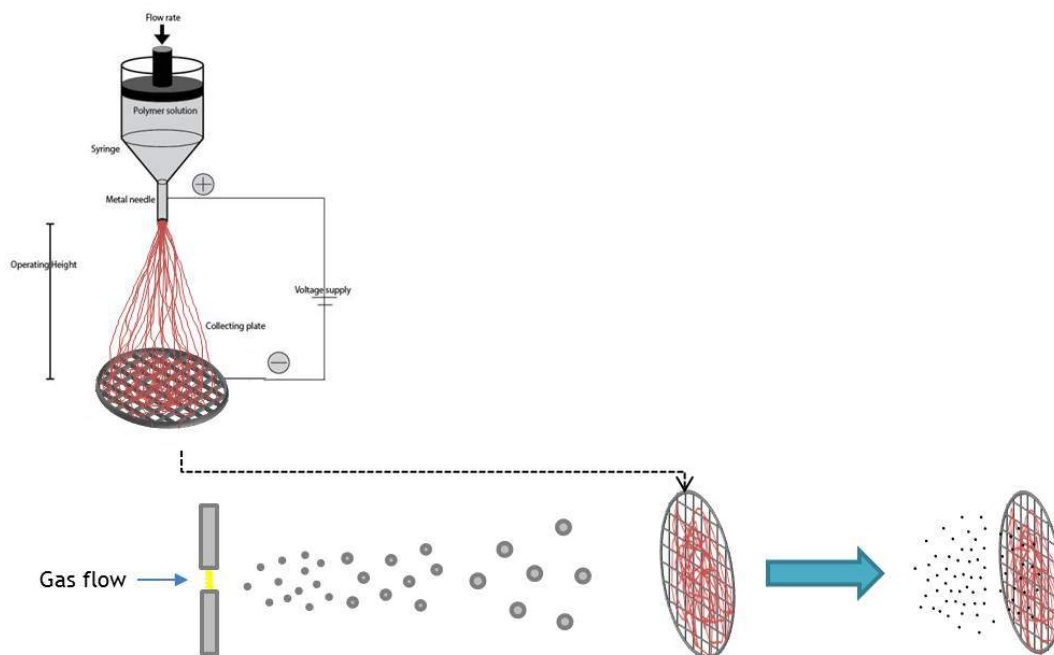
Figure A.1: Schematic overview of the experimental process
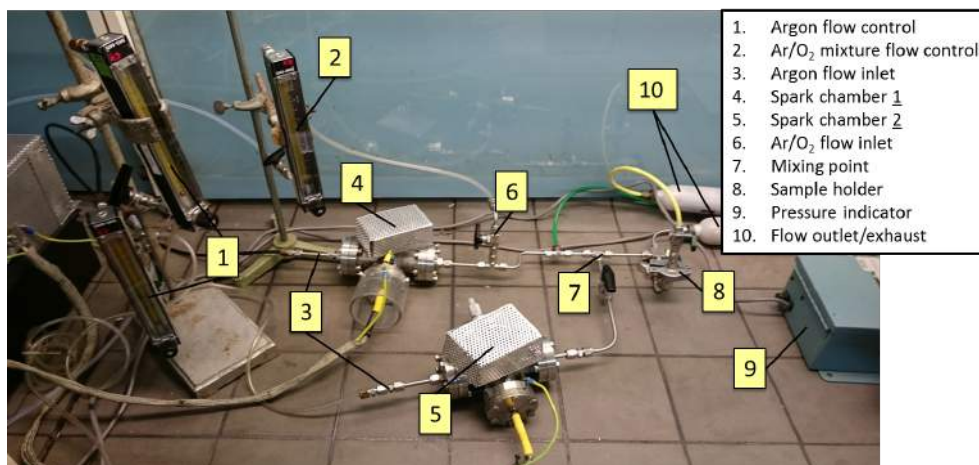
Figure A.2: Experimental set-up for spark discharge

The legend in the figure:
1. Argon flow control
2. Ar/O$_2$ mixture flow control
3. Argon flow inlet
4. Spark chamber 1
5. Spark chamber 2
6. Ar/O$_2$ flow inlet
7. Mixing point
8. Sample holder
9. Pressure indicator
10. Flow outlet/exhaust

A.1 Electrospinning

The electrospinning set-up that was used in this research is shown in figure A.3 (a). The legend next to the figure shows the different parts of the set-up. The fibers were spun on a metal mash that was placed upon the aluminium collector plate to be able to later deposit the nanoparticles, produced via spark discharge, onto these fibers. The optimal operating conditions that were used for the electrospinning throughout the experiments are as follows:

- Flow rate: 5 mL/h

- Polymer solution: 15wt% of PVA, dissolved in toluene

- Applied voltage: 20 kV

- Operating height: 13 cm

To perform TEM measurements, the fibers needed to be spun on the TEM grid and later on placed in the spark discharge set-up. To be able to do this, the TEM grids were placed on the metal mashes and on top of that the fibers were spun, as shown in figure A.3 (b). The metal mashes were made of stainless steel and were punched from a larger sheet to make circles with a diameter of 14 millimeter that would fit the sample holder of the spark discharge process.

A.2 Spark discharge - one spark chamber

The first of two experimental spark discharge processes that was used is a process where nanoparticles are created in one spark chamber and than transferred to the polymer nanofibers. With this experimental set-up different different electrode configurations can be tested to form agglomerates of different kinds of particles before oxidation. In light of this research two sets of electrodes were used:

- Two titanium electrodes

- separate titanium and gold electrode

II

(a) Experimental set-up for electrospinning

(b) Schematic overview of fiber deposition on TEM grids
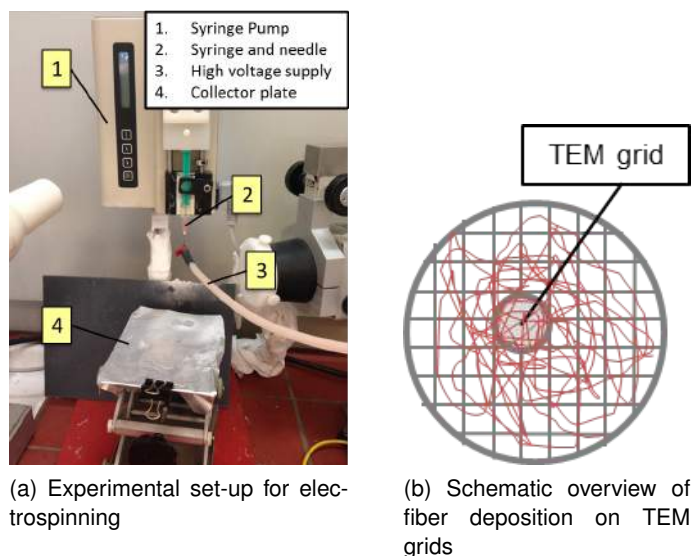
Figure A.3: Experimental set-up of electrospinning

Below, in figure A.4, an overview of the used set-up is given. A gas inlet controls the flow of the carrier gas flowing through the spark discharge chamber where the nanoparticles are formed. The carrier gas transfers the nanoparticles to the sample holder where the metal mashes with the polymer nanofibers are being held. During this process a second inlet controls the flow of the O_2. The operating conditions that were used for these experiments were:

- Gas flow of carrier gas: 5 L/min of Argon

- Spark settings: various (discussed in section A.4)

- Gas flow of oxygen inlet: 2 L/min of Ar/O_2 mixture of 80/20 vol% (resulting in $\pm$ 5 vol% of O_2 in final flow).

- Total gas flow at the nanofibers: 7 L/min Ar/O_2 mixture of 95/5 vol%.

A.2.1   Two titanium electrodes

To investigate the oxidative behaviour of titanium, titanium electrodes were used to produce the needed nanoparticles. After the spark discharge process and the production of the nanoparticles, the nanoparticles were either:

1. Oxidized *before* deposition on the fibers with a *low* O_2 vol%.

2. Oxidized *after* deposition on the fibers with a *high* O_2 vol%.

More on this subject will be discussed in the experimental section where the results of the different experiments are shown.

1. Argon flow inlet
2. Spark chamber
3. Ar/O₂ flow inlet
4. Sample holder
5. Pressure indicator
6. Flow outlet/exhaust
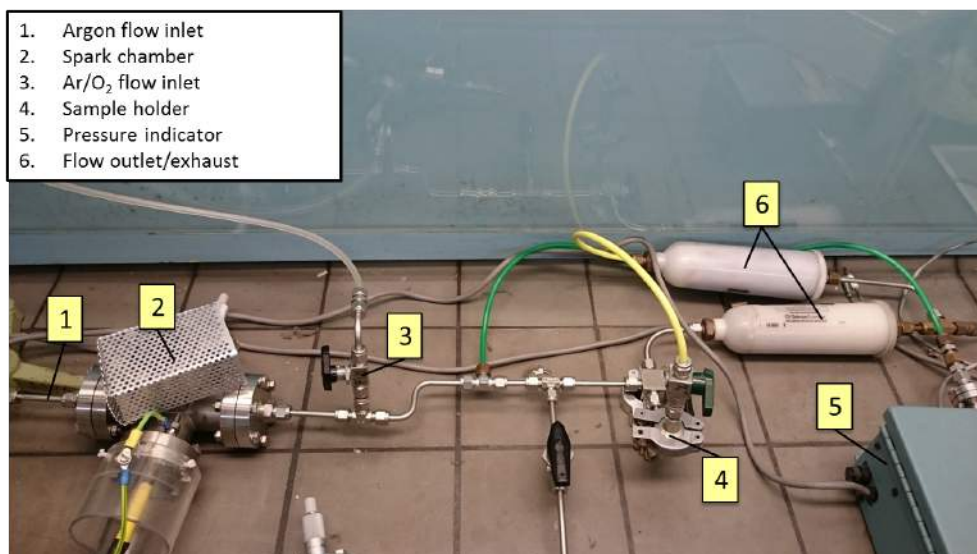
Figure A.4: Experimental set-up for one spark

A.2.2 Separate titanium and gold electrodes

In this research, a configuration was used were a titanium and a gold electrode were the positive and negative electrode in the spark discharge chamber. This electrode configuration was used to investigated the possibility of producing both titanium and gold nanoparticles with each spark at the same time and then coagulate to form primary particles and agglomerates. A schematic overview of such a two different electrode configuration is given in figure A.5.

For this process the same experimental set-up was used as in section A.2 (figure A.4) to place the particles on top of the polymer nanofibers, but with different electrodes. For this electrode configuration both oxidation *before* deposition on the fibers with a *low* O_2 vol% and oxidation *after* deposition on the fibers with a *high* O_2 vol% was performed.
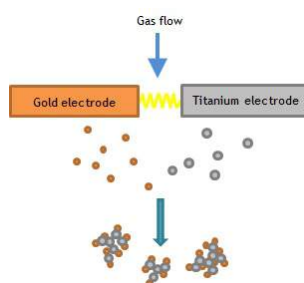
Figure A.5: Spark discharge process with two different electrodes

A.3 Spark discharge - parallel spark chambers

The second experimental process is a process where two different spark chambers were used to produce the Au-TiO₂ catalysts. With the use of a second spark chamber, the oxidation of titanium nanoparticles, the point of addition of Au and the TiO₂/Au ratio can be better monitored
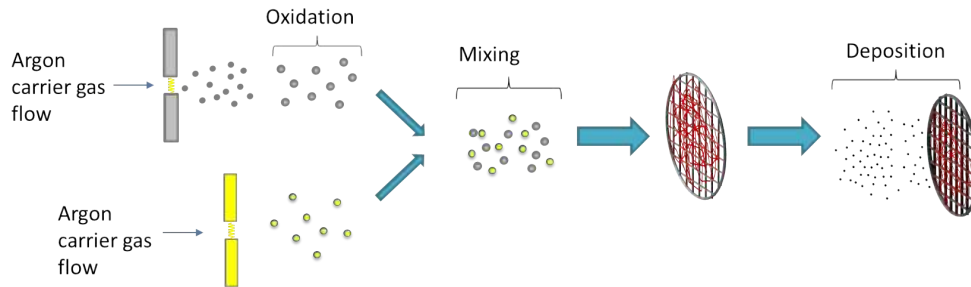
Figure A.6: Schematic overview of a dual spark set-up

and tuned. The process described in A.2 is altered by the addition of a second spark chamber, this "new" process is depicted in figure A.6. The optimal operating conditions used in these experiments were:

- Gas flow of carrier gas through spark chamber nr. 1: 2.8 L/min of Argon

- Gas flow of carrier gas through spark chamber nr. 2: 1.9 L/min of Argon

- Spark settings: various (discussed in section A.4)

- Gas flow of oxygen inlet: 1 L/min of Ar/O_2 mixture of 80/20 vol% (resulting in $\pm$ 3.5 vol% of O_2 in final flow).

- Total gas flow at nanofibers: 5.7 L/min Ar/O_2 mixture of 96.5/3.5 vol%
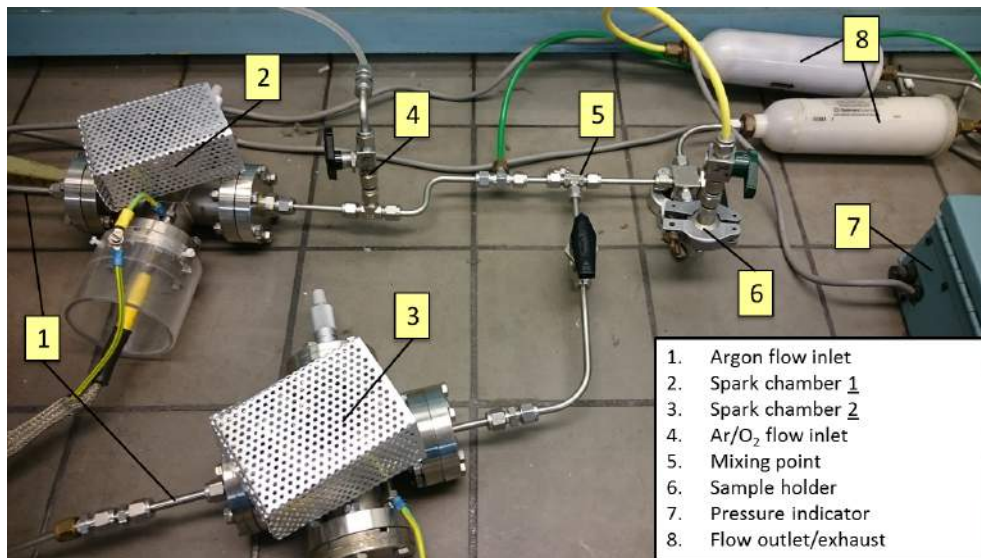
Figure A.7: Experimental set-up for two sparks

A.4   Spark Settings

To investigate the effect the spark settings had on the deposition process of the produced nanoparticles (Ti-Au ratios, amount of particles etc.), the settings of the spark generators in
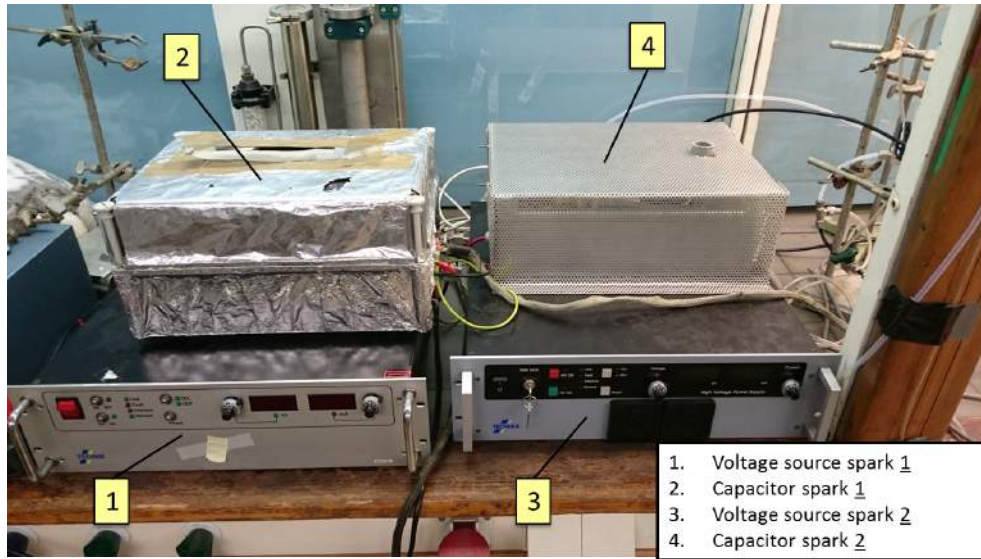
Figure A.8: Power supply for a two spark set-up

the dual spark set-up were varied. In the tables below, various settings and their respective Ti-Au atomic ratios are shown and from these tables the optimal settings for the spark discharge process were derived. Furthermore, figure A.8 shows the power supply for the (dual) spark discharge process.

With an oscilloscope the spark breakdown voltage, frequency and consistency were measured. Figure A.9 shows the oscilloscope graph from which these parameters can be measured and calculated.

- The gold electrodes had an average breakdown voltage of 0.75 kV.

- The titanium electrodes had an average breakdown voltage of 1 kV.

- The frequency of the spark between the gold electrodes was approximately 133 Hz.

- The frequency of the spark between the titanium electrodes was approximately 2250 Hz.

- The spark between the gold electrodes was relatively consistant; the breakdown voltage was in a range of 0.7 - 0.8 kV and the frequency was relatively steady.

- The spark between the titanium electrodes was not very consistant; the breakdown voltage was in a range of 0.8 - 1.2 kV and the frequency varied a lot.

Table A.1: Au-Ti ratios for various voltage and current combinations

(a) Ti-Au ratios for variable current

	mA	5	3	2	1
		0.35 kV			
1 kV	5	2.21	4.14	8.01	9.31
	7	2.13	6.23	9.86	13.13

(b) Ti-Au ratios for variable voltage

	kV	0.35	0.5	0.6
		5 mA		
5 mA	1	2.21	1.51	-
	1.5	1.74	0.85	0.41
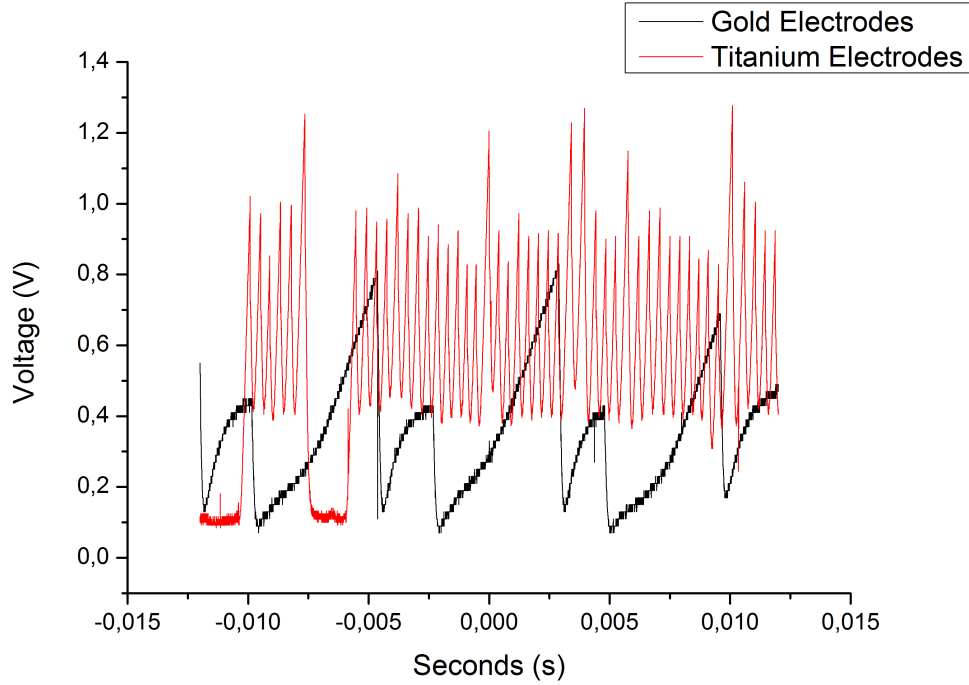
Figure A.9: Graphical representation of the spark discharge mechanism

Several mathematical relation are being used to relate the different parameters of the spark discharge process. The various parameters that can be calculated with these equations are energy (E), current (I) and the frequency (f) of the spark [11]. These relations are given in equations A.1 through A.3.

$$E = \frac{1}{2}CV_d^2 \tag{A.1}$$

$$I_c = C\frac{dV_d}{dt} \tag{A.2}$$

$$f = \frac{I}{CV_d^2} \tag{A.3}$$

With the help of these equations, the spark settings can also be calculated instead of measured.

Appendix B

Overview of Characterization Techniques

To analyze the various samples that were made during the course of this project, different characterization techniques were used. These techniques, ranging from structure analysis by transmission electron microscopy to catalytic activity testing by both CO and propane oxidation. The following analysis techniques will be discussed:

- Transmission Electron Microscopy (TEM)

- Scanning Electron Microscopy (SEM)

- CO and propane oxidation

B.1   Transmission Electron Microscopy (TEM)

To analyze the produced samples on a nanoscale (magnifications up to 300.000x) TEM was used. With TEM the primary particles (<10nm) produced by the spark discharge process could be visualized and with this the fractal-like nanostructures can be analyzed. The fundamental principle of TEM is the transfer of a high energy electron beam through the sample that needs investigation. The interactions of the electrons in the beam with the particles in the sample result in a two-dimensional image that is displayed onto either a fluorescent screen, photographic film or a sensor/camera. The sample needs to be thin (<100nm) to be able to construct a useful 2-D image of the 3-D sample, since particles that lie behind eachother are viewed as one. The electrons are scattered elastically (meaning their kinetic energy is conserved, but their direction is modified) or inelastically (meaning their kinetic energy is not conserved upon collision) and these two can be used to generate the two-dimensional image.

Next to creating an image on a nanoscale, TEM can also be used to perform Selected Area Diffraction (SAD). In SAD the electrons in the beam are visualized as waves passing through the sample. The wavelength of electrons is approximately a hundred times smaller than the spacing between atoms and will therefor easily pass through the sample. However the atoms in the sample act as a diffraction grating for the electron beam and will therefor diffract (part of) the electrons. By scattering the electrons to particular angles (defined by the crystal structure of the material), while others continue through the sample without being diffracted, a pattern can be made that depicts the crystalline structure of the material.
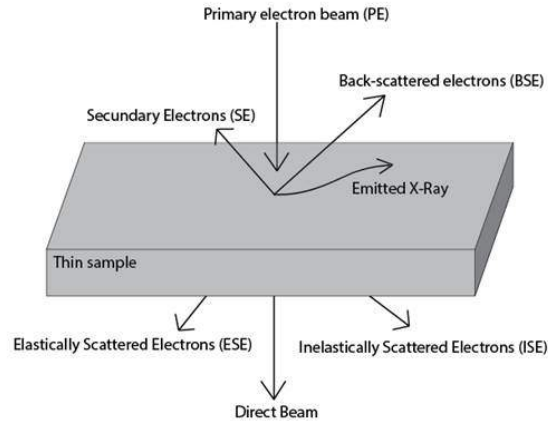
Figure B.1: Schematic representation of SEM and TEM, from A.W. van Vugt [2]

B.2   Scanning Electron Microscopy (SEM)

For this research scanning electron microscopy was used to determine the micro structure and roughly the amount of nanoparticles deposited on the polymer nanofibers. The microscope that was used was the device located at the Chem-E faculty of the TU Delft which is a Philips JOEL-JSM 6010 LA. SEM is a process were electrons are being shot at the sample that needs to be analyzed. The narrow focused electron beam scans the surface of the sample to generate a three dimensional picture with a high resolution, revealing details of nanometer sizes. The acceleration of the electrons can be controlled and usually the applied voltage that is used for the electron beam ranges from 5kV to 20kV. There are three types of signals that are used by SEM to characterize the sample, these consist of Secondary Electron (SE), Back-Scattered Electron (BSE) and characteristic X-ray signals.

- **Secondary Electrons** are electrons generated by ionization of a material. Low energy (<50 eV) secondary electrons that are ejected from the k-shell of the atoms of the sample by the primary electrons of the electron beam of the SEM. These SE are collected to yield the images shown by the microscope and are generally used to generate the surface picture of the sample.

- **Back-Scattered Electrons** are high energy electrons of the initial electron beam that are reflected or so called back-scattered by the sample that is being analyzed. Heavy elements ("bigger elements") reflect the electrons more easily than lighter ("smaller") elements and thus give a higher intensity. BSE is often used to detect areas of different chemical composition in one sample.

- **Characteristic X-ray signals** are used to determine the chemical composition of the sample. The X-rays that are produced by the electron beam interactions with the sample are collected and can be used in a process that is called energy-dispersive X-ray spectroscopy (EDX). EDX is the name of the analytical technique to determine the chemical composition of the sample. The fundamental principle behind this technique lies in the fact that each element has a unique atomic structure that corresponds with a unique x-ray emission pattern allowing the characterization via X-ray emission.

B.3   Propane oxidation reaction

To analyze the samples on photocatalytic activity, the conversion of propane to carbon dioxide under the influence of light was tested in a propane oxidation reaction. These measurements were performed by Bindikt Fraters from the University of Twente. An overview of the procedure is given below.

- The gas mixture used consisted of 0.5% vol. propane, which was mixed with 19.5% vol. oxygen diluted in nitrogen.

- The samples were placed on the bottom of the reactor and the gas mixture was led over it.

- The oxidation reaction was induced by A 365 nm UV-LED at an intensity of 25 mW/cm^2 for a reaction time of 30 minutes.

- An Agilent 7820 GC system was used to analyze the product gas. The Agilent 7820 GC system had a Varian CP7584 column and a Methanizer-FID combination for detection.

Appendix C

Dual Filter Test

To determine the penetration of the nanoparticles through the PVA filters and get an estimate of the total uptake of nanoparticles by these filters a so called 'filter test' was done. In this experiment, two samples with PVA fibers were placed behind each other and compared to each other to determine the filter efficiency of the samples. The analysis of the nanoparticle penetration was done by performing scanning electron microscopy on both samples. A dual spark experiment was done on the samples with the following spark settings. In spark chamber 1, two solid titanium electrodes were used with a spark voltage of 1 kV and a current of 7 mA. In spark chamber number 2 two hollow gold electrodes were used and a spark voltage of 0.35 kV and a current of 1 mA. The SEM images are shown in C.1. Van Vugt [2] stated that the nanoparticle penetration was related to the particle (or agglomerate) size. Assuming that the filter efficiency of two filters approaches 100%, it can be stated that the efficiency of a single filter is about 66 %

$$\frac{\frac{3.148+3.148+3.680+2.550}{4}}{\frac{1.358+1.844+1.504}{3} + \frac{3.148+3.148+3.680+2.550}{4}} = 66\% \tag{C.1}$$

However one can argue that the penetration of nanoparticles is related to the fiber density of the sample, meaning that a higher fiber density gives a lower penetration rate of the particles. Since it is hard to control this fiber density, this experiment could provide a lower boundary of particle deposition.
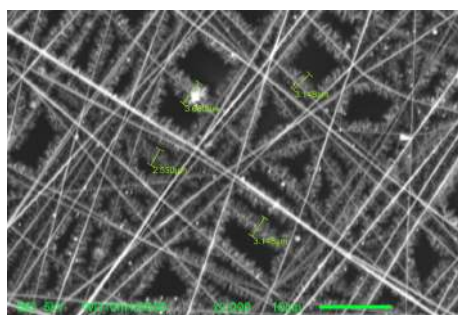
(a) SEM image of filter #1   (b) SEM image of filter #2
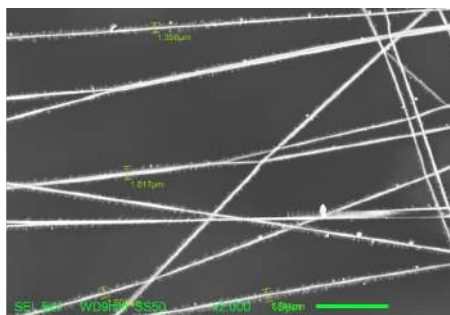
Figure C.1: Micrograph images of filter test with mixed titanium dioxide-gold nanostructures

Appendix D

Large Filter Test

The samples produced in the experimental section of this report are rather small. The amounts of deposited material are not measurable on a weighing scale and the experimental set-up was not prepared for in detail particle counting before and after the filter to indicate the amount of deposited particles. To still make an estimation of the amount of material that is deposited on the fibers, a long run experiment was done on a large fiber filter. A larger filter was needed, because only a small amount can be deposited on the 14 mm filters without them becoming overgrown with particles. A larger filter would ensure that no closing up of the filters would take place and still a measurable quantity could be deposited.

Sample Preparation

Usually a metal mash substrate of 14 mm for the polymer fibers was used, in this experiment however the metal support for the polymer fibers was 90 mm in diameter. The metal support was covered with a layer of PVA nanofibers and placed in the same dual spark set-up used in the other experiments, replacing the small sample holder. Subsequently the same procedure was followed as described in appendix A.3, only running one spark; once with titanium electrodes and a second time with aluminium electrodes. The flow through the second spark chamber kept on running, to precisely replicate the conditions the metal oxide nanoparticles are subject to in the other experiments. The difference with the other experiments was the run time, because of the variance in filter size. A total run time of 420 minutes with titanium electrodes and 480 minutes with aluminium electrodes ensured a measurable quantity was deposited on the filters. The quantities were measured at certain times during the experiment by stopping the experiment, taking out the filter, weighing the filter, putting the filter back in the set-up and continue the experiment. This was done three times, ending the experiment after weighing point three.

Results

The main goal of this section was to get an insight in the amount of nanoparticles produced and deposited on the polymer nanofiber filters. The graphs in figure D.1 show the material build up over time of the different materials tested. The results show that total amounts of 0.33 mg of titanium dioxide was deposited after 420 minutes and 0.49 mg of aluminium oxide after 480 minutes. By adding a linear trendline through the experimental data, the production per minute
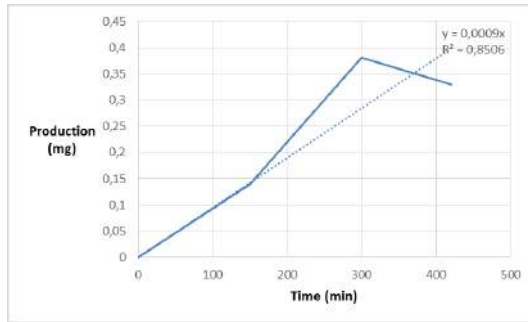
(a) Titanium dioxide deposition over time (b) Aluminium oxide deposition over time
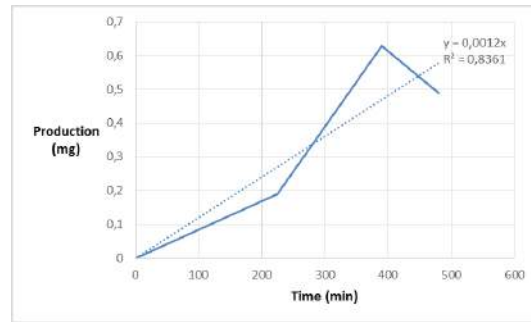
Figure D.1: Production rate of titanium dioxide and aluminium oxide on large polymer fiber filter over time
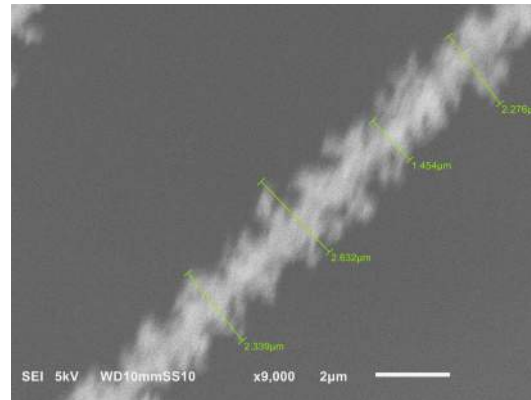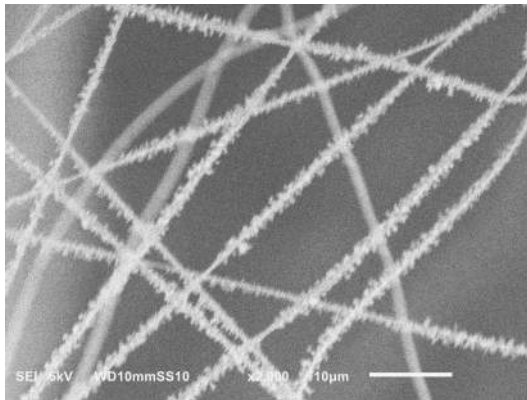
Figure D.2: SEM images of the large polymer fiber filter test with titanium dioxide nanostructures

of the spark discharge process can be calculated. A production of 0.0009 mg/min of titanium can be observed and a production of 0.0012 mg/min of aluminium. Taking these numbers, one can calculated back what the total amount of material on the other samples was. For example, the findings of this experiment would suggest a production of 0.024 mg for a titanium dioxide sample for which the runtime was 30 minutes.

To check if the conditions were the same, SEM measurements were done on large filter with titanium dioxide. These images are shown in figure D.2. The figure shows that the same (micro-) structures can be observed for the large sample as are observed in the experiment on a smaller sample with titanium dioxide in section 3.1.2.

Discussion

This experiment indicates that the total amount of material that is being made is very small, only several milligrams per day. However in light of the current research the experiment does give a nice insight in the amount of material being produced under the conditions used in the other experiments. It was found that the production rate of titanium dioxide is 0.0009 mg/min and the rate of production for aluminium dioxide is 0.0012 mg/min.

The R-squared of the regression analysis on both samples is due to an anomaly that is observed in both the aluminium large filter test and the large filter test with titanium electrodes.

In both samples it can be observed that the weight of the filter is lower than the weight at the interval measurement before that. This could be due to the fact that the weighing scale is not precise enough. The weighing scale that was used was accurate until tenths of a milligram, making the total error in the measurements relatively large. However the experiment was run for quite some time, generating enough material that could be collected on the polymer fibers to do a relatively accurate measurement. Looking at the R-squared value of both measurements, both are still in the 95 percentile of a normal distribution. Both the R-squared value of titanium dioxide (0.8506) and of aluminium oxide (0.8361) result in a standard deviation below 5% (3.8% and 4.04% for titanium dioxide and aluminium oxide respectively). Knowing that one minus R-squared is the variance of sample in a linear regression, the standard deviations are calculated using the following formula.

$$\sigma = \sqrt{1 - R^2} \tag{D.1}$$

One could argue that the fiber density of the filters has an influence on the amount of particles that are deposited on each filter. This is true and since the process of electrospinning cannot easily be controlled, which could result in a relatively large error. To minimize this error, the samples were at least produced with the same electrospin settings. To get an insight into the influence of the fiber density on the total amount of particles deposited on the filter, more research needs to be done in controlling the electrospinning, measuring the fiber density and the filter efficiency of a fiber. However these parameters were outside of the scope of my project.

Results

The main results acquired from this experiment were the production rate of titanium dioxide and aluminium oxide on the polymer fiber filters. The same settings were used as in the other experiments, resulting in a generalizable production rate with which deposition amounts for other experimental samples can be calculated. It was found that, with the desired spark settings, flow rate and electrospin settings, the production rates were 0.0009 mg/min and 0.0012 mg/min for titanium dioxide and aluminium oxide respectively. Both production rates were in the 95% confidence interval according to the R-squared value of the linear regression analysis.

Appendix E

Sample Instability induced by TEM

To analyze the various samples that were made during this project, transmission electron microscopy was used. As is explained in appendix B.1, TEM makes use of a high energy electron beam to analyze structures on a nanoscale. The obvious upside of this analysis method is that one can make images of the nanostructures, making the nanoworld very touchable and understandable. A downside of this technique is the influence the beam has on the structure itself; part of the energy of the electrons is being transformed to heat, inducing changes in the material. In figure E.1 one can see the influence that zooming in (increase in beam energy) has on the sample.
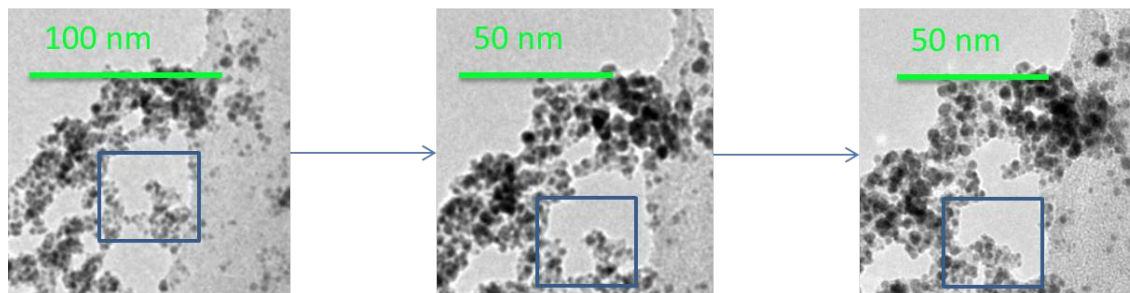
Figure E.1: TEM images of mixed titanium dioxide - gold nanostructures. Increasing in intensity from left to right.

The figure above shows that the structure significantly changes when zooming in. One can see that a gap in the structure (the part shown in the block) closes with increasing intensity, forming a more stable structure for the nanoparticles. If one looks more closely, more changes in morphology can be observed; closing and opening up of gaps, overall creating a more stable (energetically favourable) environment for the particles.

Appendix F

Nanoparticle mixing

When making the nanostructures on top of the polymer nanofibers, the particles needed to be mixed. In this research, mixing is done before the particles hit the polymer nanofiber filter. This is done because it is expected that ones the fractal-like nanostructures are formed, other particles cannot diffuse far into the structure. If one, for example, would first make a titanium dioxide fractal-like nanostructure and in a second run try to add the gold nanoparticles, these gold nanoparticles cannot diffuse far into the titanium dioxide matrix. The gold nanoparticles are thus expected to stay in the outer region of the titanium dioxide matrix. No specific experiment is done to test this hypothesis, however from figure F.1 it can be argued that the hypothesis is indeed correct.
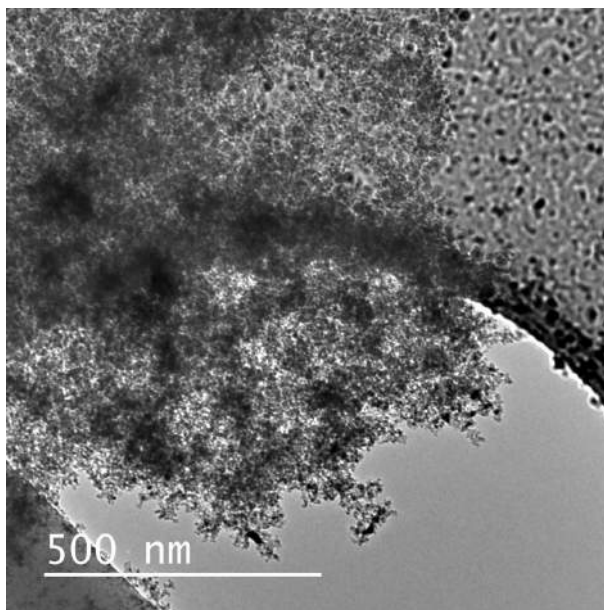
Figure F.1: TEM image of titanium dioxide nanoparticle agglomerate mixed with gold nanoparticles

The figure shows a titanium dioxide agglomerate with only gold nanoparticles in the outer regions of this agglomerate. The size of the agglomerate suggests that the agglomerate had

been circling in the spark chamber for quite some time, causing it to grow to the current size (> 500nm in diameter). However, since the agglomerate had not left the spark chamber while growing, there was no possibility for synthesized gold nanoparticles to mix with the titanium nanoparticles. Only when the agglomerate left the chamber, there was time for the gold to mix and diffuse into the agglomerate. As one can see in figure F.1 the gold is only observed in the outer region of the titanium dioxide agglomerate, assuming that the darkest dots represent gold nanoparticles. This supports the hypothesis that the fractal-like structure formed by the titanium dioxide is not easily penetrable for other nanoparticles added later. An upside of this could be that a layered structure can be formed, consisting of different types of nanoparticles (e.g. a layered structure of titanium dioxide, then gold and again titanium dioxide).

Appendix G

SEM and TEM deposition differences

Looking at the different TEM and SEM micrographs, one of the first things that catches the eye is the difference in amount of deposited particles. Figure G.1 shows TEM and SEM images of the same sample; the TEM image is taken from the nanostructures on fibers on TEM grid and SEM from nanostructures of fibers deposited on the metal mash, a schematic overview is given in figure G.1. Even though both samples are synthesized in the same way, a big difference in amount of deposited material can be observed (TEM shows less than 1 micron of material in diameter around the fiber, while SEM are more than 2 microns).
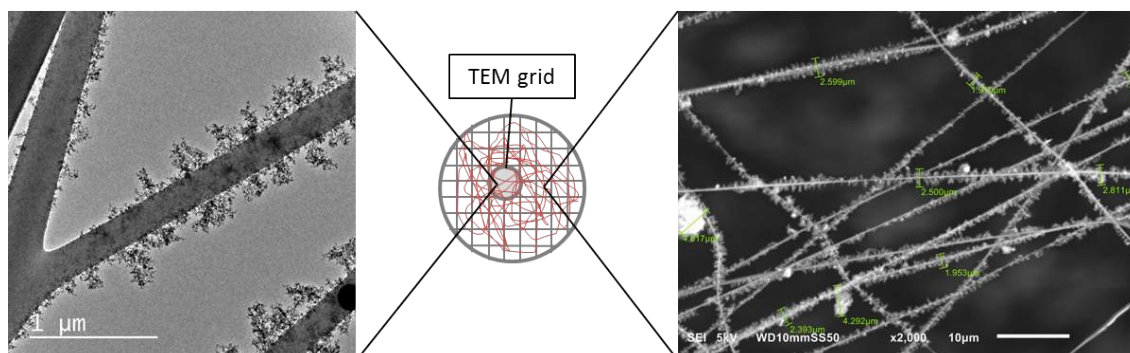
Figure G.1: TEM and SEM images (left and right respectively) of mixed titanium dioxide - gold nanostructures

The difference in deposited material on the polymer fibers can be explained by taking into account that the flow of gas and nanoparticles looks for the path with the least resistance. Since the TEM-grids used in this case have a carbon film as a support, the flow needs to pass through holes with a diameter of approximately 1.5 microns. This will most likely cause the flow to pass around the grid, making most of the nanoparticles flow around the TEM grid.

Appendix H

Diffusion Limited Aggregation Simulation

In this appendix a description of the simulation of the DLA system is provided. Simulating the DLA process for the nanoparticles and fibers was useful for two reasons. First it could provide an insight in the structure on a nanoscale; it might be especially useful to get an indication about the fractal dimension. Secondly it might give an insight in the amount of particles deposited on the fibers for certain diameters of the fractal-like structures. To simulate the diffusion limited aggregation system, a MATLAB model was made. The MATLAB software version used was R2013b and this data was processed in OriginPro 9.0. Below the simulation scatter graphs made in OriginPro is given (shown in figure H.2).

The model is based on a the assumption of discrete movement of the particles. Each particle enters the simulation space (a 3-dimensional grid) at a certain radius from the polymer fiber and makes discrete steps towards the fiber, based on the process of diffusion. When the particle hits the fiber (and later in the process the fractal-like structure) it sticks and the process is repeated. The process was monitored by plotting the 3-dimensional scatter graphs for every 20000 particles, these graphs are shown in figure H.2. The lattice size is chosen to be the size of the primary particles that are produced in the experiments, which is taken to be 7 nm.
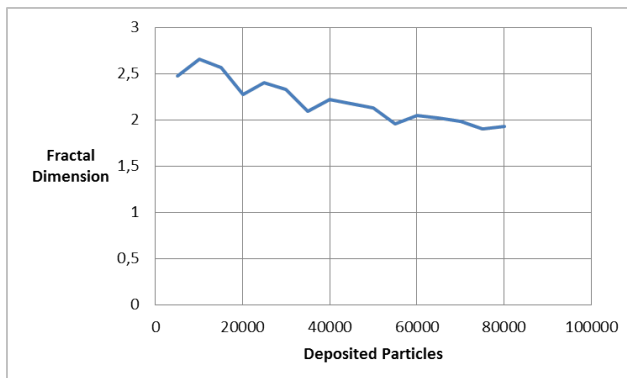
Figure H.1: Graphical representation of the fractal dimension as a function of amount of deposited particles on a polymer fiber
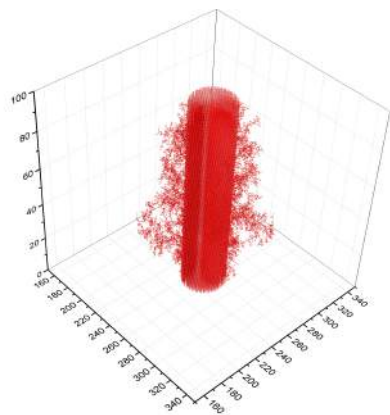
(a) 3D Simulation with 20000 particles
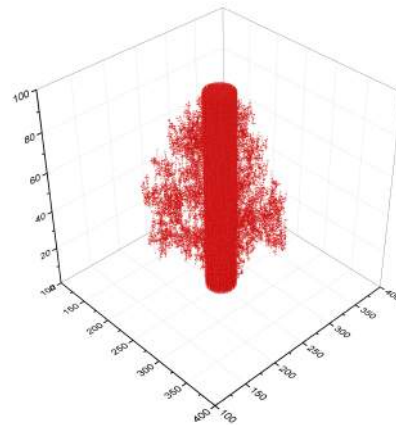
(b) 3D Simulation with 40000 particles
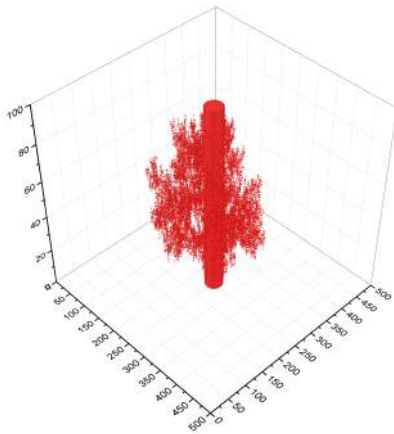
(c) 3D Simulation with 60000 particles
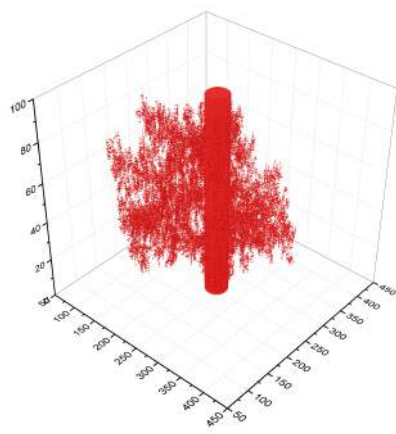
(d) 3D Simulation with 80000 particles

Figure H.2: Simulated structure growth of the fractal-like nanostructures on a polymer fiber

The fractal dimensions were calculated for these structures, which was done with a box-counting model. The results of these simulations are shown in H.1, where the fractal dimension is taken for the smallest box size. It can be seen that, if the model is indeed correct, the fractal dimension of the larger structures will level out at a value of approximately 2. This is lower than the fractal dimension for 3-dimensional diffusion limited aggregation systems that can be obtained from literature (around 2.5). However this could be explained by the fact that in this system, the particles cannot really grow in three dimensions. They are deposited on the larger fibers, in contract to the assumptions in literature where the structures grow from one particle in all directions.

Other than the (to the eye) similarity in fractal-like nanostructures, no experimental data on the fractal dimension or porosity of the material was available. Therefor it was not possible to test the model on its validity and/or reliability. Furthermore it would have been nice to see whether the fractal dimension matches the result found by Hogan *et al.* [38]. To test this larger amounts of particles needed to be deposited, which was not possible with the current model and computing power of the desktops that were available.

Appendix I

Catalyst Synthesis Process

To already provide the next step to an industrial applicable process a schematic overview of the catalyst synthesis process by the proposed method is made. Figure I.1 shows this generic pathway, where rectangles represent actions and diamonds represent choices in the process.
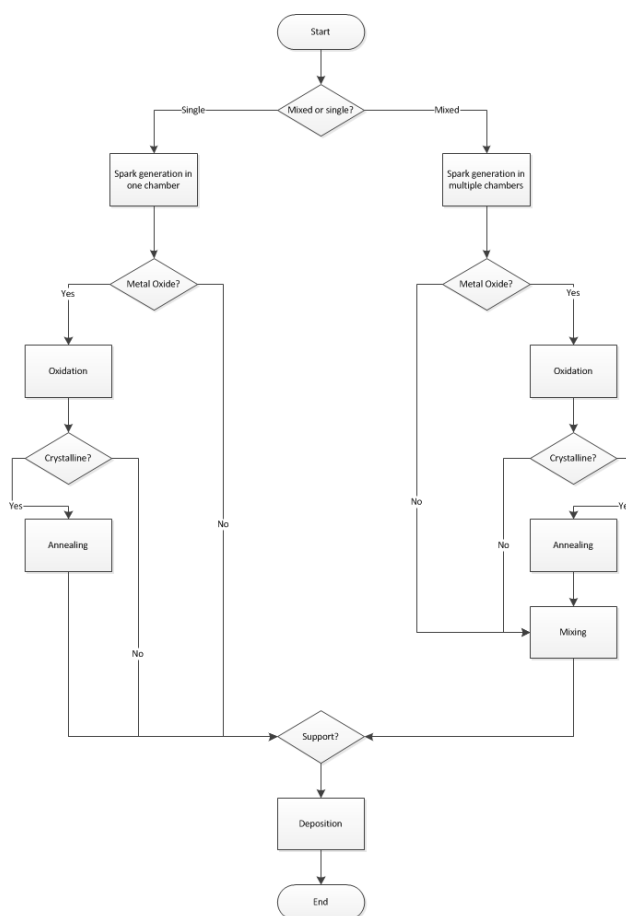
Figure I.1: Flowchart of the catalyst synthesis process

Bibliography

[1] T V Pfeiffer, J Feng, and A Schmidt-Ott. New developments in spark production of nanoparticles. *Advanced Powder Technology*, 25:56–8831, 2014.

[2] A.W. van Vugt. A clean and flexible method of catalyst synthesis. 2014.

[3] Mikhaylo A Trunov, Mirko Schoenitz, Xiaoying Zhu, and Edward L Dreizin. Effect of polymorphic phase transformations in Al_2O_3 film on oxidation kinetics of aluminum powders. *Combustion and Flame*, 140(4):310–318, 2005.

[4] Alan D McNaught and Alan D McNaught. *Compendium of chemical terminology*, volume 1669. Blackwell Science Oxford, 1997.

[5] Haakon Johnson. Catalyst Market Analysis Size, Share, Trends, Growth And Forecast to 2020 - Grand View Research, 2014.

[6] F Llewellyn Jones. Electrode erosion by spark discharges. *British Journal of Applied Physics*, 1(3):60, 1950.

[7] Heinz Burtscher and Andreas Schmidt-Ott. Enormous enhancement of van der Waals forces between small silver particles. *Physical Review Letters*, 48(25):1734, 1982.

[8] S Schwyn, E Garwin, and A Schmidt-Ott. Aerosol generation by spark discharge. *Journal of Aerosol Science*, 19(5):639–642, 1988.

[9] Bengt O Meuller, Maria E Messing, David L J Engberg, Anna M Jansson, Linda I M Johansson, Susanne M Norlén, Nina Tureson, and Knut Deppert. Review of spark discharge generators for production of nanoparticle aerosols. *Aerosol Science and Technology*, 46(11):1256–1270, 2012.

[10] R Reinmann and M Akram. Temporal investigation of a fast spark discharge in chemically inert gases. *Journal of Physics D: Applied Physics*, 30(7):1125, 1997.

[11] Nooshin Salman Tabrizi, M Ullmann, V A Vons, U Lafont, and A Schmidt-Ott. Generation of nanoparticles by spark discharge. *Journal of Nanoparticle Research*, 11(2):315–332, 2009.

[12] W Koch and S K Friedlander. The effect of particle coalescence on the surface area of a coagulating aerosol. *Journal of Colloid and Interface Science*, 140:419–9797, 1990.

[13] N S Tabrizi, Q Xu, N M van der Pers, U Lafont, and A Schmidt-Ott. Synthesis of mixed metallic nanoparticles by spark discharge. *Journal of nanoparticle Research*, 11(5):1209–1218, 2009.

[14] N S Tabrizi, Q Xu, N M van der Pers, and A Schmidt-Ott. Generation of mixed metallic nanoparticles from immiscible metals by spark discharge. *Journal of Nanoparticle Research*, 12(1):247–259, 2010.

[15] Darrell H Reneker and Iksoo Chun. Nanometre diameter fibres of polymer, produced by electrospinning. *Nanotechnology*, 7(3):216, 1996.

[16] Dan Li and Younan Xia. Electrospinning of nanofibers: reinventing the wheel? *Advanced*

materials, 16(14):1151–1170, 2004.

[17] Geoffrey Taylor. Electrically driven jets. *Proceedings of the Royal Society of London. A. Mathematical and Physical Sciences*, 313(1515):453–475, 1969.

[18] A L Yarin, S Koombhongse, and Darrell Hyson Reneker. Bending instability in electrospinning of nanofibers. *Journal of Applied Physics*, 89(5):3018–3026, 2001.

[19] Erika AdomavičiÅńtÄÛ and Rimvydas Milašius. The Influence of Applied Voltage on Poly (vinyl alcohol)(PVA) Nanofibre Diameter. *Fibres & Textiles in Eastern Europe*, 15(5-6):63, 2007.

[20] Nandana Bhardwaj and Subhas C Kundu. Electrospinning: a fascinating fiber fabrication technique. *Biotechnology advances*, 28(3):325–347, 2010.

[21] Roland Saur. Stability of Al and Pt nanostructures grown on polymer nanofibers. 2014.

[22] G V Ivanov and F Tepper. Special Topics in Chemical Propulsion. In *4th International Symposium on Special Topics in Chemical Propulsion*, volume 636, 1997.

[23] E L Dreizin. Phase changes in metal combustion. *Progress in Energy and Combustion Science*, 26:57–1285, 2000.

[24] T A Brzustowski and I Glassman. Vapor-phase diffusion flames in the combustion of magnesium and aluminum: II. Experimental observations in oxygen atmospheres. *Preprint*, pages 63–490, 1964.

[25] E W Price and R K Sigman. Combustion of aluminized solid propellants. *Solid propellant chemistry, combustion, and motor interior ballistics(A 00-36332 09-28), Reston, VA, American Institute of Aeronautics and Astronautics, Inc.(Progress in Astronautics and Aeronautics.*, 185:663–687, 2000.

[26] L F Ernst, F L Dryer, R A Yetter, T P Parr, and D M Hanson-Parr. Aluminum droplet combustion in fluorine and mixed oxygen/fluorine containing environments. *Proceedings of the Combustion Institute*, 28(1):871–878, 2000.

[27] P Bucher, L Ernst, F L Dryer, and R Yetter. Detailed studies of the flame structure of aluminum particle combustion. *Solid propellant chemistry, combustion, and motor interior ballistics(A 00-36332 09-28), Reston, VA, American Institute of Aeronautics and Astronautics, Inc.(Progress in Astronautics and Aeronautics.*, 185:689–722, 2000.

[28] K Park, D Lee, A Rai, D Mukherjee, and M R Zachariah. Size-resolved kinetic measurements of aluminum nanoparticle oxidation with single particle mass spectrometry. *The Journal of Physical Chemistry B*, 109:6106–7290, 2005.

[29] Ashish Rai, Donggeun Lee, Kihong Park, and Michael R Zachariah. Importance of phase change of aluminum in oxidation of aluminum nanoparticles. *The Journal of Physical Chemistry B*, 108:14793–16106, 2004.

[30] A Rai, K Park, L Zhou, and M R Zachariah. Understanding the mechanism of aluminium nanoparticle oxidation. *Combustion Theory and Modelling*, 10:843–7830, 2006.

[31] I E Molodetsky, E P Vicenzi, E L Dreizin, and C K Law. Phases of titanium combustion in air. *Combustion and Flame*, 112(4):522–532, 1998.

[32] V V Karasev, A A Onishchuk, S A Khromova, O G Glotov, V E Zarko, E A Pilyugina, and C J Tsai. Formation of Metal Oxide Nanoparticles in Combustion of Titanium and Aluminum Droplets. 42(6):649–662, 2006.

[33] T A Witten Jr and Leonard M Sander. Diffusion-limited aggregation, a kinetic critical phenomenon. *Physical review letters*, 47(19):1400, 1981.

[34] Hans Sagan. *Space-filling curves*, volume 18. Springer-Verlag New York, 1994.

[35] Kenneth Falconer. *Fractal geometry: mathematical foundations and applications*. John Wiley & Sons, 2004.

[36] Helge Von Koch. On a continuous curve without tangent constructible from elementary

geometry. *Classics on Fractals (Westview Press, 2004) pp*, 25:45, 1993.

[37] Bernard Sapoval. *Universalités et fractales*. Flammarion, 1997.

[38] Gustaf J Lindquist, David Y H Pui, and Christopher J Hogan. Porous particulate film deposition in the transition regime. *Journal of Aerosol Science*, 74:42–51, 2014.

[39] Pramod Kulkarni and Pratim Biswas. A Brownian dynamics simulation to predict morphology of nanoparticle deposits in the presence of interparticle interactions. *Aerosol science and technology*, 38(6):541–554, 2004.

[40] Paul Meakin. Formation of fractal clusters and networks by irreversible diffusion-limited aggregation. *Physical Review Letters*, 51(13):1119, 1983.

[41] Paul Meakin. Diffusion-controlled deposition on surfaces: Cluster-size distribution, interface exponents, and other properties. *Physical Review B*, 30(8):4207, 1984.

[42] Shipra Mital Gupta and Manoj Tripathi. A review of TiO2 nanoparticles. *Chinese Science Bulletin*, 56:1639–6538, 2011.

[43] Shipra Mital Gupta and Manoj Tripathi. An overview of commonly used semiconductor nanoparticles in photocatalysis. *High Energy Chemistry*, 46:1–1439, 2012.

[44] Meng Ni, Michael K H Leung, Dennis Y C Leung, and K Sumathy. A review and recent developments in photocatalytic water-splitting using TiO2 for hydrogen production. *Renewable and Sustainable Energy Reviews*, 11(3):401–425, 2007.

[45] Amy L Linsebigler, Guangquan Lu, and John T Yates Jr. Photocatalysis on TiO2 surfaces: principles, mechanisms, and selected results. *Chemical reviews*, 95(3):735–758, 1995.

[46] Hui Han and Renbi Bai. Buoyant photocatalyst with greatly enhanced visible-light activity prepared through a low temperature hydrothermal method. *Industrial & Engineering Chemistry Research*, 48(6):2891–2898, 2009.

[47] Brian OâĂŹregan and M Grfitzeli. A low-cost, high-efficiency solar cell based on dye-sensitized. *nature*, 353:737–740, 1991.

[48] Michael R Hoffmann, Scot T Martin, Wonyong Choi, and Detlef W Bahnemann. Environmental applications of semiconductor photocatalysis. *Chemical reviews*, 95(1):69–96, 1995.

[49] W K Wong and M A Malati. Doped TiO2 for solar energy applications. *Solar Energy*, 36(2):163–168, 1986.

[50] K Ravindranathan Thampi, John Kiwi, and Michael Gratzel. Methanation and photo-methanation of carbon dioxide at room temperature and atmospheric pressure. *Nature*, 327(6122):506–508, June 1987.

[51] J Papp, H S Shen, R Kershaw, K Dwight, and A Wold. Titanium(IV) oxide photocatalysts with palladium. *Chemistry of Materials*, 5(3):284–288, March 1993.

[52] Donia Beydoun, Rose Amal, Gary Low, and S McEvoy. Role of nanoparticles in photocatalysis. *Journal of Nanoparticle Research*, 1:439–764, 1999.

[53] Vaidyanathan Subramanian, Eduardo Wolf, and Prashant V Kamat. Semiconductor-metal composite nanostructures. To what extent do metal nanoparticles improve the photocatalytic activity of TiO2 films? *The Journal of Physical Chemistry B*, 105:11439–16106, 2001.

[54] Maria Vittoria Dozzi, Laura Prati, Patrizia Canton, and Elena Selli. Effects of gold nanoparticles deposition on the photocatalytic activity of titanium dioxide under visible light. *Physical chemistry chemical physics*, 11:7171–7180, 2009.

[55] A.Valentine Rupa, D Divakar, and T Sivakumar. Titania and Noble Metals Deposited Titania Catalysts in the Photodegradation of Tartazine. *Catalysis Letters*, 132(1-2):259–267 LA – English, 2009.

[56] Mark Turner, Vladimir B Golovko, Owain P H Vaughan, Pavel Abdulkin, Angel Berenguer-

Murcia, Mintcho S Tikhov, Brian F G Johnson, and Richard M Lambert. Selective oxidation with dioxygen by gold nanoparticle catalysts derived from 55-atom clusters. *Nature*, 454(7207):981–983, August 2008.

[57] M Albert, Y M Gao, D Toft, K Dwight, and A Wold. Photoassisted gold deposition of titanium dioxide. *Materials research bulletin*, 27(8):961–966, 1992.

[58] Y M Gao, H S Shen, K Dwight, and A Wold. Preparation and photocatalytic properties of titanium (IV) oxide films. *Materials research bulletin*, 27(9):1023–1030, 1992.

[59] Hexing Li, Zhenfeng Bian, Jian Zhu, Yuning Huo, Hui Li, and Yunfeng Lu. Mesoporous Au/TiO2 Nanocomposites with Enhanced Photocatalytic Activity. *Journal of the American Chemical Society*, 129(15):4538–4539, March 2007.

[60] Adel A Ismail, Detlef W Bahnemann, Inga Bannat, and Michael Wark. Gold nanoparticles on mesoporous interparticle networks of titanium dioxide nanocrystals for enhanced photonic efficiencies. *The Journal of Physical Chemistry C*, 113:7429–7447, 2009.

[61] Herman Pines and Werner O Haag. Alumina: Catalyst and Support. I. Alumina, its Intrinsic Acidity and Catalytic Activity1. *Journal of the American Chemical Society*, 82(10):2471–2483, May 1960.

[62] H Knözinger and Ph Ratnasamy. Catalytic aluminas: surface models and characterization of surface sites. *Catalysis Reviews Science and Engineering*, 17(1):31–70, 1978.

[63] Henrik Topsø e, Bjerne S Clausen, and Franklin E Massoth. *Hydrotreating catalysis*. Springer, 1996.

[64] Carlos MárquezâĂŘAlvarez, Naděžda Žilková, Joaquín PérezâĂŘPariente, and JiÅŹí Čejka. Synthesis, Characterization and Catalytic Applications of Organized Mesoporous Aluminas. *Catalysis Reviews*, 50(2):222–286, April 2008.

[65] D L Trimm and A Stanislaus. The control of pore size in alumina catalyst supports: A review. *Applied Catalysis*, 21(2):215–238, March 1986.

[66] Masatake Haruta. Catalysis of Gold Nanoparticles Deposited on Metal Oxides. *CATTECH*, 6(3):102–115 LA – English, 2002.

[67] Mitsutaka Okumura, Shyunichi Nakamura, Susumu Tsubota, Toshiko Nakamura, Masashi Azuma, and Masatake Haruta. Chemical vapor deposition of gold on Al2O3, SiO2, and TiO2 for the oxidation of CO and of H2. *Catalysis Letters*, 51(1-2):53–58, 1998.

[68] Jifei Jia, Kenta Haraki, Junko N Kondo, Kazunari Domen, and Kenzi Tamaru. Selective hydrogenation of acetylene over Au/Al2O3 catalyst. *The Journal of Physical Chemistry B*, 104(47):11153–11156, 2000.

[69] Hee Dong Jang, Seong-Kil Kim, and Seung-Jin Kim. Effect of particle size and phase composition of titanium dioxide nanoparticles on the photocatalytic properties. *Journal of Nanoparticle Research*, 3:141–764, 2001.

[70] Dorian A H Hanaor and Charles C Sorrell. Review of the anatase to rutile phase transformation. *Journal of Materials science*, 46(4):855–874, 2011.

[71] Robert D Shannon and Joseph A Pask. Kinetics of the AnataseâĂŘRutile Transformation. *Journal of the American Ceramic Society*, 48(8):391–398, 1965.

[72] Masanori Hirano, Chiaki Nakahara, Keisuke Ota, Osamu Tanaike, and Michio Inagaki. Photoactivity and phase stability of ZrO2-doped anatase-type TiO2 directly formed as nanometer-sized particles by hydrolysis under hydrothermal conditions. *Journal of Solid State Chemistry*, 170(1):39–47, January 2003.

[73] O Carp, C L Huisman, and A Reller. Photoinduced reactivity of titanium dioxide. *Progress in Solid State Chemistry*, 32(1âĂŞ2):33–177, 2004.

[74] Clifford A Hampel. *The Encyclopedia of the Chemical Elements*. 1968.

[75] Akira Fujishima. Electrochemical photolysis of water at a semiconductor electrode. *nature*,

238:37–38, 1972.

[76] David B Williams and C Barry Carter. *The transmission electron microscope*. Springer, 1996.

[77] Zheng-Ming Huang, Y-Z Zhang, M Kotaki, and S Ramakrishna. A review on polymer nanofibers by electrospinning and their applications in nanocomposites. *Composites science and technology*, 63(15):2223–2253, 2003.

[78] Snejana Bakardjieva, Vaclav Stengl, Lorant Szatmary, Jan Subrt, Jozef Lukac, Nataliya Murafa, Daniel Niznansky, Karel Cizek, Jaromir Jirkovsky, and Nadia Petrova. Transformation of brookite-type TiO 2 nanocrystals to rutile: correlation between microstructure and photoactivity. *Journal of Materials Chemistry*, 16(18):1709–1716, 2006.